LARGE DEFORMATION ANALYSIS IN GEOMECHANICS USING ADAPTIVE FINITE ELEMENT METHODS

By

Mina Kardani

B.Sc., Software Engineering

A Thesis submitted for the

Degree of Doctor of Philosophy at

The University of Newcastle

March 2012

DECLARATION

"*This Thesis contains no material which has been accepted for the award of any other degree or diploma in any university or other tertiary institution and, to the best of my knowledge and belief, contains no material previously published or written by another person, except where due reference has been made in the text. I give consent to this copy of my thesis, when deposited in the University Library, being made available for loan and photocopying subject to the provisions of the Copyright Act 1968.* "

(Signed) _____

ACKNOWLEDGEMENTS

This research study would not have been possible without the support of many people who have helped and inspired me during my study.

First and foremost I offer my sincerest thanks to my supervisor Prof. Daichao Sheng for his unending help and invaluable assistance, support and guidance from the initial to the final level of my research. His unlimited availability and encouragement made my research life smooth and rewarding. Also, I would like to appreciate my co-supervisors Prof. Scott Sloan and Dr. Andrew Abbo for their helpful advice.

I was delighted to have valuable discussion with Prof. Peter Wriggers in some critical stages of this research work. His guidance is really appreciated.

I offer my regards and blessings to the colleagues and postgraduates in the Geotechnical Group of the University of Newcastle who supported me in many respects and provided a convivial environment to work.

I acknowledge the University of Newcastle for giving me a postgraduate scholarship and providing the financial support for this research.

I owe my deepest gratitude to my husband Majid, for his unflagging love and support and encouragement. I am indebted to him for his abundant help, guidance and valuable assistance in the preparation and completion of this study. Last but not least, I am grateful to my gorgeous son who has constantly reminded me that life without a challenge is going to be really boring.

CONTENTS

ABSTRACT

The finite element method (FEM) is extensively used in analysis of a wide range of nonlinear geotechnical problems. The finite element method can handle simple and complex constitutive soil models, and solve problems with complicated geometries and boundary conditions with reasonably accurate results. On the other hand, mesh distortion and entanglement of elements, occurring inevitably in failure zones with high stress/strain concentration, are main drawbacks of the common finite element solutions such as the Updated Lagrangian method. In addition, efficacious application of the method requires experience and a certain amount of trial and error, particularly when choosing an optimal time and spatial discretisation.

Adaptive finite element methods provide a means for obtaining more reliable solutions by continuously adjusting the discretisation in time and space according to the current solution. These procedures automatically refine, coarsen, or relocate a mesh to achieve a solution with a specified accuracy in an optimal fashion. Although a significant amount of research has been devoted to adaptive finite element analysis in solid mechanics, the application of adaptive methods has been less considered in nonlinear geotechnical problems due to the complexity. Modelling of problems in geomechanics is typically sophisticated due to nonlinear constitutive laws, large deformations, changing boundary conditions and time-dependent behaviour. A variety of adaptive finite element techniques have been developed to tackle nonlinear problems in solid mechanics. However, the

application of these methods to geomechanics is still a challenge. Amongst the various adaptive techniques, the *r*-adaptive and *h*-adaptive finite element methods are probably the most favoured and most established. *r*-adaptive finite element method attempts to eliminate the mesh distortion by refining the mesh in the finite element domain. On the other hand, *h*-adaptive finite element method is based on the idea of generating a new mesh by dividing the area of original elements where the interpolation should be improved to achieve higher accuracy or to avoid mesh distortion.

In this Thesis, the *h*-adaptive finite element technique will be employed to solve some complex geotechnical problems involving material nonlinearity, large deformation, changing boundary conditions and time-dependent nonlinearity. To achieve this, the main features of the technique including advanced mesh generation algorithms, error estimation methods and a procedure for remapping of state variables will be discussed and developed in company of a robust analysis program. The performance of the *h*-adaptive finite element method is then represented by considering the accuracy and efficiency of the method in solving some classical geomechanics problems such as the bearing capacity of footings, expansion of cavities, and the stability of slopes.

In addition, this Thesis will address the performance and the efficiency of alternative error estimation techniques for particular geotechnical applications involved with changing boundary conditions and inertia forces, such as static and dynamic penetration of an object into soil. Such problems are categorised as one of the most sophisticated problems of computational geomechanics due to their extreme nonlinearity.

This Thesis will also present a new and innovative combined adaptive method for tackling geotechnical problems with relatively large deformations. This robust method is based upon an elegant combination of the Arbitrary Lagrangian-Eulerian (ALE) method and the *h*-adaptive finite element method developed as a part of the Thesis. The proposed method takes advantage of *r*-refinement as well as *h*-refinement finite element techniques, and yet eliminates the individual drawback of each method.

PREFACE

The research work presented in the Thesis has been performed in the Discipline of Civil, Surveying and Environmental engineering, school of Engineering, at the University of Newcastle, Australia under supervision of Prof. Daichao Sheng from September 2007 to September 2011. During the term of candidature, a number of papers were published which are listed below:

Kardani M, Nazem M, Abbo AJ, Sheng D, Sloan SW, "Refined *h*-adaptive finite element procedure for large deformation geotechnical problems", *Computational Mechanics*, Vol 49, 21-33, 2012

Nazem M, Kardani M, Carter JP, Sheng D, "A comparative study of error assessment techniques for dynamic contact problems of geomechanics", *Computer and Geotechnics*, Vol 40, 62-73, 2012

Kardani M, Nazem M, Sheng D, Carter JP, "Large deformation analysis of geomechanics problem by combined *rh*-adaptive finite element method", *Under co-authors' review*

Kardani M, Nazem M, Abbo AJ, Sheng D, "A study of adaptive finite element methods in solving large deformation problems in geomechanics", *IV European Conference on Computational Mechanics (ECCOMAS2010)*, Paris, France, 2010

Kardani M, Nazem M, Abbo AJ, Sheng D, "A comparative study of *h*-adaptive and *r*-adaptive finite element methods in geomechanics", *Proceedings of 9th World*

Congress on Computational Mechanics and 4th Asian Pacific Congress on Computational Mechanics (WCCM2010), Sydney, Australia, 2010

Nazem M, Kardani M, Carter JP, Sheng D, "Application of h-adaptive FE method for dynamic analysis of geotechnical problems", *Proceeding of the 2nd International Symposium on Computational Geomechanics (COMGEO2011)*, Cavtat-Dubrovnik, Croatia, 590-495, 2011

Kardani M, Nazem M, Sheng D, "Application of *h*-adaptive FE method for analysis of dynamic contact problems in geomechanics", *International Conference on Computational Contact Mechanics*, Hannover, Germany, 2011

Kardani M, Nazem M, Carter JP, "A combined *rh*-adaptive finite element method for geotechnical problems", *Twelfth Pan American Congress of Applied Mechanics (PACAM 2012)*, Port of Spain, Trinidad, 2012

CHAPTER 1

INTRODUCTION

1.1. MOTIVATION

The finite element method (FEM) is a robust method for analysing a large number of problems in engineering where analytical solutions cannot be obtained. In geotechnical engineering, involved with a wide range of nonlinear problems, this method can obtain reasonable solutions. Nonlinearity may arise in a problem due to several reasons: nonlinear stress-strain relations, large deformation, changing boundary conditions and time-dependent behaviour. These resources, when combined, make the analysis of nonlinear problems a very challenging task. Adaptive finite element techniques have been developed to tackle nonlinear problems arising in solid mechanics over the past decades. Although these methods have been well established in the literature for solving many problems of solid mechanics, their application in geomechanics, due to the complex and nonlinear nature of problems, is still a challenge.

Adaptive finite element techniques have been the interest of many researchers over the last three decades, and a variety of adaptive techniques have been proposed in the literature. These mainly include *p*-adaptive, *r*-adaptive, *h*-adaptive and *hp*-adaptive methods. *r*-adaptive and *h*-adaptive FE methods are probably the most favoured and common techniques among engineering applications, and are well established in solid mechanics. The *r*-adaptive FE method has recently been considered in solving some geotechnical problems. A variant of this method, namely as Arbitrary Lagrangian-Eulerian method, is able to solve a large number of geotechnical problems involving, particularly, large deformations. The method, however, is not efficient in providing a solution to some

complex problems in geomechanics since its accuracy severely depends on the initial density of its finite element mesh. This issue becomes more pronounced in problems involving strain localisation and shear bands. On the other hand, standard finite element procedures, such as the Updated-Lagrangian method, can fail to provide a solution to large deformation problems. An example where this failure may take place is the deep penetration of frictional piles or penetrometers into a soil layer. Such penetration problems usually cause severe mesh distortion. A typical distorted mesh occurring during penetration of a cone into a layer of soil is depicted in Figure 1.1. Such a distortion results in a negative Jacobian of an element, leading to a spontaneous termination of the analysis.

The *h*-adaptive finite element technique, on the other hand, has attracted less attention in geomechanics, due to the complex features involved. The implementation of this method requires robust and efficient numerical algorithms for mesh generation, mesh optimisation, error estimation and remapping of state variables. Despite these complexities, the main advantage of the *h*-adaptive finite element method is that the numbers of nodes and elements, unlike *r*-adaptive finite element method, can vary during the analysis and the elements can be resized based upon a prescribed precision. The analysis of geotechnical problems by this method may provide more accurate results which in turn lead to cheaper and safer designs. In this study the main aims are to develop the *h*-adaptive finite element method into a suitable framework for solving

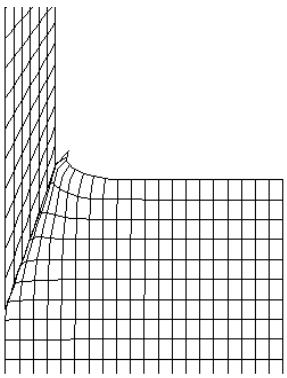

Figure 1.1. Mesh distortion under a cone.

nonlinear problems of geomechanics and to study the performance and reliability of the method in analysing such problems. The main outputs of this research work will include a detailed study of efficiency of the *h*-adaptive finite element method in geotechnical problems as well as a robust numerical analysis tool for a wide range of nonlinear problems of solid mechanics, particularly geomechanics.

1.2. OBJECTIVES

The goal of this study is to improve *h*-adaptive FE technique as well as to develop a new combined *rh*-adaptive FE technique to solve nonlinear problems in geomechanics. It includes the development of accurate numerical algorithms for efficiently analysing geotechnical problems involving material nonlinearity, large deformations, time-dependent behaviour and changing boundary conditions. Some important aspects of the *h*-adaptive FE method which will be addressed in this study are as follows:

- To develop the *h*-adaptive FE method into a computer program and compare the robustness and efficiency of the method with standard FE method and *r*-adaptive technique.
- To study alternative methods of mesh generation and mesh optimisation in 2D domains and to find an appropriate and effective meshing technique for *h*-adaptive FE method in geomechanics problems.
- To study the performance of error estimation methods and to address the applicability of each method in geotechnical problems.

- To implement an effective technique for remapping state variables between two finite element meshes with different topology and to study the efficiency as well as accuracy of this technique.
- To demonstrate the efficiency of *h*-adaptive FE method in specific problems of geomechanics involving large deformation and contact mechanics such as installation of piles and penetration of objects into a soil layer.
- To generalise *h*-adaptivity to geotechnical problems involved with dynamic loads.
- To develop a new combined *rh*-adaptive technique to analyse large deformation problems of geomechanics.

1.3. OUTLINE

This Thesis consists of eight chapters including this introduction. A summary of each chapter is given here.

Chapter 2 provides a brief literature review of finite element method and adaptivity. This chapter also introduces alternative adaptive finite element techniques. The chapter concludes with an introduction to the governing equations of nonlinear finite element analysis.

In Chapter 3 the *h*-adaptive FE, which is the main subject of this study, is described. The chapter begins with an introduction to *h*-adaptive FE techniques and its main components. The chapter then discusses several methods of mesh generation. Various error estimation

methods are also discussed in this chapter. Finally, the chapter explains a procedure for remapping nodal and state variables between two meshes with different topology.

The implementation of the *h*-adaptive FE technique into the existing code at the University of Newcastle, SNAC, is the subject of Chapter 4. A brief introduction to the *Triangle* code, the mesh generator employed in this study, is presented. Then the format of the data file including the topology of domain, material properties, loading conditions and analysis configuration are explained. The chapter also describes the adopted methods for estimating error. Also the remapping procedure applied in this study is explained in this chapter.

Chapter 5 addresses the aspects of implementation of the *h*-adaptive finite element method in problems of geomechanics involving dynamic forces and changing boundary conditions. A literature review followed by the finite element formulation and an introduction to contact mechanics for *h*-adaptivity are provided in this chapter.

Chapter 6 introduces a new *rh*-adaptive finite element method for analysing nonlinear problems in geotechnical engineering. The philosophy as well as the numerical algorithm of the proposed method is explained in this chapter.

The adaptive finite element method developed in Chapters 3-5 and the *rh*-adaptive finite element method presented in Chapter 6, are used to analyse several numerical examples in Chapter 7. These examples include the problem of cavity expansion, biaxial test, rigid strip footing on an undrained layer of soil subjected to static as well as dynamic loads, static and dynamic penetration of objects into a layer of soil, the analysis of a vertical cut, the

indentation of a cylinder object into a soil layer, and the bearing capacity of a two-layered soil under a rigid footing.

Chapter 8 presents a summary of important conclusions obtained from this Thesis.

CHAPTER 2

FINITE ELEMENTS AND ADAPTIVITY

2.1. INTRODUCTION

The basic idea of the finite element method is that a region of continuum can be approximated by a finite number of interrelated subregions or elements. In fact, the region can be substituted and be modelled by a broken continuum. The process of creating these subregions is often called discretization. The discretization strategy depends on the region and the aim of the analysis. It is noticeable that the finite element method was originally developed by structural engineers, where the skeletal structures naturally resolve into finite-size elements. On the other hand, the aircraft industry made early contribution to the breaking of solid structures into elements (meshing). This method was mainly used where the exact solution to a problem cannot be obtained. Obviously, the denser the discretization is the more accurate the result would be. Therefore, obtaining an accurate result could be a time consuming process. Adaptive finite element techniques are generally used to adjust the discretization throughout the analysis process in the way to lead to a more robust and reliable solution in a shorter time.

In geotechnical engineering, there is a wide range of nonlinear problems for which adaptivity can improve the accuracy of numerical solutions. For example, adaptive time stepping for controlling the time (load) discretisation has been used successfully to solve many geotechnical problems (Sloan and Abbo, 1999a, 1999b; Sheng and Sloan, 2001, 2003; Allix et al. 2010). Automatic substepping in explicit stress integration, which adjusts the strain increment size according to the current stress state, is another form of adaptivity

that has proved to be highly effective in implementing advanced constitutive models (Sloan, 1987; Sloan et al., 2001). In contrast, adaptive spatial discretisation has attracted less attention in the field of geomechanics, perhaps because of the prevalence of the small-deformation assumption.

The finite element method with adaptive spatial discretisation has been an active research area over the last three decades. A number of techniques have been developed, with the most common ones in dealing with large deformation problems being the *r*-adaptive and *h*-adaptive methods (Li and Bettess, 1997). The *r*-adaptive method adjusts the spatial discretisation, but usually does not increase the overall number of elements and the nodes. The *h*-adaptive method, on the other hand, adjusts the spatial discretisation by continuously increasing the mesh density in zones where a more accurate response is expected. Although it is well established in solid mechanics, the *h*-adaptive finite element method has attracted less attention in geomechanics with the work of Hu and Randolph (1998, 1999) being a notable exception. As finite element analysis becomes increasingly common in geotechnical engineering, with many practical problems involving the complex features listed above, there is a pressing need for reliable methods that control the discretisation error within a desired limit.

This chapter presents a brief literature review of *h*-adaptive finite element method. Alternative adaptive finite element techniques are introduced. The chapter ends up with the equations governing the nonlinear large deformation problems.

2.2. LITERATURE REVIEW

A normal procedure for solving the engineering problems by using an *h*-adaptive finite element method includes continuously increasing the number of discretization points in a defined region and resolving the global system of equations to calculate the relative change in the numerical solution. An *h*-adaptive method starts with an initial model of the mesh which also describes the geometry of the region and boundary conditions as well as specifying an error tolerance according to a desired criterion. The *h*-adaptive FE strategy subdivides the integration region into successively smaller sub-regions (Huerta et al., 1999), thus changing the density of the elements to yield a more accurate solution while keeping the element order constant. In the case of small deformations, where the mesh geometry does not change throughout the solution process, the *h*-adaptive method can be used to generate a better mesh at the end of the analysis with a repeated analysis being expected to improve the solution accuracy.

In the literature, it is common to use the *h*-adaptive method in this way for small deformations (e.g. Boroomand and Zienkiewicz, 1999; Rannacher and Suttmeier, 1999; Khoei et al., 2007). In the case of large deformations, where the mesh is continuously updated according to the current displacements, the *h*-adaptive method provides a natural strategy for controlling the discretisation error as the solution proceeds. The approach is thus well suited to handling problems associated with large deformations, such as mesh distortion, but reports of its use in the literature for this purpose are scarce. Another advantage is that, for the same level of accuracy, an *h*-adaptive solution is usually

substantially cheaper than a conventional solution that is based on a constant (perhaps substantially higher) number of elements.

The three main components of an *h*-adaptive finite element method are: error estimation, which controls the mesh refinement process; mesh generation, in which a new mesh is generated from scratch or by refining a previous old mesh; and remapping, which transfers the state parameters between two meshes.

The first papers on adaptive finite element methods appeared in the late seventies (e.g. Carey, 1976; Hyman, 1977; Babuska and Rheinboldt, 1978). Since then a vast number of publications have been devoted to this subject aiming to develop new algorithms and to improve the existing techniques of adaptivity components.

An important task in solving a problem by finite element method is to divide the main region into a number of small subregions known as elements. This process, mainly described as mesh generation, provides the input data for the analysis. To decrease the analyst's interaction with the mesh and therefore increasing the accuracy and efficiency of the adaptive method, development of an automatic mesh generation scheme is deemed necessary. Several automatic mesh generation algorithms which have been introduced in the last decades can be found in e.g. Ho-Lo (1988), George (1991) and Owen (1998). The importance of an efficient mesh generator is emphasized by using *h*-adaptive algorithms where based upon the result of an error estimator, the new element sizes are obtained from the previous element distributions and a mesh refinement needs to be undertaken.

Another essential procedure in an adaptive technique is assessing the error of the solution computed within a given mesh. The error measurement procedure attempts to control the spatial discretisation error in the finite element domain which, in turn, determines the distribution of the elements in future mesh discretisation. Two most common approaches for evaluating the error are: error indication and error estimation. Error indicators are usually based on the value of intuitive parameters (geometrical, mechanical, etc.) which can be easily computed to keep the processing cost low. The error indicators usually take advantage of some readily available quantities from finite element computation to evaluate the error. The main drawback of using error indicators is that they are problem dependent, i.e., the analyst needs to choose a proper indicator for the specific application. Moreover, error indicators only specify the regions where the mesh requires to be refined but the error is not quantified and it needs the user's judgment on the density of the mesh. Error estimators, on the other hand, approximately evaluate the error of a given norm. They are based on mathematical foundations and are usually more expensive to apply. However, because of their alibility to provide the quantity of the error, they have attracted more attention than the error indicators in the literature.

A vast literature review on error estimation and adaptive methods was presented by Babuska et al. (1986) and Brebbia and Aliabadi (1993). Ladevèze and Oden (1998) edited a book presenting the latest advances in adaptive techniques in engineering field. The adaptive finite element methods are also discussed in books by Zienkiewicz and Taylor (1989) and Szabo and Babuska (1991).

Babuska and Rheinboldt (1978) introduced an initial posterior error estimator by using the norms of negative Sobolev space corresponding to the given bilinear form. In their method, they estimated the error by evaluating the residuals of the approximate solution and obtained more accurate answers. In their method, they developed the mathematical basis of self-adaptive techniques. By applying a self-adaptive strategy, one can achieve to a desired accuracy in a finite element domain just by refining certain elements. Their research was later followed and improved by themselves and the others (e.g. Kelly et al., 1983; Bank and Weiser, 1985). Later around 1982 the computer graphics techniques had started to be used in mesh generation programs.

Shephard (1986) presented a self-adaptive procedure by combining Babuska's error estimation method with a geometric model and automatic mesh generation. Zienkiewicz and Zhu (1987) introduced recovery based error estimators which use the recovered solution instead of the exact solution to estimate the error. This technique (generally referred to as Zienkiewicz-Zhu or Z^2 error estimator), is based on obtaining recovered values of gradients by averaging or using the L_2 projection, to achieve a reasonable estimation of error. In 1992, the same authors corrected and improved their recovery technique and named it Superconvergent Patch Recovery (SPR) method (Zienkiewicz and Zhu, 1992a, 1992b, 1994). This method uses a least square smoothing technique to recover a more accurate value of the stresses at a node using the stresses at Gauss points in a small set of elements (a patch) around the node.

Later, researchers attempted to improve the recovery process by combining equilibrium

and boundary conditions, e.g. Wiberg and Abdulwahab (1993), Wiberg et al. (1994), Blacker and Belytschko (1994), Tabbara et al. (1994) and Lee et al. (1997). Babuska et al. (1994a, 1994b) successfully proved the robustness of Superconvergent patch recovery method over residual-type approaches by considering optimum robustness index in many performed tests. Boroomand and Zienkiewicz (1997) introduced a new Superconvergent method called Recovery by Equilibrium in Patches (REP) in which the stress field that satisfies the equilibrium in a weak form can replace the one of the finite element approximation. Therefore, in this method there is no need of considering superconvergent points. Paulino et al. (1997) introduced a new error estimation based on nodal sensitivities. Mahomed and Kekana (1998) suggested an error estimating method by using strain energy equalisation. Until then, the improvement in the error estimation methods was mainly focused on elastic problems. Boroomand and Zienkiewicz (1999) generalised their previous energy norm recovery procedure in estimating error for adaptivity in nonlinear problems of elasto-plasticity. Huerta and Diez (2000) introduced a residual type error estimation including pollution assessment for nonlinear finite element analysis. It is also possible to use an incremental form of error estimation based upon a global error measure in the constitutive equations (Gallimard et al. 1996). In recent years a new approach to a posteriori error estimation has been introduced which is known as Goal-oriented error estimation or dual method. This method is based on controlling the local quantities or other quantities of interest like a specific displacement or stress rather than controlling global quantities such as energy norm. The related mathematical analysis of this method is described by Rannacher and Suttmeier (1998). Also, some researchers have applied this

method to solve the different problems in engineering applications. For example, Wriggers et al. (2000) applied this method to problems including contact. Oden and Prudhomme (2001) presented a study of this method for two dimensional applications.

After estimating the error, the next step in an adaptive method is to optimise the mesh to achieve a better accuracy in solution. Therefore, a criterion needs to be defined for optimising the mesh. Various mesh optimality criteria have been presented in the literature. Among them, there is a simple strategy proposed by Zienkiewicz and Zhu (1987), (ZZ), which is based on an equal distribution of discretisation error between the elements in the current mesh**.** Onate and Bugeda (1993) proposed a different mesh optimality criterion (OB) based on the equal distribution of the density of error (ratio of the square error norm over every element and its measure). Later, Li and Bettess (1995, 1997) improved the ZZ strategy by relating the desired size of element to their current size (LB) based on equal distribution of error in each element in the new mesh. Diez and Huerta (1999) proved that using the LB criterion provides the cheapest mesh with the lowest number of elements and minimum number of degrees of freedom for a given accuracy.

Comparatively, the condition implied as the mesh optimality criteria in the strategy proposed by Onate and Bugeda (1993) leads to a very dense mesh where the number of elements can be even five times more than the LB and ZZ strategies. Diez and Huerta (1999) introduced an alternative refinement criterion which is a combination of the LB technique and OB strategy known as ULA. The major feature of ULA strategy is to associate the global relative error with a local prescribed accuracy.

After assessing the error, a new mesh is generated according to the refinement criterion. Then, two different approaches are available to continue the analysis. One is to restart the analysis with the new mesh from time zero. This avoids the cumbersome process of transferring variables from one mesh to another, but is only appropriate for small deformations. For large deformations, the new mesh represents the current deformed configuration and cannot be used as the initial undeformed configuration, thus making a restart of the analysis infeasible (e.g., in penetration problems such as those described by Sheng et al., 2009). An alternative strategy, which is known as remapping or convection, is to transfer the history-dependent variables and displacements from the old mesh to the new mesh. Different approaches for remapping are available in the literature such as global least square projection (Oden and Brauchli, 1971), element-based transfer which uses an extrapolation algorithm based on shape functions, and patch-based transfer or least-square approximation techniques (Boroomand and Zienkiewicz, 1999). By remapping state variables, the analysis continues with the new mesh for the next load increment. Thus, the total number of load increments is not increased, but with a cost of remapping the state variables between the old and new meshes.

Various *h*-adaptive finite element strategies can be devised by combining different forms of error estimators, mesh generators, and remapping techniques. For example, Hu and Randolph (1998) proposed an *h*-adaptive finite element procedure for geotechnical problems in which the error is estimated using the Superconvergent Patch Recovery (SPR) technique to recover the strains at Gauss points. The mesh refinement procedure is based on a minimum element size criterion. To transfer the stresses and soil properties from the old

mesh to the new mesh two interpolation strategies, a modified form of the unique element method and the stress-SPR method, were applied. This method has been used to analyse the bearing capacity of strip and circular foundations on non-homogeneous soil where the strength increases linearly with depth. The strategy proposed by Hu and Randolph (1998) is based upon small strain analysis where the effect of rigid body rotations is neglected.

As mentioned above, the *h*-adaptive method has been used mostly for small deformation problems with only a few studies focusing on large deformations mainly on other areas rather than geomechanics (Peric et al., 1999; Hu and Wriggers, 2002). The key aim of previous work was to improve the accuracy of the solution, with little attention being devoted to important issues such as mesh distortion (Khoei and Lewis, 2002).

2.3. FINITE ELEMENT METHOD

The finite element method is a powerful tool for analysis of many problems in several engineering disciplines. Although it is difficult to find the exact orientation date of this method, by tracing it back, it seems to have been first introduced to the engineering in the mid 1950s by Argyris and Kelsey (1954) and Turner et al. (1956). The term “finite element” was, however, applied for the method by Clough (1960) for the first time. This method and its aspects have attracted the interest of many researchers over the past decades and a vast range of publications is available in the literature.

To use the finite element method for solving physical problems, first a mathematical model of the problem needs to be generated. This model can be governed by differential equations

assumptions on geometry, material law, loading, and boundary conditions. Then the finite element analysis solves the mathematical model. It is clear that the finite element solution will be based on the selected mathematical model with all its specific assumptions. Therefore, the choice of an appropriate mathematical model is one of the most important steps in engineering analysis.

The finite element method has also been known as a robust tool for solving nonlinear problems in many engineering applications such as solid mechanics and fluid dynamics. In geotechnical problems, nonlinearity may occur for several reasons; material nonlinearity, geometrical nonlinearity, changes in boundary conditions, time dependency. Material nonlinearity happens when the stress-strain relationship is not linear. In geomechanics, there are several well-established material models for predicting nonlinear behaviour of soil under different situations. Geometrical nonlinearity is observed when deformations, including displacements and rotations, are so large that the effect of geometry change may not be neglected during the analysis. In other words, the volume of body changes due to large deformations and it cannot be considered as a constant. In some problems, the boundary conditions are not constant during the analysis resulting in a nonlinear behaviour. Such problems usually involve contact mechanics. Some time dependant problems may also represent a nonlinear behaviour. For instance, this behaviour may be observed when the external forces are changing with time in a dynamic analysis. Consolidation of soils is another well-known time dependent problem in geomechanics.

2.4. ADAPTIVE FINITE ELEMENT METHODS

The finite element solution technique is a numerical procedure which usually starts with an initial mesh and aims to generate a solution with a desirable accuracy in a specific parameter. However, we do not have an initial sufficient knowledge of the model to meet the accuracy criteria in a single try. A common finite element strategy to solve problems involved with large deformation is the Updated-Lagrangian (UL). In the UL method the material particles are connected to a computational grid. The spatial position of this computational grid is updated according to incremental displacements at the end of each time step. Potentially, mesh distortion and entanglement of elements can occur in the material mesh due to continuous change in geometry, leading to a negative Jacobian of finite elements or a significant loss of accuracy in the solution. Mesh distortion and overlapping of elements in zones with high stress and strain concentration is almost inevitable if the finite element mesh is fine enough to achieve acceptable results. This phenomenon can be observed while solving a wide range of geotechnical problems such as bearing capacity of relatively soft soils under a footing, penetration of objects into soil layers, lateral movements of pipelines on seabeds, pull-out capacity of anchors embedded in soft soils, and slope stability analysis.

Consequently, adaptive finite element methods try to achieve a solution with a specific accuracy in a determined parameter by refining, coarsening or relocating a mesh. The analysis by these methods usually adapts an initial mesh which requires no specific consideration as a priori. Then an incremental analysis begins to provide the error in a

prescribed parameter. If the error does not satisfy the prescribed accuracy, the mesh will be adjusted through adaptive methods aiming to achieve the desirable accuracy with least effort. Incremental solving method for nonlinear equations which is the nature of finite element method will help the adaptive mesh generation to refine the mesh based on the partial results of the previous increment. Therefore, adaptive finite element techniques can eliminate the mesh distortion by, if necessary, generating an undistorted new mesh at the end of the UL analysis.

Although the development of adaptive finite element methods started in the second part of 1970s and many researchers have devoted their study to this subject during last three decades ,e.g., Babuska et al. (1983,1986,1995), Flaherty et al. (1989), Duncan(1998) and Bern et al. (1999), there is not enough information to suggest which strategy is most efficient. The adaptive finite element methods are usually classified as:

- *p*-adaptive FE method
- *r*-adaptive FE method
- *h*-adaptive FE method
- *hp*-adaptive FE method

These methods are briefly reviewed in the following.

2.4.1. *p*-adaptive FE method

In a *p*-adaptive finite element method, mesh is refined by locally increasing the degree of interpolating polynomial functions, p, (Figure 2.1). During the analysis by this method,

number of nodes and the type of generated elements may change to obtain a more accurate solution. This strategy is acceptably powerful when used with hierarchical basis, since portions of the stiffness and mass matrices and load vector will not change by increasing the polynomial degree of the basis. The use of hierarchical *p*-adaptive method was first introduced by Zienkiewicz et al. (1970) and was successfully applied by Peano et al. (1979) and Szabo (1979, 1986). Schwab (1999) has explained the theory and application of this method in solid and fluid mechanics in details. According to Partheymuller et al. (1995) while this method is less common than *h*-adaptivity and *r*-adaptivity, it is widely considered to be more accurate and efficient for smooth elemental integrands.

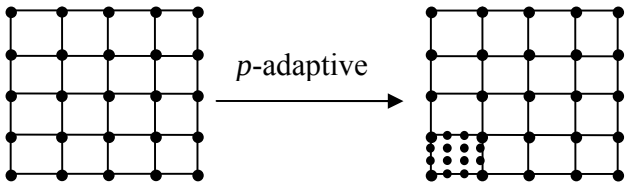

Figure 2.1. *p*-adaptive finite element method

2.4.2. *r*-adaptive FE method

r-adaptive finite element method tries to improve the solution to a problem by relocating the nodes in the finite element domain (Figure 2.2). In this method, the topology of the problem, i.e. the number of nodes and the elements connectivity, remains constant. For the refinement the nodes are moved to desired locations so that the mesh would be finer in some areas and coarser in others. It might seem that *r*-adaptive alone is not sufficient to

find a solution with a specific accuracy as it relies completely on the initial mesh. Therefore, if the analysis is started with a very coarse mesh, it would be impossible to achieve a high level of precision at any time. To achieve a more precise solution one needs to start the analysis with a fine mesh which is normally increasing the computation cost.

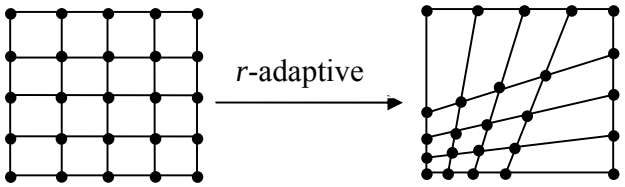

Figure 2.2. *r*-adaptive finite element method

A classic example of this approach is the so-called Arbitrary Lagrangian-Eulerian method. Nazem et al. (2006) demonstrated the ability of this method in solving general large deformation problems of geomechanics. Khoei et al. (2008) presented an extended finite element formulation based the ALE technique for large deformation analysis of solid mechanics problems. Although powerful, the *r*-adaptive method does not directly address problems like localised deformation or stress concentration.

2.4.3. *h*-adaptive FE method

h-adaptive finite element method is based on generating a new mesh, using the same type of element, by dividing the area of basic elements where the interpolation must be improved to achieve more accuracy. In this method, the connectivity of the elements and

the total number of degree of freedom may change but the degree of interpolation

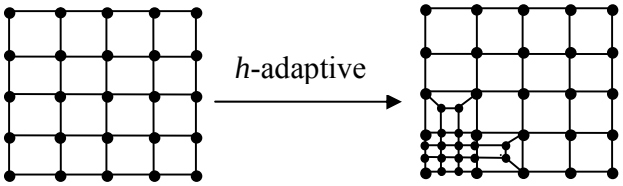

Figure 2.3. *h*-adaptive finite element method

polynomial functions remains the same. This approach is particularly effective in improving the solution accuracy for problems involving large deformation, localised deformation, moving boundaries, post-failure response, steep gradients and sharp fronts. As finite element analysis becomes increasingly common in geotechnical engineering, with many practical problems involving the complex features listed above, there is a pressing need for reliable methods that control the discretisation error to within a desired limit.

Since *h*-adaptive finite element method is the main subject of this Thesis, the method will be explained in details in Chapter 3.

2.4.4. *hp*-adaptive FE method

An alternative way to apply adaptivity is to combine two different adaptive methods simultaneously. The most well-known combination is *hp*-adaptivity. The *hp* version combines both *h*-adaptive and *p*-adaptive strategies to exploit the strength of each method while avoiding their individual weaknesses. The purpose of developing this strategy is to minimise the computational cost by requiring a minimum number of parameter according

to Oden et al. (1989) while still obtaining accurate approximate solution. Each new adaptive mesh is created by estimating the error on the previous mesh and executing the *h*-adaptive and *p*-adaptive refinement procedures on the existing mesh according to the result of adaptive method. With this combination, high rates of convergence can be achieved when singularities are present. A review and application of this method was presented by Verfurth (1996) and Schwab (1999).

2.5. GOVERNING EQUATIONS

In this section, the general formulation of a nonlinear finite element analysis is prescribed. This formulation considers material nonlinearity as well as geometrical nonlinearity. A nonlinear analysis by finite element method is usually performed by increments (or time steps). At each increment, a portion of the loads, including external loads and body forces, is applied on the body and the correspondent incremental displacements are obtained by solving the nonlinear global equations. The incremental strains can be computed from the incremental displacements and these strains are then used to determine the stresses within the continuum. This procedure usually requires a stress-integration scheme provided that the relation between the stresses and strains is nonlinear. The stresses are then used to find the internal forces which must be, to a tolerance, equal to external forces so that the equilibrium is satisfied. In the following, the fundamental equations in a nonlinear finite element analysis are briefly discussed.

Note that the governing equations presented in this chapter are for static analysis.

Later, the *h*-adaptive method also applied to solve the problem involving dynamic analysis and contact mechanics. The related governing equations of those problems are presented in detail in Chapter 5.

2.5.1. Equilibrium equation

Assume that the analysis starts at time 0 and all state variables which satisfy equilibrium at time t are known. If further loading is applied at time $t+\Delta t$ the domain of the problem will deform, and equilibrium will need to be checked and satisfied. In theory, equilibrium will be achieved if the following equation satisfied

$$\int_{V^{t+\Delta t}} \sigma_{ij}^{t+\Delta t} \cdot \delta\varepsilon_{ij} \cdot dV^{t+\Delta t} - \int_{V^{t+\Delta t}} b_i^{t+\Delta t} \cdot \delta u_i \cdot dV^{t+\Delta t} - \int_{A^{t+\Delta t}} T_i^{t+\Delta t} \cdot \delta u_i \cdot dA^{t+\Delta t} = 0 \qquad (2.1)$$

where δu denotes a displacement field that satisfies the displacement boundary conditions, σ_{ij} is the Cauchy stress tensor, $\delta\varepsilon_{ij}$ represents the variation of the linear strain tensor consistent with the virtual displacements δu_i, V is volume of the body, b_i is the applied forces per unit volume, T_i are the components of the surface traction per unit area and A is the surface area. For the adaptive finite element methods developed in this study, including the *h*-adaptive as well as the combined *rh*-adaptive technique, an Updated-Lagrangian (UL) framework has been adopted. In the UL method, all variables are referred to the last equilibrium configuration. Therefore, to solve Equation (2.1), all quantities must be transferred to the configuration at time t. Moreover, the Cauchy stress tensor may change significantly due to possible rigid body motion occurring in a large deformation analysis.

To avoid this, objective stress rate is introduced into Equation (2.1). In this study we use the Jaumann stress rate, $\sigma^{\nabla J}$, one of the most commonly used stress rates , which is defined as follows

$$\sigma_{ij}^{\nabla J} = \frac{d\sigma_{ij}}{dt} - \sigma_{ik} \cdot w_{jk} - w_{ik} \cdot \sigma_{kj} \tag{2.2}$$

where *w* is the spin tensor, and is given by

$$w_{ij} = \frac{1}{2}\left(\frac{\partial \dot{u}_i}{\partial x_j} - \frac{\partial \dot{u}_j}{\partial x_i} \right) \tag{2.3}$$

and *u* represents the displacement vector.

Linearization of Equation (2.1) in an UL frame-work and employing the Jaumann stress rate in Equation (2.2) provide

$$\begin{aligned} &\int_{V^t} \left(C_{ijkl}\, d\varepsilon_{kl} \right) \delta\left(d\varepsilon_{ij} \right) dV^t + \int_{V^t} \left(\sigma_{ij}^t \right) \delta\left(d\eta_{ij} \right) dV^t + \int_{V^t} \left(\sigma_{ik}^t d\Omega_{jk} + \sigma_{jk}^t d\Omega_{ik} \right) \delta\left(d\varepsilon_{ij} \right) dV^t \\ &= \int_{V^{t+\Delta t}} b_i^{t+\Delta t} \cdot \delta u_i \cdot dV^{t+\Delta t} + \int_{A^{t+\Delta t}} T_i^{t+\Delta t} \cdot \delta u_i \cdot dA^{t+\Delta t} - \int_{V^t} \left(\sigma_{ij}^t \right) \delta\left(d\varepsilon_{ij} \right) dV^t \end{aligned} \tag{2.4}$$

where

$$\eta_{ij} = \frac{1}{2} \frac{\partial u_k}{\partial x_i} \frac{\partial u_k}{\partial x_j} \tag{2.5}$$

Linearisation of Equation (2.4) by the finite element method provides the matrix equation

governing the equilibrium of the body. In its rate form, the equilibrium equation is expressed by

$$\dot{\mathbf{F}}^{int} = \mathbf{K}^{ep}\dot{\mathbf{U}} = \dot{\mathbf{F}}^{ext} \tag{2.6}$$

where $\mathbf{K}^{ep}$ represents the stiffness matrix, and $\mathbf{F}^{ext}$ and $\mathbf{F}^{int}$ represent the external and the internal force vectors, respectively. The stiffness matrix and the internal force vector are obtained by

$$\mathbf{K}^{ep} = \int_{V^t} \mathbf{B}_l^T \mathbf{C}^{ep} \mathbf{B}_l \, dV^t + \int_{V^t} \mathbf{B}_{nl}^T \boldsymbol{\sigma}^t \mathbf{B}_{nl} dV^t + \int_{V^t} \mathbf{B}_l^T \bar{\boldsymbol{\sigma}}^t \bar{\mathbf{B}}_l \, dV^t \tag{2.7}$$

$$\mathbf{F}^{int} = \int_{V^t} \mathbf{B}_l^T \boldsymbol{\sigma} dV^t \tag{2.8}$$

where, for two dimensional plane strain conditions, the corresponding **B** matrices at the i^{th} node of an arbitrary element, and the stress matrices are defined as

$$\mathbf{B}_l = \begin{bmatrix} \dfrac{\partial N_i}{\partial x_1} & 0 & \dfrac{\partial N_i}{\partial x_2} \\ 0 & \dfrac{\partial N_i}{\partial x_2} & \dfrac{\partial N_i}{\partial x_1} \end{bmatrix}^T \tag{2.9}$$

$$\mathbf{B}_{nl} = \begin{bmatrix} \dfrac{\partial N_i}{\partial x_1} & \dfrac{\partial N_i}{\partial x_2} & 0 & 0 \\ 0 & 0 & \dfrac{\partial N_i}{\partial x_1} & \dfrac{\partial N_i}{\partial x_2} \end{bmatrix}^T \tag{2.10}$$

$$\overline{\mathbf{B}}_I = \begin{bmatrix} 0 & 0 & \frac{1}{2}\frac{\partial N_i}{\partial x_2} \\ 0 & 0 & -\frac{1}{2}\frac{\partial N_i}{\partial x_1} \end{bmatrix}^T \tag{2.11}$$

$$\boldsymbol{\sigma}^t = \begin{bmatrix} \sigma_{11}^t & \sigma_{12}^t & 0 & 0 \\ \sigma_{21}^t & \sigma_{22}^{\prime t} & 0 & 0 \\ 0 & 0 & \sigma_{11}^t & \sigma_{12}^t \\ 0 & 0 & \sigma_{21}^t & \sigma_{22}^t \end{bmatrix} \tag{2.12}$$

$$\overline{\boldsymbol{\sigma}}^t = \begin{bmatrix} 2\sigma_{11}^t & 0 & 2\sigma_{12}^t \\ 0 & 2\sigma_{22}^t & -2\sigma_{12}^t \\ \sigma_{12}^t & \sigma_{12}^t & \sigma_{22}^t - \sigma_{11}^t \end{bmatrix} \tag{2.13}$$

$$\boldsymbol{\sigma} = \begin{Bmatrix} \sigma_{11}^t & \sigma_{22}^t & \sigma_{12}^t \end{Bmatrix}^T \tag{2.14}$$

Note that *N* denotes the nodal displacement shape functions.

2.5.2. Constitutive equations

Based on the theory of plasticity, the constitutive equations governing the elastoplastic behaviour of the material are usually derived by the following assumptions:

- The incremental strain tensor, $\dot{\varepsilon}_{ij}$, is decomposed into an elastic part, $\dot{\varepsilon}_{ij}^e$, and a plastic part, $\dot{\varepsilon}_{ij}^p$.

$$\dot{\varepsilon}_{ij} = \dot{\varepsilon}_{ij}^e + \dot{\varepsilon}_{ij}^p \tag{2.15}$$

- A yield function of the form $f\left(\sigma_{ij},\kappa_i\right)=0$ describes the elastic domain, and κ represents a set of hardening parameters.
- As yielding occurs, the stress state must not lie outside the yield surface as the plastic deformation occurs , i.e.,

$$\dot{f}=\frac{\partial f}{\partial \sigma_{ij}^t}\cdot\dot{\sigma}_{ij}^t+\frac{\partial f}{\partial \kappa_i^t}\cdot\dot{\kappa}_i^t=0 \tag{2.16}$$

- The direction of the plastic strain is normal to a surface called the plastic potential *g*. This rule is known as the associated flow for $f=g$ and non-associated flow for $f\neq g$, and is expressed by

$$\dot{\varepsilon}_{ij}^p=\dot{\lambda}\cdot\frac{\partial g}{\partial \sigma_{ij}} \tag{2.17}$$

where $\dot{\lambda}$ is a plastic multiplier.

The stress rate can be obtained by

$$\dot{\sigma}_{ij}=C_{ijkl}^e\cdot\dot{\varepsilon}_{kl}^e \tag{2.18}$$

where C^e represents the elastic constitutive matrix. Substituting (2.15) and (2.17) into (2.18) gives

$$\dot{\sigma}_{ij}=C_{ijkl}^e\cdot\dot{\varepsilon}_{kl}-\dot{\lambda}\cdot C_{ijkl}^e\cdot\frac{\partial g}{\partial \sigma_{kl}} \tag{2.19}$$

To find the plastic multiplier, we may assume a common hardening law

$$\dot{\kappa}_i = B_i\left(\sigma,\kappa\right)\cdot\dot{\lambda} \tag{2.20}$$

where B is a variable derived from the hardening laws and is typically a function of the current stresses and hardening parameters. Inserting (2.19) and (2.20) into (2.16), $\dot{\lambda}$ can be found as follows

$$\dot{\lambda} = \frac{\dfrac{\partial f}{\partial \sigma_{ij}}\cdot C^e_{ijkl}\cdot\dot{\varepsilon}_{kl}}{\dfrac{\partial f}{\partial \sigma_{ij}}\cdot C^e_{ijkl}\cdot\dfrac{\partial g}{\partial \sigma_{kl}} - \dfrac{\partial f}{\partial \kappa_m}\cdot B_m\left(\sigma,\kappa\right)} = D_{kl}\cdot\dot{\varepsilon}_{kl} \tag{2.21}$$

The elastoplastic constitutive relation is obtained by substituting (2.21) into (2.19) according to

$$\dot{\sigma}_{ij} = C^{ep}_{ijkl}\cdot\dot{\varepsilon}_{kl} \tag{2.22}$$

where

$$C^{ep}_{ijkl} = C^e_{ijkl} - \frac{C^e_{ijmn}\cdot\dfrac{\partial f}{\partial \sigma_{mn}}\cdot C^e_{klpq}\cdot\dfrac{\partial g}{\partial \sigma_{pq}}}{\dfrac{\partial f}{\partial \sigma_{pq}}\cdot C^e_{pqrs}\cdot\dfrac{\partial f}{\partial \sigma_{rs}} - \dfrac{\partial f}{\partial \kappa_m}\cdot B_m\left(\sigma,\kappa\right)} \tag{2.23}$$

Equations (2.22) and (2.20) define a system of ordinary differential equations which must be integrated at each integration point to find the stresses. For a given strain increment, this

integration takes the following form

$$\sigma_{ij}^{t+\Delta t} = \sigma_{ij}^{t} + \int_{0}^{\Delta\varepsilon_{kl}} C_{ijkl}^{ep}(\sigma,\kappa)\cdot d\varepsilon_{kl}$$
$$\kappa_{i}^{t+\Delta t} = \kappa_{i}^{t} + \int_{0}^{\Delta\varepsilon_{kl}} B_{i}(\sigma,\kappa)\cdot d\lambda = \kappa_{i}^{t} + \int_{0}^{\Delta\varepsilon_{kl}} B_{i}(\sigma,\kappa)\cdot D_{kl}(\sigma,\kappa)\cdot d\varepsilon_{kl} \tag{2.24}$$

Considering large deformations, the constitutive equations must be objective, i.e., a rigid body rotation should change neither the stress components nor the strain in the material. This condition, termed as the principle of stress objectivity, may be satisfied by adopting the so-called rate-type formulation in the finite strain plasticity, and, therefore, replacing the stress rate in Equation (2.22) by an objective stress rate. As mentioned before the Jaumann stress rate defined by Equation (2.2) is adopted in this study. Thus, Equation (2.22) may be rewritten as following

$$\dot{\sigma}_{ij}^{\nabla J} = C_{ijkl}^{ep}\cdot\dot{\varepsilon}_{kl} \tag{2.25}$$

Introducing (2.2) and (2.25) into (2.24) the following integration equations are obtained

$$\sigma_{ij}^{t+\Delta t} = \sigma_{ij}^{t} + \int_{0}^{\Delta\varepsilon_{ij}} d\sigma_{ij} = \sigma_{ij}^{t} + \int_{0}^{\Delta\omega_{kl}} \left(\sigma_{ik}\cdot d\omega_{jk} + \sigma_{jk}\cdot d\omega_{ik}\right) + \int_{0}^{\Delta\varepsilon_{kl}} C_{ijkl}(\sigma,\kappa)\cdot d\varepsilon_{kl}$$
$$\kappa_{i}^{t+\Delta t} = \kappa_{i}^{t} + \int_{0}^{\Delta\varepsilon_{kl}} B_{i}(\sigma,\kappa)\cdot D_{kl}(\sigma,\kappa)\cdot d\varepsilon_{kl} \tag{2.26}$$

which describe the stress-strain relations, and need to be solved at every integration point during each equilibrium iteration. Note that ω_{ij} in (2.26) is defined by

$$\omega_{ij} = \frac{1}{2}\left(\frac{\partial u_i}{\partial x_j} - \frac{\partial u_j}{\partial x_i} \right) \tag{2.27}$$

CHAPTER 3

h-ADAPTIVITY AND ITS ASPECTS

3.1. INTRODUCTION

In this chapter the *h*-adaptive finite element method is discussed in detail. In an *h*-adaptive finite element procedure, the analysis starts with a relatively coarse mesh. During a typical time-step, necessary iterations are performed until equilibrium is achieved. Then an automatic procedure, based upon error estimators or error indicators, usually determines the regions where the mesh requires refinement for the future increments. After generating a new mesh, all state variables such as stresses and hardening parameters must be transformed from the old mesh to the new mesh. It is clear that three main components of an *h*-adaptive FE procedure include error estimation, mesh generation and mapping of state variables. This chapter describes these three important aspects of an *h*-adaptive FE method.

3.2. *h*-ADAPTIVE FINITE ELEMENT METHOD

h-adaptivity is probably the most common adaptive technique used in modern finite element applications. However, its implementation is quite a challenge, since in every stage of refinement a new mesh which can be totally different from the old mesh is generated.

This approach is based on subdividing the integration region into successively smaller sub regions. In this way a new mesh is produced using the same type of elements used in the old mesh by changing the density of the elements to satisfy the requirements of the solution. Therefore, the topology of the main domain is changed to obtain a desired accuracy. In fact, *h*-adaptive procedures generate a sequence of approximate meshes which are aimed at converging to a proper mesh gradually or eliminating mesh distortion in the

finite element domain. In order to verify the accuracy in each stage, an error assessment is used to provide a clue for the later mesh refinement. During error assessment, the error in each element is calculated and is compared with a prescribed limit. If the error is above the limit, the element must be divided into some new smaller elements in the next mesh. The new area of element is calculated using an optimality criterion. The computational cost of an *h*-adaptive finite element analysis is normally higher than an *r*-adaptive method because at each step, if required, a new mesh must be generated based upon an error measure and then all the state parameters need to be recalculated by transferring data from the old mesh to the new mesh. In this method, the projections of the state parameters can be quite a challenge as the topology of the new mesh may significantly differ from the topology of the old mesh. *h*-adaptive finite element method, on the other hand, does not depend on an initial mesh to find a solution and the accuracy of the solution improves as the analysis proceeds. In other words, the number of degrees of freedom can change arbitrarily to achieve a prescribed accuracy. This method is generally more accurate than *r*-adaptive and *p*-adaptive techniques but the implementation of the method is rather more complicated and challenging.

As mentioned before, three main components of an *h*-adaptive finite element analysis include error estimation, mesh generation, and remapping of state variables. These components will be explained in the followings.

3.3. ERROR ESTIMATION

In an *h*-adaptive finite element analysis, since an exact solution is usually not available, a posteriori error estimation is always a necessary requirement. The error estimators measure the quality of the approximate solution and serve as a guide through the mesh refinement procedure which is aimed at decreasing the discretization error. Two major types of error estimators are residual error estimators and recovery based error estimators. The residual type of error estimator was first introduced by Babuska and Rheinboldt (1978). It uses the residual of the finite element solution implicitly or explicitly to estimate the error. In the implicit type, an approximation of the error is obtained by solving local boundary value problems which are involved with the residuals of the finite element solution as data. The accuracy of this type of error estimators depends on the way boundary conditions are set and the local problem is solved. The explicit type, on the other hand, directly uses the residuals of the mesh solution to estimate the error. Babuska et al. (1994a) showed that the accuracy and robustness of this type of error estimators depends on regularity of the problem and the mesh used for the finite element analysis. Recovery based error estimators were first introduced by Zienkiewicz and Zhu (1987). In this method a more accurate or super convergent solution which is computed from the finite element approximation through recovery techniques replaces the exact solution to compute the error. In the present work the recovery based error estimation is chosen over the residual type for its following advantages:

- The concept is simple as the error is defined as the difference between the recovered solution u^* and the finite element approximation $\hat{u}$ and can be shown as

$$\left\| e^* \right\| = \left\| u^* - \hat{u} \right\| \tag{3.1}$$

where the exact solution u in any norm can be replaced by the recovered one.

- As some parts of recovered solution are automatically computed during the finite element computation process, little additional computations are involved. Therefore the method is computationally more efficient.
- If the recovery process is superconvergent, as Zienkiewicz and Zhu (1992a) have shown, the estimator will always be asymptotically exact.

By solving several numerical benchmark problems as well as a 'patch test', Babuska et al. (1994a, 1994b) showed that the recovery type of error estimators is more robust and more accurate than the residual based methods in all cases.

As been noted first by Rank and Zienkiewicz (1987) and later by Ainsworth and Oden (1993), for every residual based estimator there is a corresponding recovery- based process with the exact same performance. However, the reverse is not true. Therefore, not only every residual based error estimator can be replaced by its identical recovery based one but also the recovery method offers even more possibilities.

In the following, recovery based error estimation is explained in more details.

3.3.1. Recovery based error estimation

In general, error is known as the difference between the exact value of a specific parameter in a solution and its value which is obtained through the finite element approximation. So the error can generally be shown as

$$e = s - \hat{s} \tag{3.2}$$

where s is the exact solution and $\hat{s}$ is the finite element approximation. Some of the parameters considered in the error assessment are displacement, strain and stress.

The direct use of the local error calculated from Equation (3.2) is not convenient as the exact solution is not available. Therefore, the mathematical norms, such as energy or L_2 norms are usually used to measure the discretization error. The L_2 norm can be associated with errors of any quantity. For the stress in an element, *i*, the L_2 norm of the error is defined in form

$$\|e\|_{L2} = \left[\int_{\Omega} (\sigma - \hat{\sigma})^T (\sigma - \hat{\sigma}) d\Omega \right]^{\frac{1}{2}} \tag{3.3}$$

where σ is the exact stress, $\hat{\sigma}$ denotes the finite element approximation and Ω is the defined problem region.

On the other hand, the error in each increment can be quantified using energy norm expressed as

$$\|e\| = \left[\int_{\Omega} \left| \left(\sigma - \hat{\sigma}\right)^T \left(\Delta\varepsilon - \Delta\hat{\varepsilon}\right) \right| d\Omega \right]^{\frac{1}{2}} \tag{3.4}$$

in which, $\Delta\varepsilon$ and $\Delta\hat{\varepsilon}$ are representing the exact and the finite element incremental strain fields. In the specific case of elasticity the Equation (3.4) can be written as

$$\|e\| = \left[\int_{\Omega} \left(\sigma - \hat{\sigma}\right)^T \left(\sigma - \hat{\sigma}\right) D^{-1} d\Omega \right]^{\frac{1}{2}} \tag{3.5}$$

Clearly the only difference between the energy norm formulation for elasticity and the L_2 norm is the weighting *D*.

Again, as σ is generally unknown it is replaced with σ^* which is the recovered stress obtained from a recovery procedure such as local nodal-point averaging (ZZ) by Zienkiewicz and Zhu (1987) , Superconvergent Patch Recovery (SPR) by Zienkiewicz and Zhu (1992a, 1992b) or Recovery by Equilibrium of Patches (REP) by Boroomand and Zienkiewicz (1997). So for example the estimated relative error in elastic mode can be obtained from

$$\|e\|_{es} = \left[\int_{\Omega} \left(\sigma^* - \hat{\sigma}\right)^T \left(\sigma^* - \hat{\sigma}\right) D^{-1} d\Omega \right]^{\frac{1}{2}} \tag{3.6}$$

For each specific element *i*, Equation (3.6) can be re-written as

$$\left\|e\right\|_{es}^{i}=\left[\int_{\Omega}\left(\sigma^{*}-\hat{\sigma}\right)^{T}\left(\sigma^{*}-\hat{\sigma}\right)D^{-1}\left|J\right|d\Omega_{i}\right]^{\frac{1}{2}} \tag{3.7}$$

in which $i\in\Omega_i$ when $\bigcup_{i=1}^{n}\Omega_i=\Omega$. Also, $\left|J\right|$ is the determinant of the Jacobean transformation matrix.

Clearly, no matter how we calculate the error in each element (using energy norm or L_2 norms) the relationship between the error on whole domain and the element contributions is shown as

$$\left\|e\right\|=\left[\sum_{i=1}^{n}\left\|e\right\|_{i}^{2}\right]^{\frac{1}{2}} \tag{3.8}$$

where *i* represent an element contribution and *n* is the total number of elements.

The error obtained this way is then used to refine the area of the elements in current mesh. Therefore, a new finer mesh is generated as the result. In *h*-adaptive method, this process is repeated and it generates meshes which are expected to converge to a proper mesh. In practical computations, the refinement must no longer take place when an acceptability criterion is satisfied. The acceptability criterion sets a threshold of the prescribed computational accuracy, so when the criterion is satisfied the solution has achieved enough accuracy. In general, the acceptability criterion can be stated as

$$\mu_{es}\leq\mu_{prs} \tag{3.9}$$

where μ_{prs} is the prescribed accuracy and μ_{es} is defined by

$$\mu_{es} = \frac{\|e\|_{es}}{\left(\|\eta_h\|^2 + \|e\|_{es}^2\right)^{1/2}} \tag{3.10}$$

in which $\|\eta\|_h$ represents the energy norm obtained from finite element solution. In an optimal mesh a high convergence rate can be achieved by equally distribution of the error among elements. Therefore for each element *i*, the criterion is given by

$$\|e\|_{es}^i < \mu_{prs}\left(\frac{\|\eta_h\|^2 + \|e\|_{es}^2}{n}\right)^{\frac{1}{2}} = \overline{e}_m \tag{3.11}$$

So considering the ratio

$$\theta_i = \frac{\|e\|_{es}^i}{\overline{e}_m} \tag{3.12}$$

it is obvious that the refinement must be stopped if

$$\theta_i \le 1.0 \tag{3.13}$$

Otherwise, the new size of the element for the refinement process can be calculated from

$$A_{new}^i = \frac{A_{old}^i}{\sqrt[p]{\theta_i}} \tag{3.14}$$

where A^i_{old} represents the current element size, A^i_{new} is the prescribed size of the element in the next mesh and *p* is the polynomial order of the approximation.

3.4. MESH GENERATION

Mesh generation is the procedure of dividing the problem domain into some elements which are used as the input of finite element programs for analysis. Modelling the geometry is an essential part of the analysis as the mesh can tremendously influence the accuracy and efficiency of the solution. It is also a time-consuming task. The mesh generators can be categorized in various fashions based on their aspects. They can be classified based upon the dimension and the shapes of the generated elements as:

- 2-dimensional triangles
- 2-dimensional rectangles
- 3-dimensional tetrahedral
- 3-dimensional bricks

On the other hand, from the connectivity point of view, two main categories can be distinguished as follows:

- Structured
- Unstructured

Different methods of two or three dimensional structured or unstructured mesh generation have been presented in the reviews and surveys which are available in references by Ho-Le

(1988) and El-Hamalawi (1997). The latest of above classification is more noticeable and will be explained further in the following sections.

3.4.1. Structured mesh generation

A structured mesh generator produces elements with regular connectivity that can be expressed as a two or a three dimensional array. In this approach nodal placement are computed directly from some given functions by using some simple algorithms which are referred as algebraic algorithms like in Laplacian mesh generation or by manually decomposing the problem domain into simple patches. The patches are necessarily non-intersecting and their union results in the parent domain (isoparametric and transfinite methods). This type of mesh generators are computationally easy to handle as only the spatial coordinates of the points needs to be stored. However, according to Ho-Le (1988) the density of the mesh is not easily controllable and the shape of mesh can be disturbed if the patch itself has a disturbed shape or has a large aspect ratio. Three most known structured mesh generation methods include Laplacian mesh generation, isoparametric mapping by Zienkiewicz and Philips (1971), and transfinite mapping method. Due to their limitations, the structured mesh generation methods are not considered in this study.

3.4.2. Unstructured mesh generation

Unstructured mesh generators are generally boundary based and typically require some form of boundary discretisation to be specified. Then, in every step of element generation, the geometry of the unmeshed region will be assessed and the boundary definition is

preserved. Unstructured meshes are often characterized by irregular connectivity, and are efficient in the sense that they permit elements to be highly concentrated in zones where they are needed. Unstructured mesh generators have now superseded structured ones, noticeably in the engineering applications, due to their flexibility and robustness specially for meshing complicated and irregular regions. However, the need of keeping the track of connectivity as well as coordinates of elements makes these methods computationally expensive. Two most known unstructured mesh generation methods are advancing front method and Delaunay method which will be described in the following.

a) Advanced front method

Advanced front method was introduced by George (1971) for generating unstructured meshes. Later, Lo (1985) presented a new mesh generation algorithm where the initial advancing front boundary of the region is defined by a set of lines known as segments and all nodes are generated within the boundary of the region. Then each triangular element is formed by connecting the end nodes of a segment to an interior node assuming that it does not intersect the advancing front. Peraire et al. (1987) presented a new version of advancing front method for steady state solution of Euler equations in two dimensions. His work made the basis of all other researches in this field which are more concerned with the methods of generating the elements and the nodes simultaneously. In this method, nodes are generated along the boundary of the region, which establishes a front. Then, based on the element densities at different positions, the internal nodes are produced to link sets of double nodes on the front. At this stage a layer of elements is created which does not necessarily have

the same shape as the front. Afterward, the front end is replaced with the new element edges and the process is continued by generating the new interior nodes until the whole region has been meshed, as shown in Figure 3.1.

There has been a great progress in the mesh generation schemes which use the advancing front method in the last few years. These schemes are mainly concerned with procedures for controlling the direction of mesh stretching and the element size. More recent modification and development in this method can be found in Lo and Lee (1994), Lau and Lo (1996) and Zienkiewicz and Wu (1994). The advancing front method usually generates nicely graded meshes with high quality triangles. Also by considering the domain boundary as the initial front, the consistency of the boundary is preserved. However, checking the intersection of edges and overlapping of elements can be really time-consuming and in complicated regions identifying and selecting points based on a selected front and then validation of new elements can be a major problem.

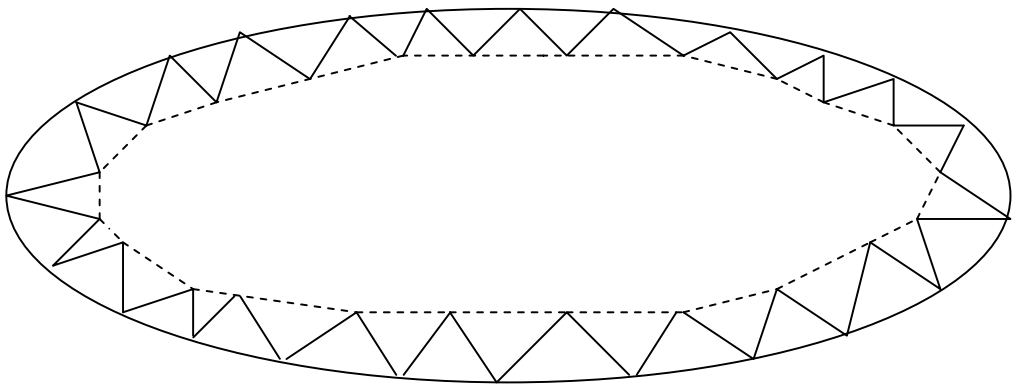

Figure 3.1. Advancing front with one layer of triangles

b) Delaunay method

Delaunay method is probably the most popular and the most time-efficient method available for generating triangular unstructured meshes. The main characteristic feature of this method is that the circumcircle (or circumsphere in 3D) of every triangle (or tetrahedral) does not contain any other nodal points of the triangulation. This type of triangulation is generally known as Delaunay triangulation (DT).

The idea of DT was presented by Boris Delaunay based on mathematical work of Dirichlet and Voronoi in 1934. A two dimensions Voronoi diagram (also known as Dirichlet Tessellation) is based on a group of vertices which divide a plane region into subregions bound by line segments. Each subregion is indicated with a Voronoi cell and belongs to one vertex and contains that part of the main region which is closer to this vertex than any other vertex in the group. Delaunay showed that the Voronoi diagram could form a unique triangulation just by connecting each of its two neighboured vertices, by a new edge. The Voronoi diagram for eight vertices in the plane is shown in Figure 3.2.

Later, various algorithms using the main feature of DT were established by researchers which no longer need to construct Voronoi diagram. Lawson (1977) presented topological flipping technique which is used to obtain the DT directly from any arbitrary triangulation. As an alternative to Lawson's technique, Sibson (1973) introduced the flipping algorithm for two dimensional domains, where an arbitrary triangulation is converted into a Delaunay triangulation by flipping the diagonals of two neighbouring triangles. Then, Chew (1989)

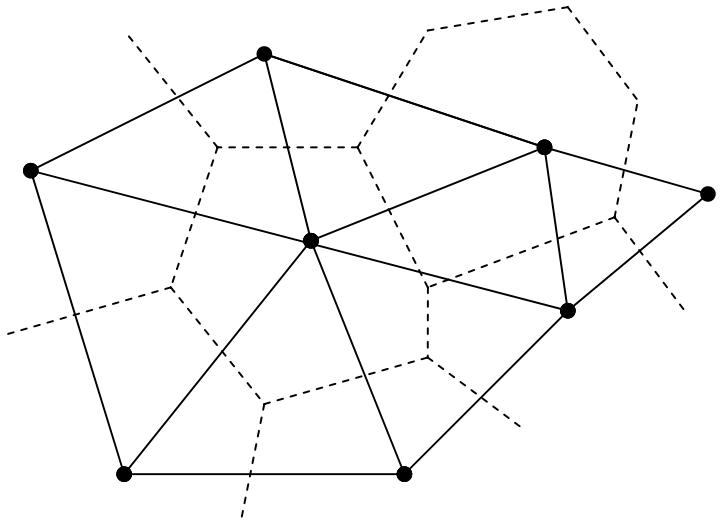

Figure 3.2. The Voronoi diagram (dotted lines) and the Delaunay triangulation (solid lines)

proposed a constrained version of the Delaunay method for domains with irregular non-convex boundaries. Also a basic algorithm was introduced by Rebay (1993) for meshing a two dimensional irregular region using the Bowyer-Watson node insertion method.

In early eighties DT attracted the attention of researchers as not only a mathematical method for triangulation but also a robust and highly efficient technique for generating the computational meshes. However, as a mesh generator, it needs to be combined with a fast and effective node insertion technique.

Based on the point insertion scheme, mesh generation methods using DT can be classified into non-incremental and incremental methods. In non-incremental methods, positions of all vertices are determined before triangulation. Works by Lee and Schechter (1980) which developed “divide-and-conquer” method and Fortune (1987) and O’Rourke (1993) which presented sweeping methods are examples of the non-incremental methods. On the other

hand, in incremental methods, vertices are added one at the time to a gradually growing triangulation starting from a single triangle. An example of this method is presented by Green and Sibson (1978).

Using Delaunay triangulation increases the quality of mesh and computational efficiency even for complex domains by reducing the user intervention. Also as noted by Lawson (1977), the DT maximizes the minimum angle in the triangulation. Therefore it minimizes the largest circumcircle that can be constructed around any triangle. In other words, Delaunay triangulation automatically avoids the creation of long thin triangles with small internal angles. Sloan (1993) presented a fast algorithm for generating constrained DT using the Voronoi diagram. Sloan's scheme is based on permitting certain edges to be specified in the final triangulations, such as those that correspond to region boundaries or natural interface. Therefore, it allows more control on the way mesh is distributed and it is suitable for contour plotting applications.

3.5. REMAPPING

In an adaptive mesh refinement the result of error estimation is used to regenerate an efficient finite element mesh based upon the new areas of the elements. Then, two different approaches are available to continue adaptivity process up to achieving the accessibility criteria. One solution is to restart the analysis with the new mesh. By doing so, one can avoid the necessity for transferring variables between meshes and can get stable numerical results. However, this increases the number of increments which are required to complete

the analysis. Also, in more complicated problems, analysis may begin with meshes which are totally inappropriate for the earlier stages of loading. An alternative strategy, which is known as remapping, is to transfer the history-dependent variables and displacements from the old mesh to the new mesh. A remapping process must consider the following important aspects:

- Conservation of plasticity consistency,
- Equilibrium achievement,
- Compatibility of the history-dependent internal variables transfer with new displacement field,
- Keeping the numerical diffusion of remapping at a minimum.

After remapping the state variables, the analysis will be continued with the new mesh from the start of the next load increment. Therefore, there is no need for re-analysing the previous increments and the total number of increments does not change. Although applying remapping to an adaptive method makes it computationally more complicated, the total required time to achieve the result is dramatically decreased. For this reason, the adaptive method with remapping process has been considered in the present work.

CHAPTER 4

IMPLEMENTATION OF *h*-ADAPTIVITY

4.1. INTRODCUTION

In this chapter, the procedure of analysis by an *h*-adaptive finite element technique, being adopted in this study, is described in more details. Here, *h*-adaptive finite element method is discussed for two dimensional domains using a mesh generator tool in combination with a robust finite element analysis program, *SNAC*. *SNAC* is a robust analysis program written in *FORTRAN*, and has been developed and improved at the University of Newcastle, Australia, during the past two decades.

The algorithm of the *h*-adaptive finite element procedure developed in the present work is shown in Figure 4.1. The analysis starts with generating a coarse mesh on the domain based upon the user information.

In the first increment, UL step use a relatively coarse mesh over the domain of the problem. In this step, an adaptive implicit time-stepping (Sloan and Abbo, 1999a) is used to solve the nonlinear global equations, during which an automatic explicit stress-integrator solves the nonlinear differential constitutive equations due to material nonlinearity. At the achievement of equilibrium, the nodal coordinates are updated according to the incremental displacements and the error in the finite element mesh is evaluated by an error estimator. If the error satisfies an acceptability criterion, the analysis will be continued using the same mesh in the next increment. Otherwise, the new area of each element will be calculated according to the estimated error and a new mesh will be generated. Then, all state variables such as stresses and hardening parameters are transferred from the old mesh to the

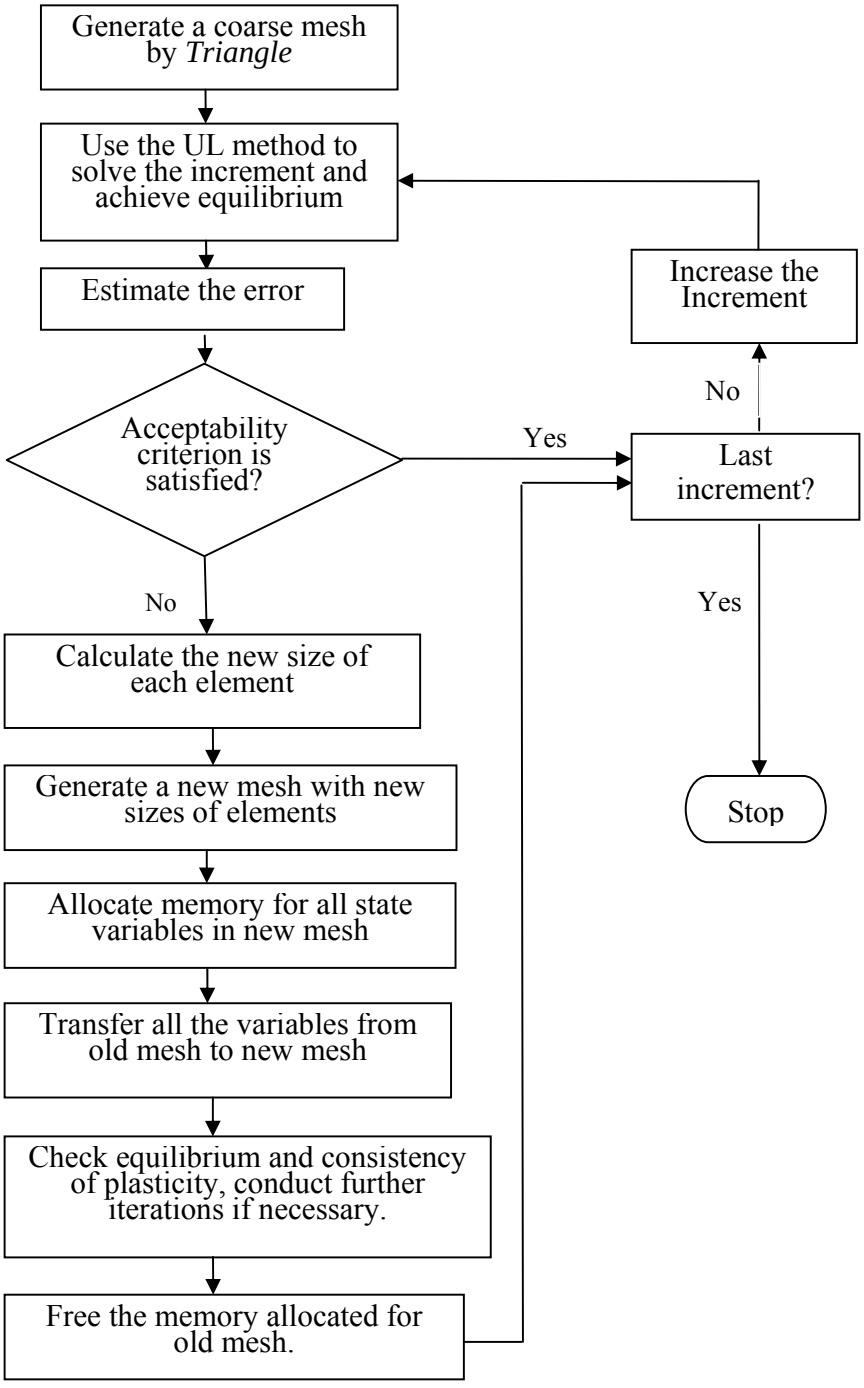

Figure 4.1. Procedure for *h*-adaptive finite element analysis

new mesh and the analysis will be performed using the new mesh in next increment. This transfer process occurs at integration points as well as nodal points. Since the topology of the new mesh is potentially different to the topology of the old mesh, the code must store the information of two meshes in memory simultaneously, demanding a precise memory reallocation routine. This information must include the total number of nodes and their spatial coordinates, the number of elements and their connectivity, the boundary conditions, the applied loading, and all state variables at the Gauss points.

In some stages of the process it may be observed that further refinement may not improve the results and also lead to mesh distortion due to the generation of very small elements. To avoid this problem, a minimum element area is prescribed for every region inside the meshed domain. This guarantees that the area of each individual element will not be smaller than a minimum value, even if the associated error estimator indicates otherwise. In addition, the solution algorithm can terminate the mesh refinement at any time-step, thus allowing the analysis to be continued with the last generated mesh for the remaining load increments.

In the following sections, the components of the *h*-adaptive method will be explained in more details. In the first part, the implementation of error estimation process is described in details. Then, the mesh generator, which is used to generate a coarse mesh as well as refining the current mesh based upon specific element areas, is explained. In the next section, the format of the input file and the necessary considerations are discussed. At the end, the implementation of remapping procedure is presented.

4.2. ERROR ESTIMATOR

Among others, three different techniques of error assessment are employed in this work, and their application as well as their efficiency in solving different geotechnical problems will be addressed. In the following, these techniques will briefly explain. The first method used to estimate the error in the finite element domain is the one introduced by Boroomand and Zienkiewicz (1999) based on the energy norm in nonlinear problems of elasto-plasticity. In this method, the error in an increment can be calculated by an energy norm defined as

$$\|e\| = \left[\int_{\Omega} \left| \left(\sigma - \hat{\sigma}\right)^T \left(\Delta\varepsilon - \Delta\hat{\varepsilon}\right) \right| d\Omega \right]^{\frac{1}{2}} \tag{4.1}$$

in which, $\Delta\varepsilon$ and $\Delta\hat{\varepsilon}$ represent the exact and the finite element incremental strain fields, σ and $\hat{\sigma}$ denote the exact and the finite element approximation of stresses, respectively and Ω is the problem domain.

To estimate the error, the stress and strain fields are replaced by their recovered values, σ^* and $\Delta\varepsilon^*$, which are calculated by using the superconvergent patch recovery procedure. So the Equation (4.1) can be rewritten as

$$\|e^*\| = \left[\int_{\Omega} \left| \left(\sigma^* - \hat{\sigma}\right)^T \left(\Delta\varepsilon^* - \Delta\hat{\varepsilon}\right) \right| d\Omega \right]^{\frac{1}{2}} = \left[\sum_{i=1}^{nel} \left\| e_{el}^* \right\|_i \right]^{\frac{1}{2}} \tag{4.2}$$

where nel is the total number of elements in the domain Ω and $\left\|e_{el}^{*}\right\|$ represents the estimated error in each element calculated by

$$\left\|e_{el}^{*}\right\| = \sum_{i=1}^{ngp} w_i \left(\sigma_i^{*} - \hat{\sigma}_i\right)\left(\Delta\varepsilon_i^{*} - \Delta\hat{\varepsilon}_i\right) \tag{4.3}$$

in which ngp is the total number of Gauss points in an element and w_i is the standard Gauss quadrature weight.

Also, the error in the finite element domain, E, can be obtained by

$$E = \left(\sum_{i=1}^{nel} \sum_{j=1}^{ngp} w_j \sigma_{ij}^{*T} \Delta\varepsilon_{ij}^{*} \right)^{\frac{1}{2}} \tag{4.4}$$

For elastoplastic materials, particularly in problems involving large deformation, the error indicator based on the stress field may not be the most efficient since the stresses in the plastic zones tend to remain on the yield surface while large plastic strains may occur due to further loading. Belytschko (1996) suggested an error indicator based on the recovered Green-Lagrange strain tensor, and showed that this indicator is effective in mesh refinement of plastic zones. For dynamic contact problems of geomechanics, such as dynamic penetration of an object into a soil layer, this type of error assessment is potentially a good candidate due to the highly localised deformations occurring around the contact surfaces. Based on the Green-Lagrange strain tensor, E_G, the error in each element and the error in the finite element domain can be obtained by

$$\left\| e_{el}^{*} \right\| = \left(\int \left| \left(E_G^{*} - E_G^{h} \right)^T \left(E_G^{*} - E_G^{h} \right) \right| dV_{el} \right)^{\frac{1}{2}} \tag{4.5}$$

$$E = \left(\sum_{i=1}^{N_{nel}} \sum_{j=1}^{N_{ngp}} w_j E_{Gij}^{*T} E_{Gij}^{*} \right)^{\frac{1}{2}} \tag{4.6}$$

Another meaningful error measurement can be defined based on the plastic dissipation and the rate of plastic work (Peric et al. 1994). The plastic dissipation function, D^p, is defined by

$$D^p = \sigma^T \dot{\varepsilon}^p - A\dot{a} \tag{4.7}$$

where ε^p is the plastic strain, A is the hardening thermodynamical force, and a represents a set of variables associated with the hardening of the elastoplastic material. For a non-hardening material, the errors in each element and the error in the finite element domain based on the plastic dissipation can be assessed from

$$\left\| e_{el}^{*} \right\| = \left(\int \left| \left(\sigma^{*} - \sigma^{h} \right)^T \left(\Delta\varepsilon^{p*} - \Delta\varepsilon^{ph} \right) \right| dV_{el} \right)^{\frac{1}{2}} \tag{4.8}$$

$$E = \left(\sum_{i=1}^{N_{nel}} \sum_{j=1}^{N_{ngp}} w_j \sigma_{ij}^{*T} \Delta\varepsilon_{ij}^{p*} \right)^{\frac{1}{2}} \tag{4.9}$$

With knowledge of the error in each element and the error in the finite element domain, the relative error in the solution, η, can be found from

$$\eta = \frac{\sqrt{\sum_{i=1}^{N_{nel}} \left\| e_{el}^{*} \right\|_i}}{E} \tag{4.10}$$

Again, in the mesh refinement procedure, the error is compared with a prescribed accuracy, $\overline{\eta}$, according to

$$\eta \le \overline{\eta} \tag{4.11}$$

Obviously, if the condition (4.11) is satisfied no more refinement will be needed. Otherwise, by assuming equal distribution of error over the elements, the new element area, A_{new}, can be obtained from the old element area, A_{old}, according to

$$A_{new} = \left(\frac{\overline{\eta} E}{\frac{\sqrt{N}}{\left\| e_i^{*} \right\|}} \right)^{\frac{1}{p}} \times A_{old} \tag{4.12}$$

in which N represents the total number of elements in the old mesh and p is the polynomial order of the shape functions. After calculating the new area of each element, a mesh generation algorithm, based on the Delaunay triangulation, is used to generate a new mesh for the entire domain of the problem.

4.3. THE MESH GENERATOR

In this study the mesh generation is based on a program named *Triangle* which is a mesh generation code written in *C++* by Shewchuk (1997) at Carnegie Mellon University as part

of the *Quake* project (tools for large-scale earthquake simulation). It has been improved during the last decade and its latest version (1.6), which was released in 2005, is available as a free open code. *Triangle* takes advantage of various existing Delaunay triangulation algorithms such as the incremental insertion algorithm of Lawson (1977), the divide-and-conquer algorithm of Lee and Schachter (1980) and the plane-sweep algorithm of Fortune (1987) to generate high quality meshes for two-dimensional domains. *Triangle* is a fast and robust tool to construct Delaunay triangulations, i.e. constrained Delaunay triangulations and Voronoi diagram. In this code the quality of the generated mesh is guaranteed, making sure there is no angle smaller than twenty degrees, by using Reppert's Delaunay refinement algorithm. More details about *Triangle* program is given by Shewchuk (1996).

Triangle was chosen over the other available packages for mesh generation in this work because of the facilities it provides for users to specify constrains on angles and triangle areas and to define the holes and concavities in the domain. It is a very fast procedure and it can provide a coarse mesh on a specified domain as well as a finer mesh from an existing mesh. Also, the input format of the program is very simple, which makes it possible to introduce complicated domains and necessary constrains without much effort. The availability of *Triangle*'s source code made it possible to apply new changes to the code. In this work, significant improvement has been made to *Triangle,* to make it compatible with the requirements of this study. For example, keeping track of the previous stage of the mesh for the refinement procedure, dealing with problems involving large deformation like constantly changing domain, constrains on the minimum element area and regions with different maximum and minimum element areas. Also, the order of the generated nodes is

optimised in terms of memory allocation and the time spent for analysis and it is facilitated to avoid mesh distortion during the refinement procedure. Also, some changes have been applied in the original code of *Triangle* to make it compatible with the analysing program, *SNAC*. The main body of input file is described in the section 4.5.3.

4.3.1. Pre-processing and analysis

The analysis starts with generating a coarse mesh on the domain based upon the information in the input file and the prescribed minimum area of the elements in each region. In the first increment, the global nonlinear equations are solved to achieve equilibrium. This includes the calculation of all state variables and nodal displacements. Then, the error in the current mesh is calculated by an error estimator technique and the program checks if the error is acceptable. If yes, the analysis will be continued in the next increment keeping the topology of the problem unchanged, i.e., the desirable accuracy has been achieved and no mesh refinement is necessary. Otherwise, for all the elements with the estimated error above an acceptable accuracy, a new area will be assigned to minimise the error. Then, the old mesh is refined according to the new sizes of elements. In this stage, the information of the new mesh as well as the information of the old mesh must be stored in the memory of the computer simultaneously. After generating the new mesh, all state parameters such as stresses as well as nodal displacements need to be transferred from the old mesh to the new mesh. This remapping is quite a challenging process because the topology of the new mesh, including number of the nodes, their spatial coordinates, number

of the elements and their connectivity, is totally different to the topology of the old mesh. Details of the remapping process are discussed in Section 4.4.

4.4. REMAPPING

After generating the new mesh based on the estimation of the error, all variables such as stresses and displacements need to be transferred from the old mesh to the new mesh. The state variables in general can be classified in two groups; the nodal variables and those stored at integration points.

Nodal variables can be transferred from the old nodes to the new nodes by a direct interpolation. In other words, if the new coordinates of a node matches the coordinates of an old node, the displacement will remain unchanged. If a new node is generated on one of the segments with a prescribed displacement it will inherit the characteristics of that segment. The displacements of other new nodes will be calculated by substituting their spatial coordinates in the displacement shape function of the surrounding old element.

Transferring the information from old Gauss points to the new Gauss points is quite a challenge as the new mesh can be completely different from the old mesh. In this work to compute the nodal quantities of interest (such as stresses), the super convergent patch recovery technique developed by Zienkiewicz and Zhu (1992a, 1992b) is used. This technique has been successfully used with *h*-adaptive as well as *r*-adaptive finite element methods (Hu and Randolph, 1998; Nazem et al., 2006), and assumes that the quantities in a

patch can be modelled using a polynomial of the same order as the displacements. Thus, for two-dimensional quadratic elements, the stresses over a patch may be written as

$$\sigma = \mathbf{P} \cdot \mathbf{a} \tag{4.13}$$

where the matrix notation is used instead of the component notation and

$$\mathrm{P} = \left[1, x, y, x^2, xy, y^2\right] \tag{4.14}$$

and

$$\mathrm{a} = \left[a_1, a_2, a_3, a_4, a_5, a_6\right]^T \tag{4.15}$$

Zienkiewicz et al. (1993) proposed the use of normalised coordinates in Equation (4.14) instead of global coordinates to avoid ill-conditioning of equations, particularly for higher order elements. The normalised coordinates in a two-dimensional patch, x_i^* and y_i^*, can be written as

$$\begin{aligned} x_i^* &= -1 + 2\frac{x_i - x_{\min}}{x_{\max} - x_{\min}} \\ y_i^* &= -1 + 2\frac{y_i - y_{\min}}{y_{\max} - y_{\min}} \end{aligned} \tag{4.16}$$

where $x_{\min}$ and $x_{\max}$ represent the maximum and minimum values of the x-coordinates in the patch, respectively, and $y_{\max}$ and $y_{\min}$ are defined similarly for the y-coordinates. A least square fit is then used to find the unknown values of **a** by minimising

$$F(a) = \sum_{i=1}^{m} \left(\sigma\left(x_i^*, y_i^*\right) - \mathrm{P}\left(x_i^*, y_i^*\right).\mathrm{a} \right)^2 \tag{4.17}$$

in which $\sigma\left(x_i^*, y_i^*\right)$ are the stress values at Gauss points and m is the number of Gauss points in a patch. Finally, **a** is found by

$$\mathrm{a} = A^{-1}b \tag{4.18}$$

where

$$A = \sum_{i=1}^{m} \mathrm{P}^T\left(x_i^*, y_i^*\right)\mathrm{P}\left(x_i^*, y_i^*\right) \tag{4.19}$$

$$b = \sum_{i=1}^{m} \mathrm{P}^T\left(x_i^*, y_i^*\right)\sigma\left(x_i^*, y_i^*\right) \tag{4.20}$$

The stresses at any node or Gauss point in the new mesh can be obtained by substituting its normalised coordinates in Equation (4.13) for its surrounding patch in the old mesh. As the topology of the mesh has changed, it is possible to find more than one enclosed patch for a specific Gauss point or node. In this case the final value of stresses is equal to the mean of the calculated stresses in each patch.

For elastoplastic materials, the stresses and hardening parameters remapped by this method may violate the equilibrium and consistency of plasticity in the new mesh. Ideally, transferring the state variables from an old mesh to a new mesh should not cause any straining and hence the equilibrium should be satisfied for both the old and new mesh.

Moreover, the remapped stresses must lie inside or on the yield surface. Unfortunately, there is no simple way to satisfy these two conditions. In this work, if a stress point after remapping is found to lie outside the yield surface, it is projected back to the yield surface using the stress correction procedure described in Sloan et al. (2001). In their suggested procedure, first, the total applied strain increment is divided into sub-increments according to the estimation of the local error. Then, it attempts to correct the stresses in a way that the global integration error in stresses falls below an acceptable tolerance. After these corrections are executed, equilibrium is enforced by conducting additional iterations at the global level (if needed).

New nodal restraints can be considered by projecting the old nodes restraints on their matched new nodes and also generalising the information of the restrained segments for all the new nodes which have been generated on those segments. An identical method is used to construct the loads on the new nodes and edges using the information from old mesh.

4.5. OTHER ASPECTS OF IMPLEMENTATION

4.5.1. Memory management

Developing the program including all the components of *h*-adaptivity has some difficulties in the software engineering point of view. In an *h*-adaptive procedure number of nodes and elements change in each mesh refinement. Therefore, using static arrays for storing this information is impossible. On the other hand, during the remapping process, both information (e.g. nodes, elements, state variables and etc) of the old mesh and the new

mesh need to be available simultaneously. To manage the memory in the best way in the software just dynamic arrays are considered. One of the most difficult ways to manage the memory in an *h*-adaptive finite element code is utilising dynamic arrays. The sizes of the arrays are dynamically changed to adopt the required size of the newest mesh. The information of the old mesh is only required at the time of remapping. After transferring the data from old mesh to the new mesh, the memory allocated to the information of the old mesh is freed.

4.5.2. Ordering optimisation

The order of the generated nodes may not be optimum, in terms of memory allocation and the time spent for analysis. This may lead to extra storage for some global sparse matrices such as the stiffness matrix. Consequently, the time spent for solving the global equations may increase dramatically. Any symmetric $n \times n$ can be considered as the adjacency matrix of a graph. Therefore, it is possible to reduce the bandwidth (the maximum distance between two adjacent vertices) of those matrices by using an appropriate reordering of the indices assigned to each vertex (Figure 4.2). In this study, the Reverse Cuthill-McKee (RCM) algorithm (Cuthill and McKee, 1969) has been applied for reordering the nodes. This is done by obtaining the coordinates of the nodes and their connectivity which is described in terms of a triangulation as an input. Then the algorithm computes the adjacency information, carries out the RCM algorithm to get the permutation and applies the permutation to the nodes and triangles.

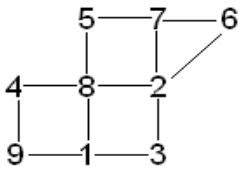

*	0	1	0	0	0	0	1	1
0	*	1	0	0	1	1	1	0
1	1	*	0	0	0	0	0	0
0	0	0	*	0	0	0	1	1
0	0	0	0	*	0	1	1	0
0	1	0	0	0	*	1	0	0
0	1	0	0	1	1	*	0	0
1	1	0	1	1	0	0	*	0
1	0	0	1	0	0	0	0	*

a) Corresponding adjacency matrix with a bandwidth of 7

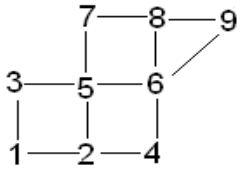

*	1	1	0	0	0	0	0	0
1	*	0	1	1	0	0	0	0
1	0	*	0	1	0	0	0	0
0	1	0	*	0	1	0	0	0
0	1	1	0	*	1	1	0	0
0	0	0	1	1	*	0	1	1
0	0	0	0	1	0	*	1	0
0	0	0	0	0	1	1	*	1
0	0	0	0	0	1	0	1	*

b) Corresponding adjacency matrix with a bandwidth of 7

Figure 4.2. Corresponding adjacency matrices (a) before reordering and (b) after RCM reordering

4.5.3. Input file

In the Input file, the necessary information for finite element analysis is introduced to the program. The information mainly includes the definition of geometry, boundary conditions, material properties, loads information and the analysis procedures.

The first two lines of the Input file ("*Snac.Poly*") are the headers which will appear in all output files. The third line includes the switches which can be set by the user to describe the way of generating mesh in *Triangle* and the desired outputs. In most cases in this work the combination of these switches has been set in a way to generate a six noded Delaunay

triangulation with a domain which has been defined in the input file considering the limit on minimum area of the elements. Clearly, the configuration of the domain in the input file is only used to generate the first coarse mesh. After that, *Triangle* retrieves its initial information of the domain from the previous mesh. Definition of the geometry should appear after the third line.

In the geometry part, the domain of the problem is defined by a combination of some points and segments. In general each point represents the intersection of two segments. A segment can be a straight line or a curve. The domain of the problem may consist of several regions. A region is a partially enclosed area of the main domain with a specific material property and element type. This facilitates the definition of a domain including several types of materials and elements. For each region a minimum area of element needs to be defined. This minimum element area represents the density of the mesh in each region during the process of mesh generation as well as mesh refinement. Also, whether the region needs to be consider as a fixed region, can be specified in the time of its definition. A region can be recognised by defining an arbitrary internal point. The mesh generator automatically considers the closest enclosed area around this point as a region.

Cavities (an enclosed area in which no element is generated) can also be defined in any part of the domain. Cavities remain unchanged during the process of mesh generation and mesh refinement. A cavity can be defined in a similar fashion to a region.

Boundary conditions such as nodal restraints or contact surfaces can be applied to a point or

a segment in the input file. Note that the definition of boundary conditions here is different to the common method of assigning boundary conditions in finite element programs, where these conditions are usually applied on nodes.

As mentioned before, material properties are defined individually for each region of the domain. Obviously, all elements generated during meshing will inherit the properties of their surrounding region.

Loads including external nodal forces, body forces and prescribed displacements can also be specified for any points or segment. These loads are automatically assigned to the correspondent nodes and the elements in the mesh.

The last part of the input file includes some commands controlling the analysis procedure and outputs. In this part, the total analysis time, increment, refinement step and other commands which lead the analysis process can be specified. In this section, user can specify the frequency of remeshing and the type of error estimation technique to be used.

CHAPTER 5

h-ADAPTIVITY FOR CONTACT AND DYNAMIC ANALYSIS

5.1. INTRODUCTION

In many geomechanics problems, soil is subjected to dynamic loads while interacting with a structure or an object. Among others, examples include the dynamic penetration of an object into a layer of soil due to its initial kinetic energy, the lateral capacity of a pile subjected to a dynamic impact, and the investigation of the dynamic pullout capacity of an anchor embedded in soil. The analysis of such problems demands robust computational techniques able to deal with their highly nonlinear and complex nature, and is yet one of the most challenging and sophisticated tasks in computational geomechanics. The complexity is mainly due to nonlinear soil behaviour, large deformations accompanied by severe mesh distortion, changing boundary conditions due to contact, and time-dependent behaviour. Furthermore, in penetration problems the interfaces between the soil and the penetrometer may change continuously, which necessitates the contact mechanics formulation. A typical distorted mesh occurring during the analysis of penetration of a cone into a layer of soil is depicted in Figure 1.1. Such distortion often results in a negative Jacobian of an element, leading to a spontaneous termination of the numerical analysis.

In this chapter, the formulations of dynamic analysis and contact mechanics in an *h*-adaptive finite element framework are explained in details. Also alternative error assessment techniques to deal with such problems, based on the energy norm, the Green-Lagrange strain, and plastic dissipation, will be explained. The performance of the *h*-adaptive finite element method as well as the performance of these error assessment techniques will be investigated by solving a few numerical examples in Chapter 6.

5.2. LITERATURE REVIEW

In many problems of geotechnical engineering the loads are applied at a relatively slow rate so that the effect of the inertia forces maybe be ignored in the analysis. However, if the loads affect a domain in a short time the effect of the inertia forces needs to be considered throughout the analysis process to achieve an accurate solution. Moreover, the soil may undergo large deformations, leading to severe mesh distortion. Therefore, the adaptive techniques have attracted attention to tackle possible mesh distortion in various fields of dynamic problems of engineering. Some of the early works in this area include using an *r*-adaptive method for strain localization problems (Ortiz and Quigley, 1991) and also applying an *h*-adaptive method for transient solid mechanics problems with the aim of capturing localised shear band and strain localisation (Belytschko and Tabbara, 1993). Gallimard et al. (1996) and Ladevèze and Moës (1996) have used a residual error estimator to deal with dynamic problems. Later, Wiberg and Li (1994) suggested an *h*-adaptive finite element procedure to refine the mesh and time step automatically based on the spatial and time discretisation error. Their work was based on a recovery error estimator. The work of Deb et al. (1996) is another effort of developing an *h*-adaptive method to capture the shear band for dynamic strain localisation in elasto-plastic continuum. One of the first applications of the *h*-adaptive technique in geomechanics was presented by Hu and Randolph (1998), where the analysis is performed assuming small deformations within each load step, and is followed by updating the mesh according to the computed incremental nodal displacements and then remeshing the entire problem domain. Silva et

al. (2000) employed an *h*-adaptive strategy to deal with the plastic and visco-plastic behaviours in a two-dimensional non-linear dynamic analysis. Also, Khoei and Lewis (2002) studied the localised failure due to material instability using an *h*-adaptive finite element method in metal powder forming. Khoei et al. (2005) applied the *h*-adaptive strategy using Cosserat continuum while regularizing rotational and the conventional freedom in the governing equations to locate the shear band.

Contact problems are common challenges in various fields of engineering. The importance of the contact analysis comes from the real world where almost no movement is possible without considering the contact between at least two surfaces. Finite element method is a robust way to tackle the contact related problems. In addition, since the boundary conditions are continuously changing in contact problems *h*-adaptive finite element method is seemingly well suited to analyse such problems. Some of the early research works on using adaptivity to solve the problems involving frictionless contact has been undertaken with the emphasis on choosing a suitable error estimator. Some error estimators were introduced for small deformation frictionless contact (e.g. Kikuchi and Oden, 1988; Hlavacek et al., 1988) considering the underlying mathematical base of the problem. Johnson and Hansbo (1992) proposed a residual based error estimator to be used for unilateral membrane problems. Later, their approach was completed by Wriggers et al. (1994) and was used for the analysis of the contact between two elastic bodies. Later, the super convergent patch recovery error estimator, introduced by Zienkiewicz and Zhu (1987), attracted the researchers' attention and was adopted in some research works to solve contact problems (e.g. Wriggers and Scherf, 1998). Also, Rannacher and Suttmeier

(1998) used the concept of dual error estimation and introduced a technique for evaluating the error in linear elastic problems. Later, their technique was extended by Rieger and Wriggers (2001) to problems involved with non-linear frictionless contact in three dimensions. The method proposed by Johnson and Hansbo (1992) was also used by Buscaglial et al. (2001) to develop a posterior error estimator based on the penalized approach for frictionless contact problems. The recovery-based error estimators were effectively used by Bessette et al. (2003) for modelling three dimensional penetration and impact problems within an *h*-adaptive procedure in an explicit finite element method. Many of contact problems also include dynamic loadings. Therefore, solving this type of problems has always been a subject of interest. Armero and Petocz (1998) conducted a study of the energy and momentum conservation algorithms for dynamic contact problems. Blum et al. (2008) described a discretisation using the space-time method by Galerkin to overcome problems involving dynamic contact. Also, a comparison on the efficiency of different adaptive methods for solving two dimensional contact problems can be found in the work by Franke et al (2010).

5.3. FINITE ELEMENT FORMULATION

As explained in Chapter 4, the *h*-adaptive finite element method employs the UL approach to solve the problem in each increment. After the UL analysis a new mesh is generated based upon an error estimator followed by remapping of the state variables from the old mesh to the new mesh. Therefore, the UL method is one of the main components of the *h*-adaptive finite element method. As such, the formulation for dynamic and contact analysis

of geomechanics problems is presented in a UL framework. Then, other aspects of dynamic analysis of a continuum including alternative time-integration schemes, energy-absorbing boundaries, satisfying equilibrium in the newly generated finite element mesh, and implementation of the *h*-adaptivity will be discussed in this section.

5.3.1. Momentum equation and its discretisation

In each time step of the analysis the *h*-adaptive procedure starts with an UL step to calculate the displacements, velocities and accelerations, which satisfy the principle of virtual work according to

$$\sum_{k=1}^{P}\left(\int_{V_k}\sigma_{ij}\delta\varepsilon_{ij}dV_k+\int_{V_k}\delta u_i\rho\ddot{u}_i dV_k+\int_{V_k}\delta u_i c\dot{u}_i dV_k\right)=\sum_{k=1}^{P}\left(\int_{V_k}\delta u_i b_i dV_k+\int_{S_k}\delta u_i q_i dS_k\right)+\int_{S_c}\left(t_N\delta g_N+t_T\delta g_T\right)dS_c \tag{5.1}$$

where P denotes the total number of bodies in contact, σ is the Cauchy stress tensor, and $\delta\varepsilon$ is the variation of strain due to virtual displacement δu. The symbols u, $\dot{u}$ and $\ddot{u}$ represent material displacements, velocities and accelerations, respectively, while ρ and c are the mass density and damping of the material, b is the body force, q is the surface load acting on area S of volume V, δg_N and δg_T are the virtual normal and tangential gap displacements at contacts, and t_N and t_T represent the normal and tangential forces at contact surface S_c.

To model the contact between two bodies including large deformations the so-called node-to-segment (NTS) concept is employed, where a node on a slave surface may come into

contact with an arbitrary segment of the master contact surface, and is allowed to slide along the master surface a finite distance (Wriggers, 2006). For large deformations, this technique facilitates the sliding of a contacting node over several elements. With this assumption the last term in Equation (5.1), representing the virtual work due to normal and tangential components of the contact force, can be estimated according to

$$\int_{S_c} \left(t_N \delta g_N + t_T \delta g_T \right) dS_c \approx \sum_{i=1}^{n_c} \delta u_i^T F_{N_i}^c + \sum_{i=1}^{n_c} \delta u_i^T F_{T_i}^c \tag{5.2}$$

where F_N^c and F_T^c represent the normal and tangential components of the contact force, respectively, and n_c is the total number of slave nodes contacting the master surface. Linearisation of Equation (5.1) in the standard finite element framework provides the matrix form of the equation of motion as

$$\mathbf{M}\ddot{\mathbf{u}}^{t+\Delta t} + \mathbf{C}\dot{\mathbf{u}}^{t+\Delta t} + \mathbf{F}_{\text{int}}^{t+\Delta t} = \mathbf{F}_{ext}^{t+\Delta t} \tag{5.3}$$

where **M** is the mass matrix, **C** is the damping matrix, $\mathbf{F}_{\text{int}}$ and $\mathbf{F}_{ext}$ are the internal and external force vectors, respectively, **u** represents the displacement vector and a superimposed dot represents the time derivative of a variable.

5.3.2. Time Integration

The solution of the momentum equation in (5.1) requires a step-by-step integration scheme. In general, the dynamic time-integration schemes are classified as implicit or explicit. Explicit algorithms, such as the central difference method, find a solution for state variables

which satisfy the momentum equation at time $t+\Delta t$ based exclusively on their values at previous time increments. Such schemes circumvent the solution of nonlinear equations, but are conditionally stable due to the fact that the size of each time step must guarantee that an elastic wave will cross the smallest size of any element in the problem domain. This limitation generally results in selecting a very small time step or using a relatively coarse mesh. Implicit time-integration schemes, on the other hand, provide a solution to the dynamic quantities at time $t+\Delta t$ based upon their values at time t as well as the values at time $t+\Delta t$, requiring, however, the solution of nonlinear equations. Several time-integration algorithms have been commonly used in dynamic analysis of geotechnical problems. A recent study conducted by Kontoe et al. (2008a) revealed that the generalised-α, method, previously developed by Chung and Hulbert (1993), outperforms the other algorithms investigated. Then, Kontoe et al. (2008b) demonstrated the ability of this method in solving the dynamic coupled consolidation problems of geomechanics. The generalised-α method is second-order accurate, and is adopted in this study for solving the momentum equation in (5.1). The formulation of the method, adopting an iterative procedure based on Newton-Raphson method, is presented in the following.

In the implicit generalised-α method proposed by Chung and Hulbert (1993), the inertia forces in the momentum equation are measured at time $t+(1-\alpha_m)\Delta t$ while the damping forces and the internal forces are measured at time $t+(1-\alpha_f)\Delta t$, viz, the momentum equation in (5.3) is written as follows

$$\mathbf{M}\ddot{\mathbf{u}}^{t+(1-\alpha_m)\Delta t} + \mathbf{C}\dot{\mathbf{u}}^{t+(1-\alpha_f)\Delta t} + \mathbf{F}_{int}^{t+(1-\alpha_f)\Delta t} = \mathbf{F}_{ext}^{t+(1-\alpha_f)\Delta t} \tag{5.4}$$

in which α_m and α_f are two new integration parameters, and

$$\begin{aligned}
\ddot{\mathbf{u}}^{t+(1-\alpha_m)\Delta t} &= (1-\alpha_m)\cdot\ddot{\mathbf{u}}^{t+\Delta t} + \alpha_m\cdot\ddot{\mathbf{u}}^{t} \\
\dot{\mathbf{u}}^{t+(1-\alpha_f)\Delta t} &= (1-\alpha_f)\cdot\dot{\mathbf{u}}^{t+\Delta t} + \alpha_f\cdot\dot{\mathbf{u}}^{t} \\
\mathbf{F}_{int}^{t+(1-\alpha_f)\Delta t} &= (1-\alpha_f)\mathbf{F}_{int}^{t+\Delta t} + \alpha_f\mathbf{F}_{int}^{t} \\
\mathbf{F}_{ext}^{t+(1-\alpha_f)\Delta t} &= (1-\alpha_f)\mathbf{F}_{ext}^{t+\Delta t} + \alpha_f\mathbf{F}_{ext}^{t}
\end{aligned} \tag{5.5}$$

Substituting the equations in (5.5) into the momentum equation in (5.4) provides

$$\begin{aligned}
&\mathbf{M}\left[(1-\alpha_m)\cdot\ddot{\mathbf{u}}^{t+\Delta t} + \alpha_m\cdot\ddot{\mathbf{u}}^{t}\right] + \mathbf{C}\left[(1-\alpha_f)\cdot\dot{\mathbf{u}}^{t+\Delta t} + \alpha_f\cdot\dot{\mathbf{u}}^{t}\right] + \\
&(1-\alpha_f)\cdot\mathbf{F}_{int}^{t+\Delta t} + \alpha_f\cdot\mathbf{F}_{int}^{t} = (1-\alpha_f)\cdot\mathbf{F}_{ext}^{t+\Delta t} + \alpha_f\cdot\mathbf{F}_{ext}^{t}
\end{aligned} \tag{5.6}$$

In the generalised-α method, the displacements and velocities are computed by Newmark's equations according to

$$\begin{aligned}
\mathbf{u}^{t+\Delta t} &= \mathbf{u}^{t} + \dot{\mathbf{u}}^{t}\Delta t + \left[\left(\frac{1}{2}-\delta\right)\ddot{\mathbf{u}}^{t} + \delta\ddot{\mathbf{u}}^{t+\Delta t}\right]\Delta t^2 \\
\dot{\mathbf{u}}^{t+\Delta t} &= \dot{\mathbf{u}}^{t} + \left[(1-\beta)\ddot{\mathbf{u}}^{t} + \beta\ddot{\mathbf{u}}^{t+\Delta t}\right]\Delta t
\end{aligned} \tag{5.7}$$

in which δ and β are the Newmark's integration parameters. Rearranging the equations in (5.7), the velocities and accelerations at time $t+\Delta t$ can be expressed in terms of the displacements at time $t+\Delta t$ and other quantities at time t as follows

$$\begin{aligned}
\dot{\mathbf{u}}^{t+\Delta t} &= \frac{\delta}{\beta\Delta t}\left(\mathbf{u}^{t+\Delta t} - \mathbf{u}^{t}\right) + \left(1-\frac{\delta}{\beta}\right)\dot{\mathbf{u}}^{t} + \Delta t\left(1-\frac{\delta}{2\beta}\right)\ddot{\mathbf{u}}^{t} \\
\ddot{\mathbf{u}}^{t+\Delta t} &= \frac{1}{\beta\Delta t^2}\left(\mathbf{u}^{t+\Delta t} - \mathbf{u}^{t}\right) - \frac{\dot{\mathbf{u}}^{t}}{\beta\Delta t} + \left(1-\frac{1}{2\beta}\right)\ddot{\mathbf{u}}^{t}
\end{aligned} \tag{5.8}$$

Substituting $\dot{\mathbf{u}}^{t+\Delta t}$ and $\ddot{\mathbf{u}}^{t+\Delta t}$ in (5.8) into the equations in (5.5) and simplifying will provide

$$\begin{aligned}
\dot{\mathbf{u}}^{t+(1-\alpha_f)\Delta t} &= \frac{\delta\left(1-\alpha_f\right)}{\beta\Delta t}\left(\mathbf{u}^{t+\Delta t}-\mathbf{u}^{t}\right)+\left(\left(1-\alpha_f\right)\left(1-\frac{\delta}{\beta}\right)+\alpha_f\right)\dot{\mathbf{u}}^{t}+\Delta t\left(1-\alpha_f\right)\left(1-\frac{\delta}{2\beta}\right)\ddot{\mathbf{u}}^{t} \\
\ddot{\mathbf{u}}^{t+(1-\alpha_m)\Delta t} &= \frac{1-\alpha_m}{\beta\Delta t^2}\left(\mathbf{u}^{t+\Delta t}-\mathbf{u}^{t}\right)-\frac{\left(1-\alpha_m\right)}{\beta\Delta t}\dot{\mathbf{u}}^{t}-\left(\frac{1-\alpha_m-2\beta}{2\beta}\right)\ddot{\mathbf{u}}^{t}
\end{aligned} \tag{5.9}$$

Substituting the equations in (5.9) into the momentum equation in (5.4) and applying Newton-Raphson iterative method, the following equation is obtained which must be solved during i^{th} iteration

$$\begin{aligned}
&\mathbf{K}_{eff(i-1)}^{t+\Delta t}\cdot\Delta\mathbf{u}_{(i)}=\left(1-\alpha_f\right)\cdot\mathbf{F}_{ext}^{t+\Delta t}+\alpha_f\cdot\mathbf{F}_{ext}^{t}-\left(1-\alpha_f\right)\cdot\mathbf{F}_{int(i-1)}^{t+\Delta t}-\alpha_f\cdot\mathbf{K}_{T(i-1)}^{t+\Delta t}\cdot\mathbf{u}^{t} \\
&-\mathbf{M}\left(a_0\cdot\left(\mathbf{u}_{(i-1)}^{t+\Delta t}-\mathbf{u}^{t}\right)-a_2\cdot\dot{\mathbf{u}}^{t}-\left(a_3-1\right)\cdot\ddot{\mathbf{u}}^{t}\right)-\mathbf{C}\left(a_1\cdot\left(\mathbf{u}_{(i-1)}^{t+\Delta t}-\mathbf{u}^{t}\right)+\left(1-a_4\right)\cdot\dot{\mathbf{u}}^{t}-a_5\cdot\ddot{\mathbf{u}}^{t}\right) \\
&\mathbf{u}_{(i)}^{t+\Delta t}=\mathbf{u}_{(i-1)}^{t+\Delta t}+\Delta\mathbf{u}_{(i)}\qquad,\qquad\mathbf{u}_{(0)}^{t+\Delta t}=\mathbf{u}^{t}
\end{aligned} \tag{5.10}$$

in which $\mathbf{K}_{eff}$ represents the effective stiffness matrix and is computed by

$$\mathbf{K}_{eff}=\mathbf{M}+a_1\cdot\mathbf{C}+\left(1-\alpha_f\right)\cdot\mathbf{K}_T \tag{5.11}$$

Note that the coefficients a_0-a_5 are defined by

$$\begin{aligned}
&a_0=\frac{1-\alpha_m}{\beta\cdot\Delta t^2}\qquad,\qquad a_1=\frac{\delta\left(1-\alpha_f\right)}{\beta\cdot\Delta t} \\
&a_2=\frac{1-\alpha_m}{\beta\cdot\Delta t}\qquad,\qquad a_3=\frac{1-\alpha_m}{2\beta} \\
&a_4=\frac{\delta}{\beta}\left(1-\alpha_f\right)\ ,\qquad a_5=\Delta t\left(\frac{\delta}{2\beta}-1\right)\left(1-\alpha_f\right)
\end{aligned} \tag{5.12}$$

$\mathbf{K}_T$ in Equation (5.11) represents the tangential stiffness matrix, and it defined as

$$\mathbf{K}_T\left(\mathbf{u}_i^{t+\Delta t}\right)=\left(\frac{\partial \mathbf{R}}{\partial \mathbf{u}^{t+\Delta t}}\right)_{\mathbf{u}_i^{t+\Delta t}} \tag{5.13}$$

in which **R** is the stress divergence term. The tangential stiffness matrix is obtained by summation of the material stiffness, $\mathbf{K}_{ep}$, the stiffness due to geometrical nonlinearity, $\mathbf{K}_{nl}$, and the stiffness due to normal and tangential contact, $\mathbf{K}_{Ns}$ and $\mathbf{K}_{Ts}$, i.e.,

$$\mathbf{K}_T=\mathbf{K}_{ep}+\mathbf{K}_{nl}+\mathbf{K}_{Ns}+\mathbf{K}_{Ts} \tag{5.14}$$

In addition, the internal force vector can be calculated by the contribution of the Cauchy stress tensor and the nodal forces at the contact surfaces as follows

$$\mathbf{F}_{int}^{t+\Delta t}=\int_{V^{t+\Delta t}}\mathbf{B}^T\cdot\boldsymbol{\sigma}^{t+\Delta t}dV^{t+\Delta t}-\sum_{i=1}^{n_c}\left(\mathbf{F}_{N_i}^c+\mathbf{F}_{T_i}^c\right) \tag{5.15}$$

5.3.3. Energy absorbing boundaries

When applying the finite element method with the finite boundaries the outgoing waves from the source (normally the structure) may reflect back to their source and the accuracy of the numerical solution can be significantly affected. Therefore, simulating an infinite medium is a major concern in dynamic analysis of soil-structure-interaction (SSI) problems, and the numerical model should guarantee that the waves would dissipate in a far-field of the source.

The common way to avoid any wave reflection from truncated computational boundaries, is defining artificial boundaries which absorb the energy of incoming waves. Lysmer and

Kuhlemeyer (1969) introduced a very efficient artificial boundary known as the "standard viscous boundary" which is able to dissipate the waves in an acceptable rate and low computational cost. The standard viscous boundary is one of the most commonly used and efficient wave-absorbing boundaries provided that the boundary is not located within 1.2-1.5 times the length of the shear wave (Kellezi, 1998). Kontoe (2006) also studied the performance of the viscous boundaries by analysing a few plane strain as well as axi-symmetric problems, and found that the standard viscous boundary is able to absorb both dilatational waves (P-waves) and shear waves (S-waves) effectively. This type of boundary has been adopted in dynamic analysis of geotechnical problems addressed in this Thesis, and is briefly explained in the following.

The implementation of the viscous boundaries requires the replacement of the damping matrix, **C**, in the momentum Equation (5.3), by $\bar{\mathbf{C}}$ as

$$\mathbf{M}\ddot{\mathbf{u}}^{t+\Delta t} + \bar{\mathbf{C}}\dot{\mathbf{u}}^{t+\Delta t} + \mathbf{F}_{\text{int}}^{t+\Delta t} = \mathbf{F}_{ext}^{t+\Delta t} \tag{5.16}$$

where

$$\bar{\mathbf{C}} = \mathbf{C} + \int_L \mathbf{N}^T \mathbf{C}_c \mathbf{N} dL \quad , \quad \mathbf{C}_c = \begin{bmatrix} V_s & 0 \\ 0 & V_p \end{bmatrix} \tag{5.17}$$

in which the second term on the right hand side represents the contribution of the viscous boundary, L is the length of the side of the element modelled as the viscous boundary, **N** is the displacement shape functions of the element, and $\mathbf{C}_c$ is the constitutive viscous damping

matrix depending on the velocities of dilatational waves, V_s, and the shear waves, V_p, according to

$$V_s = \sqrt{\frac{E}{2\rho(1+\nu)}} \tag{5.18}$$

$$V_p = \sqrt{\frac{E(1-\nu)}{\rho(1+\nu)(1-2\nu)}} \tag{5.19}$$

where E and ν are Young's modulus and Poisson's ratio, respectively.

5.3.4. Definition of contact

In many geotechnical problems two solid bodies often come into contact, at a smooth or non-smooth interface, causing a nonlinear behaviour. The penetration of an object into a layer of soil is a typical example of such problems in which large deformation and material nonlinearity are combined with frictional contact nonlinearities (e.g. sliding, detaching and re-joining of the two contact surfaces) and make the analysis quite a challenge. In the literature, there are two methods available to solve a large deformation frictionless contact problem. The first approach is the node to segment element method (NTS-contact) based on the work by Wriggers and Simo (1985). Sheng et al. (2005) employed this method to model the frictional contact associated with pile penetration. Also, Sheng et al. (2006) analysed the same problem by the NTS-contact considering a smoothed discretisation in the contact surfaces. The second approach is the mortar type method, based on the mathematical framework developed by Bernardi and Patera (1993). The mortar type

method uses higher order elements, and has been applied to the large deformation contact problems by Puso and Laursen (2003) and Fischer and Wriggers (2005, 2006).

In this study, the NTS-contact method is employed to analyse problems involving changing boundary conditions. To model the interface between two bodies by the NTS-contact method, the contact surfaces are usually discredited as the slave and the master surface. There is no specific criterion to assign the slave or the master attribute to a surface. However, the choice of master and slave bodies needs to remain consistent throughout the analysis. In a large deformation problem, the size and the position of the contact surface is changing constantly but the following normal contact constraint should be always satisfied

$$g_N \geq 0 \tag{5.20}$$

in which g_N represents the gap between the two surfaces. This gap is known as the distance between the current location of a point on the slave surface, x_s, and its closest projection on the master surface, $\bar{x}_m$, and can be defined according to

$$g_N = \left(\mathbf{x}_s - \bar{\mathbf{x}}_m\right).\bar{\mathbf{n}} \tag{5.21}$$

where $\bar{\mathbf{n}}$ is the unit normal vector of the master surface at the projection point.

In contact mechanics, there are three main approaches to formulate the constitutive relations for the normal and the tangential directions. They include: (a) using the gap function and considering the related stresses as the reactions, (b) using the gap function to

define a method to calculate the stresses in two contact bodies, (c) using the penalty method. In this work the third approach was chosen due to its common use in the engineering software (Wriggers, 2010; ABAQUS, 2008). The constitutive equations for the normal and the tangential directions based on the penalty method are discussed in more details in the following.

a) Normal and tangential tractions

In the penalty method, the normal pressure at the contact area, t_N, and its time derivative, $\dot{t}_N$, are defined by

$$\begin{aligned} t_N &= \varepsilon_N . g_N \\ \dot{t}_N &= \varepsilon_N . \dot{g}_N \end{aligned} \tag{5.22}$$

in which g_N is the gap function calculated by Equation (5.21), and ε_N represents the penalty parameter in normal direction. Using the gap constraint, the two contact bodies in each time step can be sticking to or sliding on each other. In the stick condition the relative tangential displacement between the two bodies would be zero. As soon as the bodies slip on each other a tangential movement occurs, i.e., the tangential displacement is a non-zero value, known as slip. The tangential displacement, $\mathbf{t}_T$, and the tangential velocity, $\dot{\mathbf{t}}_T$, at the contact surface in a stick condition can be defined by

$$\begin{aligned} \mathbf{t}_T &= \varepsilon_T . \mathbf{g}_T^{st} \\ \dot{\mathbf{t}}_T &= \varepsilon_T . \dot{\mathbf{g}}_T^{st} \end{aligned} \tag{5.23}$$

where ε_T denotes the penalty parameter in the tangential direction and $\mathbf{g}_T^{st}$ is the stick constraint. Using the friction coefficient, μ, a slip criterion for a slave node sliding on the master boundary can be written based on the Coulomb friction law as follows

$$f_s = \|\mathbf{t}_T\| - \mu t_N \leq 0 \tag{5.24}$$

The value of μ depends on the material properties of the two bodies in contact. For a fixed contact pressure, the evolution equation for total slip can be defined as

$$\dot{\mathbf{g}}_T^{sl} = \dot{\lambda}_s \frac{\partial g_s(\mathbf{t}_T)}{\partial \mathbf{t}_T} = \dot{\lambda}_s \mathbf{n}_T \tag{5.25}$$

where $\dot{\lambda}_s$ is the slip parameter, $g_s = \|\mathbf{t}_T\|$ and $\mathbf{n}_T = \dfrac{\mathbf{t}_T}{\|\mathbf{t}_T\|}$.

In general, the slip criterion function is defined as

$$f_s(\mathbf{t}_T, t_N, g_v) = \|\mathbf{t}_T\| - h(t_N, g_v) = 0 \tag{5.26}$$

where g_v is the total sliding distance, t_N denotes the normal pressure and *h* is obtained from experimental observation. Therefore the principle of plasticity consistency yields

$$\dot{f}_s = \frac{\partial f_s}{\partial \mathbf{t}_T}\dot{\mathbf{t}}_T + \frac{\partial f_s}{\partial t_N}\dot{t}_N + \frac{\partial f_s}{\partial g_v}\dot{g}_v = \frac{\partial \|\mathbf{t}_T\|}{\partial \mathbf{t}_T}\dot{\mathbf{t}}_T + \frac{\partial h}{\partial t_N}\dot{t}_N + \frac{\partial h}{\partial g_v}\dot{g}_v = 0 \tag{5.27}$$

By considering $\dot{g}_v = \dot{\lambda}_s$ in Equations (5.25) and (5.27), the slip parameter can be obtained

using

$$\dot{\lambda}_s = \frac{1}{\varepsilon_T + \dfrac{\partial h}{\partial t_N}} \left(\varepsilon_T \mathbf{n}_T . \dot{\mathbf{g}}_T - \frac{\partial h}{\partial t_N} \varepsilon_N \dot{g}_N \right) \tag{5.28}$$

In an elasto-plastic model the total tangential velocity, $\dot{g}_T$, can be considered as the summation of the stick velocity, $\dot{g}_T^{st}$, and the slip velocity $\dot{g}_T^{sl}$. Thus, Equation (5.23) can be written in a rate form at the contact interface as

$$\dot{\mathbf{t}}_T = \varepsilon_T (\dot{\mathbf{g}}_T - \dot{\lambda}_s \mathbf{n}_T) \tag{5.29}$$

Substituting the value of $\dot{\lambda}_s$ from Equation (5.28) into (5.29) provides the incremental tangential motion at the contact interface as

$$\dot{\mathbf{t}}_T = \varepsilon_T \left[1 - \frac{\varepsilon_T}{\varepsilon_T + \dfrac{\partial h}{\partial g_v}} \mathbf{n}_T \otimes \mathbf{n}_T \right] \dot{\mathbf{g}}_T + \varepsilon_N \frac{\varepsilon_T}{\varepsilon_T + \dfrac{\partial h}{\partial g_v}} \frac{\partial h}{\partial t_N} \dot{g}_N \mathbf{n}_T \tag{5.30}$$

Therefore, the incremental tangential traction in a sliding motion can be computed knowing the tangential gap based on the total slip, $\dfrac{\partial h}{\partial g_v}$ and the normal gap based on the normal pressure, $\dfrac{\partial h}{\partial t_N}$. Comparing the Coulomb friction law in (5.24) with the general friction law in (5.26) one can consider $\dfrac{\partial h}{\partial t_N} = \mu$ provided $\dfrac{\partial h}{\partial g_v} = 0$. Therefore, Equation (5.30) can be rewritten for Coulomb friction model as

$$\dot{\mathbf{t}}_T = \varepsilon_T \left[1 - \mathbf{n}_T \otimes \mathbf{n}_T\right] \dot{\mathbf{g}}_T + \mu \varepsilon_N \dot{g}_N \mathbf{n}_T \tag{5.31}$$

b) Discretisation of the contact surfaces

In this work the node-to-segment contact method is used to solve the nonlinear finite element contact problems. In this method, the contact constraints considered for each slave node coming to contact with a straight or a curved segment on the master surface are shown in Figure 5.1. The Bezier polynomial can be used to present a smooth discretisation on the master surface. As shown in Figure 5.1, the slave node $\mathbf{x}_s$ is in contact with the segment defined by $\mathbf{x}_m^1 - \mathbf{x}_m^2$ on the master. To find the correct interpolation between $\mathbf{x}_m^1$ and $\mathbf{x}_m^2$ the neighbourhood nodes should be considered as well. Therefore, for each slave node two interpolating polynomials are defined, each including two tangent vectors and two middle nodes. The tangent vectors are formed by the lines between two adjacent nodes on the

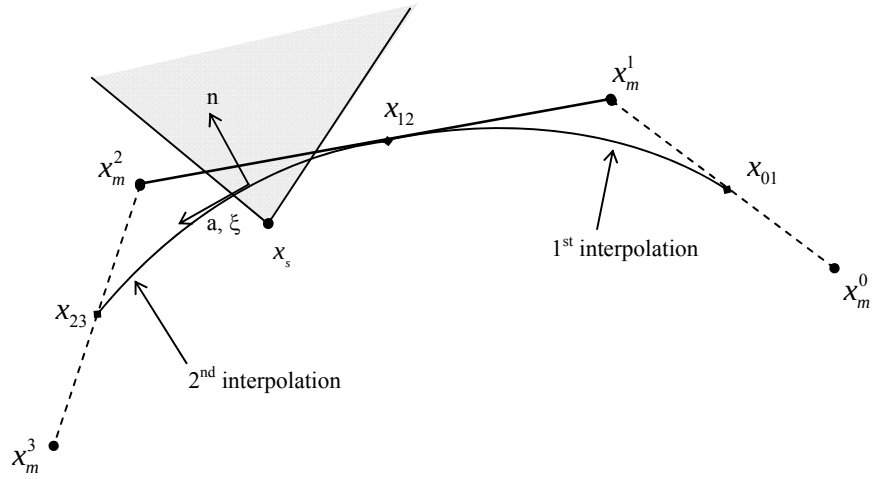

Figure 5.1. Smooth discretisation of the master surface in NTS contact

master surface. The active polynomial will be the one closer to the slave node, i.e., the second polynomial for the case shown in Figure 5.1.

Therefore, this interpolation is used to find the contact residual and the tangent matrix. Now, considering $\xi \in [-1,+1]$ as the normal projection of the slave node on the master surface the interpolation can be defined by

$$\mathbf{x}_m(\xi) = B_1(\xi)\mathbf{x}_{12} + B_2(\xi)\mathbf{x}_{12}^{+} + B_3(\xi)\mathbf{x}_{23}^{-} + B_4(\xi)\mathbf{x}_{23} \tag{5.32}$$

in which B_1, B_2, B_3 and B_4 are the Bezier interpolation functions, generally known as

$$\begin{aligned} B_1(\xi) &= \frac{1}{8}(1-\xi)^3 \\ B_2(\xi) &= \frac{3}{8}(1-\xi)^2(1+\xi) \\ B_3(\xi) &= \frac{3}{8}(1-\xi)(1+\xi)^2 \\ B_4(\xi) &= \frac{1}{8}(1+\xi)^3 \end{aligned} \tag{5.33}$$

and the nodes $\mathbf{x}_{12}$, $\mathbf{x}_{12}^{+}$, $\mathbf{x}_{23}^{-}$ and $\mathbf{x}_{23}$ form the convex hull of the interpolation. For the case shown in Figure 5.1, $\mathbf{x}_{12}^{+}$ and $\mathbf{x}_{23}^{-}$ are defined by

$$\mathbf{x}_{12}^{+} = \mathbf{x}_{12} + \frac{\alpha_B}{2}(\mathbf{x}_m^2 - \mathbf{x}_{12}), \quad \mathbf{x}_{23}^{-} = \mathbf{x}_{23} + \frac{\alpha_B}{2}(\mathbf{x}_m^2 - \mathbf{x}_{23}) \tag{5.34}$$

and the Bezier interpolation functions are based on three nodes as

$$\bar{B}_1(\xi) = \frac{1}{2}[B_1(\xi) + (1-\alpha_B)B_2(\xi)]$$
$$\bar{B}_2(\xi) = \frac{1}{2}[B_1(\xi) + (1+\alpha_B)(B_2(\xi) + B_3(\xi) + B_4(\xi))] \quad (5.35)$$
$$\bar{B}_3(\xi) = \frac{1}{2}[B_4(\xi) + (1-\alpha_B)B_3(\xi)]$$

when α_B is the parameter specifying the distance between the nodes $\mathbf{x}_{12}^{+}$ and $\mathbf{x}_{23}^{-}$ and the nodes $\mathbf{x}_{12}$ and $\mathbf{x}_{23}$, respectively. Obviously, the shape of active interpolation depends on the value of α_B. In the finite element model as the contact surfaces are deforming based on the displacement, α_B can change as the analysis proceeds. Typical value of α_B is 1/3. Since $\mathbf{x}_{12}$ and $\mathbf{x}_{23}$ are the middle points of the vectors $\mathbf{x}_m^1 - \mathbf{x}_m^2$ and $\mathbf{x}_m^2 - \mathbf{x}_m^3$, respectively, the interpolation described in Equation (5.32) can be changed to

$$\mathbf{x}_m(\xi) = \sum_{i=1}^{3} \bar{B}_i(\xi)\mathbf{x}_m^i, \quad \frac{\partial \mathbf{x}_m}{\partial \xi} = \sum_{i=1}^{3} \bar{B}_{i,\xi}(\xi)\mathbf{x}_m^i \quad (5.36)$$

c) Projection point

The projection point ξ of slave node on the master surface can be obtained using the nonlinear Equation (5.37) considering the minimal distance between the slave node and the master segment

$$\left[\mathbf{x}_s - \mathbf{x}_m(\xi)\right].\frac{\partial \mathbf{x}_m(\xi)}{\partial \xi} = 0 \quad (5.37)$$

The following equation can be solved in an iterative linear form using Newton's algorithm

$$\left\{\frac{\partial \mathbf{x}_m(\xi_i)}{\partial \xi}.\frac{\partial \mathbf{x}_m(\xi_i)}{\partial \xi}-[\mathbf{x}_s-\mathbf{x}_m(\xi_i)].\frac{\partial^2 \mathbf{x}_m(\xi_i)}{\partial \xi^2}\right\}\Delta\xi_{i+1}=[\mathbf{x}_s-\mathbf{x}_m(\xi_i)].\frac{\partial \mathbf{x}_m(\xi_i)}{\partial \xi} \qquad (5.38)$$
$$\xi_{i+1}=\xi_i+\Delta\xi_{i+1}$$

in which ξ_{i+1} represents the normal projection of the slave node on the master surface, ξ. The projection on the straight segment between $\mathbf{x}_m^1$ and $\mathbf{x}_m^2$ is considered as the starting value in the iteration, and is defined by

$$\xi_0=2\frac{(\mathbf{x}_s-\mathbf{x}_m^1).(\mathbf{x}_m^2-\mathbf{x}_m^1)}{(\mathbf{x}_m^2-\mathbf{x}_m^1).(\mathbf{x}_m^2-\mathbf{x}_m^1)}-1 \qquad (5.39)$$

d) Normal contact

The gap and its variation at the projection point ξ are obtained by

$$g_{N_s}=\left[\mathbf{x}_s-\sum_{i=1}^{3}\bar{B}_i(\bar{\xi})\mathbf{x}_m^i\right].\bar{\mathbf{n}}$$
$$\delta g_{N_s}=\left[\boldsymbol{\eta}_s-\sum_{i=1}^{3}\bar{B}_i(\bar{\xi})\boldsymbol{\eta}_i\right].\bar{\mathbf{n}}=\boldsymbol{\eta}_s^T\mathbf{B}_N(\bar{\xi}) \qquad (5.40)$$

Considering $\boldsymbol{\eta}_s^T=(\boldsymbol{\eta}_s^T,\boldsymbol{\eta}_1^T,\boldsymbol{\eta}_2^T,\boldsymbol{\eta}_3^T)$ as the vector of the nodal variations involved in desired polynomial and smoothed Bezier approximation, the gap variation can be stated as

$$\delta g_{N_s}=(\boldsymbol{\eta}_s^T,\boldsymbol{\eta}_1^T,\boldsymbol{\eta}_2^T,\boldsymbol{\eta}_3^T)\begin{Bmatrix}\bar{\mathbf{n}}\\-\bar{\mathbf{B}}_1(\bar{\xi})\bar{\mathbf{n}}\\-\bar{\mathbf{B}}_2(\bar{\xi})\bar{\mathbf{n}}\\-\bar{\mathbf{B}}_3(\bar{\xi})\bar{\mathbf{n}}\end{Bmatrix} \qquad (5.41)$$

Using the penalty method, the weak form of the normal contact can be written as

$$\int_{S_c} t_N \delta g_N dS = \int_{S_c} \varepsilon_N g_N \delta g_N dS \tag{5.42}$$

and can be approximated by

$$C_c \approx \sum_{s=1}^{n_c} \boldsymbol{\eta}_s^T [\varepsilon_N A_s g_{Ns} \mathbf{B}_N(\bar{\xi})] \tag{5.43}$$

in which, A_s, represents the area of the slave surface. Then, the contact residual for each slave node *s* and its associated active master segment can be defined in the form of below vector

$$\mathbf{F}_{N_s}^c = \varepsilon_N A_s g_{Ns} \mathbf{B}_n(\bar{\xi}) \tag{5.44}$$

To obtain the tangent matrix for one slave node, the linearisation of (5.43) is required. The variation of the normal gap is calculated by (Wriggers, 2002)

$$\begin{aligned} \Delta\delta g_N = &-(\frac{\partial \boldsymbol{\eta}^1}{\partial \xi}\Delta\xi + \Delta\frac{\partial \bar{\mathbf{u}}^1}{\partial \xi}\delta\xi + \frac{\partial^2 \bar{\mathbf{x}}_m}{\partial \xi^2}\Delta\xi\delta\xi).\bar{\mathbf{n}} + g_N\bar{\mathbf{n}} \\ &.(\frac{\partial \boldsymbol{\eta}^1}{\partial \xi} + \frac{\partial^2 \bar{\mathbf{x}}_m}{\partial \xi^2}\delta\xi)\frac{1}{\bar{a}_{11}}(\Delta\frac{\partial \bar{\mathbf{u}}^1}{\partial \xi} + \frac{\partial^2 \bar{\mathbf{x}}_m}{\partial \xi^2}\delta\xi).\bar{\mathbf{n}} \end{aligned} \tag{5.45}$$

where $\bar{a}_{11} = \frac{\partial \mathbf{x}^m(\bar{\xi})}{\partial \xi}.\frac{\partial \mathbf{x}^m(\bar{\xi})}{\partial \xi}$, and $\delta\xi$ is defined as

$$\partial\xi = \frac{1}{\bar{a}_{11} - g_N \dfrac{\partial^2 \mathbf{x}_m(\bar{\xi})}{\partial\xi^2}.\bar{\mathbf{n}}} \left\{ \left[\boldsymbol{\eta}^2 - \boldsymbol{\eta}^1 \right]. \frac{\partial \bar{\mathbf{x}}_m}{\partial\xi} + g_N \bar{\mathbf{n}}. \frac{\partial \boldsymbol{\eta}^1}{\partial\xi} \right\} \tag{5.46}$$

in which

$$\frac{\partial \boldsymbol{\eta}^1}{\partial\xi}.\bar{\mathbf{n}} = \boldsymbol{\eta}_s^T \mathbf{B}_{N,\xi}(\bar{\xi}) \tag{5.47}$$

and

$$\left[\boldsymbol{\eta}^2 - \boldsymbol{\eta}^1 \right]. \frac{\partial \bar{\mathbf{x}}_m}{\partial\xi} = \boldsymbol{\eta}_s^T \mathbf{B}_T(\bar{\xi}) \tag{5.48}$$

Equation (5.46) can be rewritten in the following form

$$\partial\xi = \boldsymbol{\eta}_s^T \left\{ H_{\xi\xi}^{-1} \left[\mathbf{B}_T(\bar{\xi}) + g_{N_s} \mathbf{B}_{N,\xi}(\bar{\xi}) \right] \right\} = \boldsymbol{\eta}_s^T \mathbf{B}_\xi(\bar{\xi}) \tag{5.49}$$

with $H_{\xi\xi}^{-1} = (\bar{a}_{11} - g_N \bar{\mathbf{n}} \dfrac{\partial^2 \mathbf{x}_m(\bar{\xi})}{\partial\xi^2})^{-1}$. Now, using the above derivation, the stiffness matrix for one slave node *s* is defined as

$$\begin{aligned} \mathbf{K}_{Ns} = \varepsilon_N A_s \{ & \mathbf{B}_N(\bar{\xi})(\mathbf{B}_N(\bar{\xi}))^T - g_{N_s} [\mathbf{B}_{N,\xi}(\bar{\xi})(\mathbf{B}_\xi(\bar{\xi}))^T \\ & + \mathbf{B}_\xi(\bar{\xi})(\mathbf{B}_{N,\xi}(\bar{\xi}))^T + \bar{b}_{\xi\xi}^1 \mathbf{B}_\xi(\bar{\xi})(\mathbf{B}_\xi(\bar{\xi}))^T \\ & - \frac{g_{Ns}}{\left\| \dfrac{\partial \bar{\mathbf{x}}_m}{\partial\xi} \right\|^2} \left[\mathbf{B}_{N,\xi}(\bar{\xi}) + \bar{b}_{\xi\xi}^1 \mathbf{B}_\xi(\bar{\xi}) \right] \left[\mathbf{B}_{N,\xi}(\bar{\xi}) + \bar{b}_{\xi\xi}^1 \mathbf{B}_\xi(\bar{\xi}) \right]^T \Big] \} \end{aligned} \tag{5.50}$$

in which $\bar{b}^1_{\xi\xi} = \dfrac{\partial^2 \bar{\mathbf{x}}_m}{\partial \xi^2}.\bar{\mathbf{n}}$.

e) Tangential contact

The incremental tangential displacement at time $t_{n+1} = t_n + \triangle t$ can be defined based on the change of the surface coordinate ξ as

$$\Delta g_{Tn+1} = (\xi_{n+1} - \xi_n) \frac{\partial \mathbf{x}_m(\xi_{n+1})}{\partial \xi} \tag{5.51}$$

Therefore, the tangential component of the traction in Equation (5.23) is given by

$$\mathbf{t}^{tr}_{Tn+1} = \mathbf{t}_{Tn} + \varepsilon_T \Delta g_{Tn+1} \tag{5.52}$$

for current time step. Using the stick and slip criterion in (5.24), the tangential force at the contact point is given by

$$\begin{aligned} \mathbf{t}_{Tn+1} &= \mathbf{t}^{tr}_{Tn+1} && \textit{in stick case} \\ \mathbf{t}_{Tn+1} &= \mu \varepsilon_N g_{Nn+1} \mathbf{n}^{tr}_{Tn+1} && \textit{in slip case} \end{aligned} \tag{5.53}$$

in which

$$\mathbf{n}^{tr}_{Tn+1} = sign(\xi_{n+1} - \xi_n) \frac{\dfrac{\partial \mathbf{x}_m(\xi_{n+1})}{\partial \xi}}{\left\| \dfrac{\partial \mathbf{x}_m(\xi_{n+1})}{\partial \xi} \right\|} = sign(\xi_{n+1} - \xi_n) \mathbf{a}^1(\xi_{n+1}) \tag{5.54}$$

Equation (5.53) can be also considered in general form $\mathbf{t}_{T_{n+1}} = \gamma_{n+1}\mathbf{a}^1(\xi_{n+1})$ with

$$\begin{aligned} \gamma_{n+1} &= \varepsilon_T(\xi_{n+1} - \xi_{n+1})\left\|\frac{\partial \mathbf{x}_m(\xi_{n+1})}{\partial \xi}\right\| \qquad stick \\ \gamma_{n+1} &= \mu\varepsilon_N g_{Nn+1} sign(\xi_{n+1} - \xi_n) \qquad slip \end{aligned} \tag{5.55}$$

The weak form of tangential contact can be approximated by

$$C_T \approx \sum_{s=1}^{n_c} \delta g_{T_s}.\mathbf{t}_{Tn+1} A_s \tag{5.56}$$

Considering the variation of relative tangential displacement as

$$\delta g_T = \delta\xi \frac{\partial \mathbf{x}_m(\xi)}{\partial \xi} \tag{5.57}$$

the residual can be written as

$$C_T \approx \sum_{s=1}^{n_c} \delta\xi \frac{\partial \mathbf{x}_m(\xi_{n+1})}{\partial \xi}.\gamma_{n+1}\mathbf{a}^1(\xi_{n+1})A_s = \delta\xi \left\|\frac{\partial \mathbf{x}_m(\xi_{n+1})}{\partial \xi}\right\| \gamma_{n+1} A_s \tag{5.58}$$

Therefore, the nodal force vector for one slave nose *s* is defined as

$$\mathbf{F}_{Ts}^c = \left\|\frac{\partial \mathbf{x}_m(\xi_{n+1})}{\partial \xi}\right\| \gamma_{n+1} A_s \mathbf{B}_\xi(\xi_{n+1}) \tag{5.59}$$

Note that g_N in Equation (5.49) can be neglected for the case of relatively small deformations and, therefore, Equation (5.59) can be written as

$$\mathbf{F}_{Ts}^{clin} = \gamma_{n+1} A_s \mathbf{B}_T(\xi_{n+1}) \tag{5.60}$$

where

$$\mathbf{B}_T = \begin{Bmatrix} \dfrac{\partial \overline{\mathbf{x}}_m}{\partial \xi} \\ -\overline{B}_1(\xi)\dfrac{\partial \overline{\mathbf{x}}_m}{\partial \xi} \\ -\overline{B}_2(\xi)\dfrac{\partial \overline{\mathbf{x}}_m}{\partial \xi} \\ -\overline{B}_3(\xi)\dfrac{\partial \overline{\mathbf{x}}_m}{\partial \xi} \end{Bmatrix} \tag{5.61}$$

The linearisation of the residual in (5.60), provides the tangent matrix for a stick and a slip case as

$$\begin{aligned} \mathbf{K}_{Ts}^{stick} &= \varepsilon_t A_s \overline{\mathbf{B}}_T(\xi_{n+1})(\overline{\mathbf{B}}_T(\xi_{n+1}))^T \\ \mathbf{K}_{Ts}^{slip} &= -\mu\varepsilon_N sign(\xi_{n+1} - \xi_n) A_s \overline{\mathbf{B}}_T(\xi_{n+1})(\mathbf{B}_N(\xi_{n+1}))^T \end{aligned} \tag{5.62}$$

5.3.5 Retrieving dynamic equilibrium

After remapping the state variables, equilibrium in the new mesh is yet to be satisfied. Moreover, for elastoplastic soil models, the principle of plasticity consistency may be violated due to some stress points lying outside the yield surface. In this study, we use the Newmark integration scheme to conduct further iterations to guarantee equilibrium as well as plasticity consistency. Employing the Newton-Raphson method, the following equation needs to be solved in each iteration

$$\left[\frac{\mathbf{M}}{\beta\cdot\Delta t^2}+\frac{\mathbf{C}}{\beta\cdot\Delta t}+\mathbf{K}_{(i-1)}\right]\cdot\Delta\mathbf{u}_{(i)}=\Delta\mathbf{F}_{ext}^{t+\Delta t}-\Delta\mathbf{F}_{int(i-1)}^{t+\Delta t}-\mathbf{M}\left[\frac{\mathbf{u}_{(i-1)}^{t+\Delta t}-\mathbf{u}^{t}}{\beta\cdot\Delta t^2}-\frac{\dot{\mathbf{u}}^{t}}{\beta\cdot\Delta t}-\frac{(1-2\beta)\ddot{\mathbf{u}}^{t}}{2\beta}\right]$$
$$-\mathbf{C}\left[\frac{\alpha\left(\mathbf{u}_{(i-1)}^{t+\Delta t}-\mathbf{u}^{t}\right)}{\beta\cdot\Delta t}+\frac{(\beta-\alpha)\dot{\mathbf{u}}^{t}}{\beta}+\Delta t\left(1-\frac{\alpha}{2\beta}\right)\ddot{\mathbf{u}}^{t}\right] \tag{5.63}$$

5.4. *h*-ADAPTIVITY AND DYNAMIC/CONTACT ANALYSIS

The dynamic/contact analysis by the *h*-adaptive finite element method presented here includes four main steps. In the first step, the Updated Lagrangian (UL) method is employed to solve the global governing equations to achieve dynamic equilibrium. Secondly, a new finite element mesh is generated based on the new sizes of the elements, usually obtained by an error estimator which calculates the error in each element and determines which regions of the mesh domain should be subdivided into smaller elements. In the third step, all nodal variables and state variables at integration points are transformed (or mapped) from the old mesh to the newly generated mesh. Finally, an automatic procedure must be employed to check that dynamic equilibrium is satisfied at the global level and to check that the principle of plasticity consistency is satisfied at each integration point inside all elements.

The implementation of the *h*-adaptive finite element method for the problems involving inertia forces and changing boundary conditions required significant improvement of several components of the finite element *h*-adaptive engine. As in nonlinear *h*-adaptivity the discretisation of the domain changes almost in each increment throughout the analysis, there are various contact/dynamic related parameters which need to be reconstructed based

on the new mesh. The energy absorbing boundaries, which are defined with a set of nodes and segments, need to be redefined considering the new nodes and segments generated on those boundaries. In contact problems considering Node-to-Segment algorithm, the discretisation on the slave body is usually finer than the mesh on the master body. In the adaptive procedure presented in this work, the slave body is free to refinement while the topology of the master body may remain unchanged during the analysis. Therefore, keeping records of the contact points between two surfaces (finding two master nodes for each slave node) is a considerable challenge as the number of mesh points on the slave surface gradually increases during the analysis. It involves reallocating the node and element related arrays which store the data such as the boundary information and contact surfaces, according to the new size of the mesh and then setting the related values (e.g. gap in contact) for each node and element based on the available values in the previous mesh. Obviously for the nodes and elements which didn't exist in the previous mesh, the corresponding data need to be calculated based on their virtual place in the old mesh. In addition, in large deformation problems the gap, a closest point projection on the slave surface to the master surface, needs to be computed in each increment. One of the main concerns is in considering the contact/dynamic related parameter such as the velocity and the mass acceleration in the equilibrium equations. Also, as the domain of the problem is consistently changing due to the necessary *h*-adaptive refinement, the velocity and the mass acceleration arrays need to be reconstructed, sufficient memory needs to be allocated for each of them and their values need to be remapped from the previous mesh to the new mesh. This can be done using the same techniques which have been used in remapping the

displacements and the state variables as explained in section 4.4. In addition, the stiffness, mass and damping matrices need to be regenerated considering their new size which is growing as the number of elements and nodes in the new mesh increase. On the other hand, it has been noticed when using the *h*-adaptive technique in a dynamic analysis, the time stepping and minimum element area considered for the refinement in each increment can have significant effects on the accuracy of the result. It is important to avoid any dramatic changes in the area of the element between two increments as it can easily lead the analysis to a severe mesh distortion.

In the present work, author has not considered adaptive time stepping to solve the problem. The current *h*-adaptive method mainly concerns on the way discretisation is refined to achieve an accurate solution. Obviously by considering an adaptive time stepping the result would tend to be more accurate. To get the better result, the time stepping has forced in the analysis by dividing the total time in small section considering different minimum element area for refinement in each section. By doing so, the element tend to refine gradually throughout the analysis.

CHAPTER 6

COMBINED *rh*-ADAPTIVE FINITE ELEMENT METHOD

6.1. INTRODUCTION

The adaptive methods have been used in a wide range of engineering problems to overcome mesh distortion issue due to large deformations or to achieve more accurate results using less number of elements. In solid mechanics the most commonly used adaptive techniques include *r*-adaptive and *h*-adaptive. Although these two adaptive methods are proved to be robust in solving different kind of problems, there are individual drawbacks within each method due to its nature. *r*-adaptive finite element method has been designed to eliminate possible mesh distortion by changing and optimising the location of nodal points without modifying the topology of the problem. Therefore, to obtain an accurate solution by this method a relatively fine mesh is required at the beginning of the analysis, which increases the analysis time. It is clear that the accuracy as well as the efficiency of the *r*-adaptive method rely critically on the density of the initial mesh, which in turn depends on the analyst's experience and the problem being studied. On the other hand, *h*-adaptive finite element method improves the accuracy of the solution by gradually decreasing the size of the elements based on an error assessment approach. In this method the initial density of the mesh is not usually important as it changes dramatically during the analysis. Based on an error assessment criterion and an acceptable error tolerance, some elements may be subdivided into new smaller elements. As the size of an element decreases, its vulnerability to distortion, viz., negative Jacobian or a large aspect ratio, increases. In the case of large deformations, a negative Jacobian of an individual element can lead to spontaneous termination of the analysis.

In solid mechanics, the combination of *r*- and *h*-adaptive methods was first presented within the framework of the boundary element method for solution of two dimensional problems (Ammons and Vable; 1998, Cao 1998; and Kita et al. 2000). Later, Askes and Rodriguez-Ferran (2001) combined these two adaptive methods in a finite element framework. Their work was based on assessing the error of the finite element domain and then finding an optimum size for each element. Based on the current element size, *r*-adaptivity or *h*-adaptivity would be applied to refine or to generate a new mesh in the finite element domain. Lang et al. (2003) used the *rh*-adaptivity in a two-dimensional moving finite element technique for solving the nonlinear time-dependent problems in fluid dynamics. Their work was an extent to some early presentation of *rh*-adaptivity in moving mesh finite element problems such as, Arney and Flaherty (1989) and Habashi et al. (2000). The combination of *r*-adaptive and *h*-adaptive finite element method in computational geomechanics has not been addressed in the literature to date.

To eliminate the individual drawbacks of the *r*- and *h*-adaptive methods, and yet preserve the accuracy of the solution, a combined *rh*-adaptive finite element method for analysis of geotechnical problems is presented in this chapter. This method can be used in static as well as dynamic analysis of sophisticated problems of geomechanics involved with large deformations and changing boundary conditions. The proposed method is designed to improve the accuracy of the solution by the *h*-refinement strategy presented in Chapters 4 and 5 while it handles mesh distortion issue by an *r*-adaptive refinement based on the Arbitrary Lagrangian-Eulerian (ALE) operator split technique developed by Nazem (2006).

This chapter is divided into two main sections. The first section discusses the *r*-adaptive finite element method based on the ALE operator split technique. The second section of this chapter is concerned with the new combined *rh*-adaptive strategy developed for nonlinear problems of geomechanics. The robustness as well as efficiency of this new *rh*-adaptive method will be presented by solving a number of numerical examples in Chapter 7 of the Thesis.

6.2. ALE METHOD

The kinematics of continuum mechanics problems are traditionally described in two main frameworks, namely as Eulerian and Lagrangian. In a Lagrangian description of motion, which is commonly used in solid mechanics, the material particles are followed by tracing their spatial position in time. On the other hand, the motion of matter can be described by recording the flow of physical particles along a fixed position in space. This approach is known as Eulerian description, and it is commonly used in fluid mechanics. In the literature, it is well recognised that the Eulerian and Lagrangian frameworks have their drawbacks, particularly when applied to a numerical analysis strategy. For instance, the finite element method based on a Lagrangian framework usually fails to provide a solution in problems with relatively large deformations because the finite element (grid) nodes are attached one-to-one to the material points. On the other hand, Eulerian grids are attached one-to-one to space, so that large boundary motion of the material cannot be accounted for accurately. An ambiguity will exist in description of the interface zone in a fluid-structure interaction problem if the structure and the fluid are described by a Lagrangian and an

Eulerian method, respectively. Such limitations motivated the researchers to develop a combined Lagrangian-Eulerian framework to describe the motion of a continuum, which is now named as the Arbitrary Lagrangian-Eulerian (ALE) method. Noh (1964) initially suggested the concept of the ALE under the term 'Coupled Eulerian-Lagrangian', and employed the method to solve hydrodynamics problems with moving fluid boundaries using a finite difference framework. Belytschko and Kennedy (1978) presented one of the first applications of the ALE method in a finite element framework to solve fluid-structure interaction problems.

Researchers soon realised that the ALE method can be used in tackling solid mechanics problems involved with mesh distortion since the motion of the mesh points can be described arbitrarily. In the ALE method, the displacement of material points and the grid points can be coupled in the global equations. This coupling introduces a set of unknown mesh displacements into the global governing equations thus requiring a supplementary set of linear equations to be solved simultaneously. In the so-called coupled ALE method, this new set of equations is usually expressed in terms of the material displacements and the mesh displacements. Therefore, in a coupled ALE method the number of unknown displacements is normally doubled, which increases the computational time significantly. Benson (1989) presented an alternative ALE strategy in a decoupled form, called the operator split technique. In this method the analysis is performed in two steps: an Updated-Lagrangian (UL) step and an Eulerian step. In the UL step, the global equations, written in terms of material displacements only, are solved to satisfy the equilibrium. Then, the spatial coordinates of the material points are updated according to the incremental

displacements. At this stage, mesh distortion may potentially occur. In the Eulerian step, a new arbitrary mesh is generated for the entire finite element domain without changing the number of nodes, the number of elements, and their connectivity. Then, all state variables at nodal points as well as the integration points, such as displacements, velocities, and stresses, are transformed from the old mesh to the new mesh. The operator split technique is more suitable to be combined with the *h*-adaptive finite element method explained in Chapter 4. Therefore, the combined *rh*-adaptive strategy developed in this Thesis is based upon the combination of the ALE operator split technique and the *h*-adaptive procedure explained previously.

Although well established in solid mechanics, the ALE operator split method has attracted less attention in geomechanics with a few exceptions. Nazem et al. (2006) presented the application of the ALE method in tackling large deformation of geomechanics by developing a new mesh refinement technique based upon the relocation of nodes along boundaries followed by a static analysis. This robust technique was then extended to the solution of consolidation problems of geomechanics by Nazem et al. (2008) as well as dynamic analysis of geotechnical problems involved with large deformations by Nazem et al. (2009). Di and Sato (2007) also employed the ALE operator split technique to solve consolidation problems involved with large deformations.

The combined *rh*-adaptive strategy explained in this chapter is based upon the operator split technique developed by Nazem et al. (2006). The ALE operator split technique attempts to eliminate the mesh distortion by refining the finite element mesh without changing the

number of nodal points, number of elements, and their connectivity. This method outperforms the coupled ALE procedure by dividing the number of unknowns in the global equations in half. The analysis by the operator split technique includes two phases. The first phase includes solving the problem by the UL method, as explained in Section 5.3. The second phase is mainly concerned with refining the finite element mesh to avoid distortion, followed by transferring the state variables from the old mesh to the new mesh.

6.2.1. Mesh refinement

The *r*-refinement procedure, coupled with the *h*-adaptive technique in this study, is based on the method developed by Nazem et al. (2006), and is slightly modified here. This method is schematically shown in Figure 6.1, and is explained in the following.

Figure 6.1a shows a typical finite element mesh at the beginning of a new time step. The boundaries of the problem, including the material interfaces and the boundaries of each discrete body, are shown by solid lines. At the end of the UL step in the operator split technique the incremental material displacements, Δu_i, are known and the current spatial coordinates of all material points, $x^{t+\Delta t}$, are obtained according to their last known position, x^t, by

$$x_i^{t+\Delta t} = x_i^t + \Delta u_i \tag{6.1}$$

In problems involved with relatively large deformations, the resulting mesh may be distorted, or vulnerable to distortion in future increments. The mesh at the end of the UL

step, representing a potential distortion, is shown in Figure 6.1b. To refine the mesh, the nodes are relocated along the boundaries considering that the normal component of displacement on a boundary is zero, viz, the nodes are only permitted to move in the tangential direction of the boundary. For this purpose, the boundaries are divided into quadratic functions (Nazem et al., 2008) using a spline interpolation technique (Lopez, 2001). Then all nodes are relocated along the boundaries, as depicted in Figure 6.1c. The nodal relocation provides the prescribed mesh displacements of the nodes on the boundaries. The values of prescribed displacements are then applied on the mesh at time *t* (Figure 6.1a), and an elastic analysis is conducted to find the incremental mesh displacement of all other nodes, Δu_i^r, assuming small deformations only. Finally, the new spatial coordinates of the nodes in the new mesh at the end of the increment, $\left(x_i^r\right)^{t+\Delta t}$, are obtained by adding the incremental mesh displacements to the nodal coordinates of the mesh at the beginning of the increment, according to

$$\left(x_i^r\right)^{t+\Delta t} = x_i^t + \Delta u_i^r \tag{6.2}$$

Note that this mesh optimisation technique guarantees that the new mesh and the old mesh share the same number of nodes, number of elements and connectivity. The nodal relocation procedure is probably the most important component of the mesh optimisation technique developed by Nazem et al. (2006), and it depends on the initial configuration of the boundaries at time 0 as it uses the normalised length of all segments on a boundary. However, when combined with the *h*-adaptive technique, the initial configuration of the

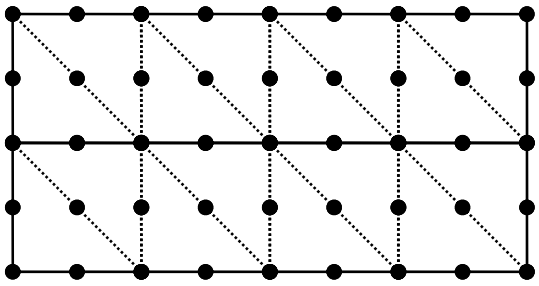

a. Finite element mesh at time t

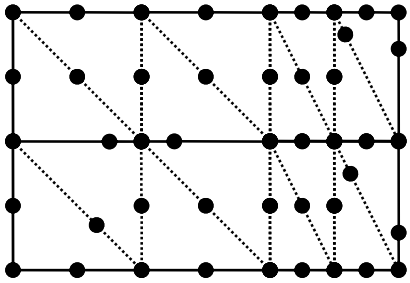

b. Deformed (possibly distorted) mesh at the end of UL step at time $t + \Delta t$

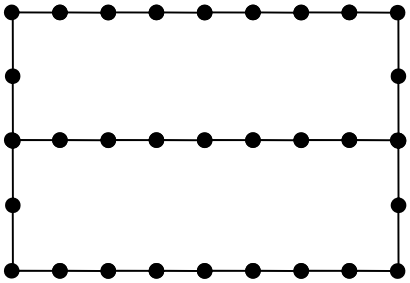

c. Boundaries after the nodal relocation at time $t + \Delta t$

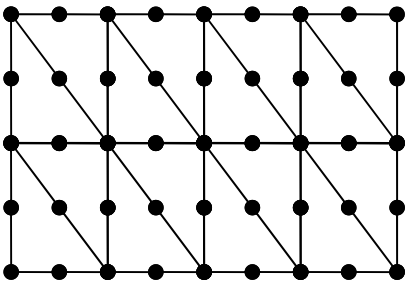

d. Refined mesh after elastic static analysis at time $t + \Delta t$

Figure 6.1. Mesh refinement procedure in the ALE method

newly generated nodes on a boundary cannot be estimated accurately. Therefore, in the combined *rh*-adaptive method developed here, the normalised lengths of the segments after the last *h*-adaptive refinement will be used.

6.2.2. Remapping of state variables

The remapping of state variables, such as stresses, is usually done by using the convection equation as

$$\Delta f^r = \Delta f + (u_i^r - u_i) \cdot \frac{\partial f}{\partial x_i} \tag{6.3}$$

where Δf^r and Δf denote the increments of an arbitrary state variable f with respect to the mesh and material coordinates, respectively, u is the material displacements and u^r represents the mesh (grid) displacements. For two-dimensional problems, the gradients of f are calculated using the chain rule according to

$$\begin{aligned} \frac{\partial f}{\partial x_1} &= \frac{\partial f}{\partial \xi} \cdot \frac{\partial \xi}{\partial x_1} + \frac{\partial f}{\partial \eta} \cdot \frac{\partial \eta}{\partial x_1} \\ \frac{\partial f}{\partial x_2} &= \frac{\partial f}{\partial \xi} \cdot \frac{\partial \xi}{\partial x_2} + \frac{\partial f}{\partial \eta} \cdot \frac{\partial \eta}{\partial x_2} \end{aligned} \tag{6.4}$$

where ξ and η, represent the normal coordinates. For an n-node element, the local derivatives of f are computed by

$$\frac{\partial f}{\partial \xi} = \sum_{k=1}^{n} \frac{\partial N_k}{\partial \xi} \cdot f^k$$
$$\frac{\partial f}{\partial \eta} = \sum_{k=1}^{n} \frac{\partial N_k}{\partial \eta} \cdot f^k \tag{6.5}$$

in which N is the nodal shape function. Note that f^k represent the nodal values of f which are obtained by the super convergent patch recovery technique explained in Section 4.4.

6.3. COMBINED *rh*_ADAPTIVE METHOD

In this section, the combined *rh*-adaptive finite element procedure will be explained. The first step of the *rh*-adaptive method includes an Updated-Lagrangian analysis. Then, the error in the finite element solution is measured by an error estimator technique. If the error is larger than a prescribed tolerance the *h*-adaptive component will be provoked to determine new element sizes. Otherwise, the analysis will proceed by the ALE strategy to eliminate possible mesh distortion. For clarity, the required algorithm is illustrated schematically in Figure 6.2. Each step of the analysis of a general problem of dynamic elastoplasticity is explained in more detail in the following.

(1) Start the analysis by generating a relatively coarse mesh.

(2) Perform Steps (3) to (26) for each time increment.

(3) Perform Steps (4) to (10) for each iteration.

(4) Form the effective stiffness matrix according to Equation (5.11).

(5) Form the global equations as in (5.10) and solve for incremental displacements $\Delta \mathbf{u}_i$.

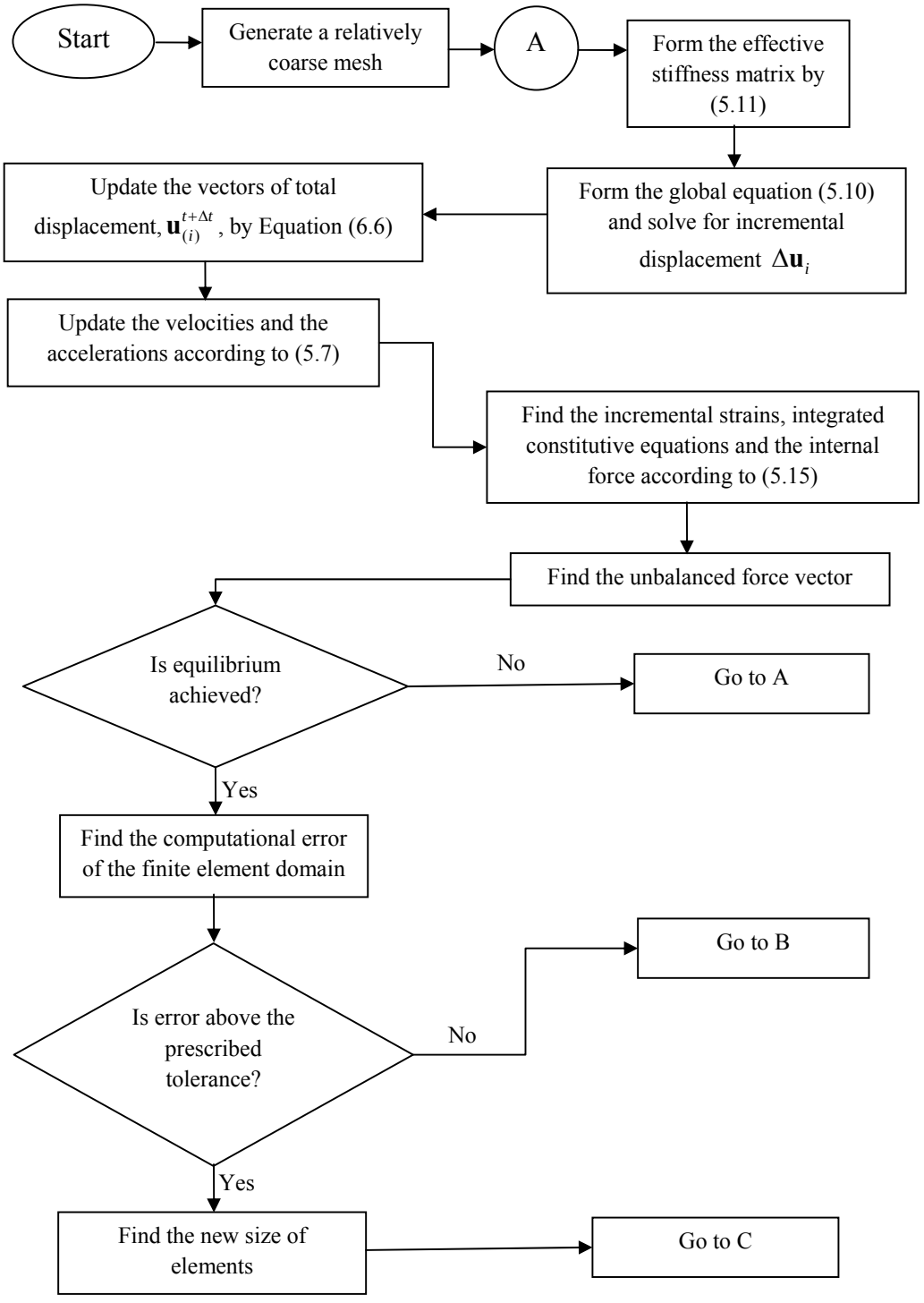

Figure 6.2. Procedure for combined *rh*-adaptive finite element analysis

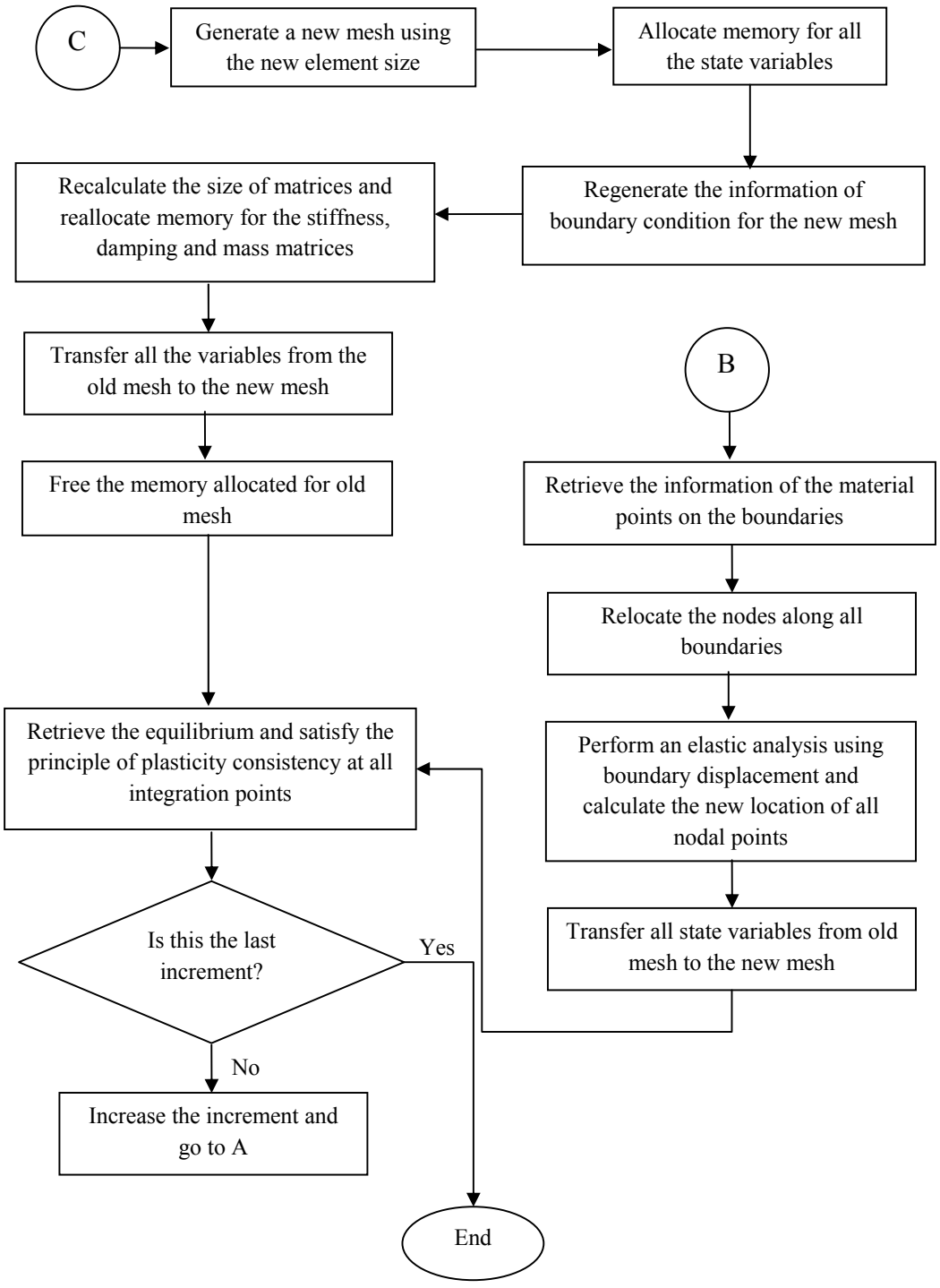

Figure 6.2. Procedure for combined *rh*-adaptive finite element analysis (cont'd)

(6) Update the vectors of total displacements, $\mathbf{u}_{(i)}^{t+\Delta t}$, by

$$\mathbf{u}_{(i)}^{t+\Delta t} = \mathbf{u}_{(i-1)}^{t+\Delta t} + \Delta\mathbf{u}_{(i)} \tag{6.6}$$

(7) Update the velocities and the accelerations according to equations in (5.7).

(8) Find the incremental strains, integrate constitutive equations, and find the internal force vector according to (5.15).

(9) Find the unbalanced force vector and check for equilibrium.

(10) If the equilibrium is achieved, exit the iteration loop. Otherwise, go to Step (4).

(11) Find the computational error of the finite element domain using an error assessment technique.

(12) If the error is greater than a prescribed tolerance, calculate the new size of each element assuming an equal distribution of error over the elements. Otherwise, go to step (18).

(13) Generate a new mesh for the entire domain of the problem based on the new size of the elements.

(14) Allocate memory for all state variables in the new mesh, including stresses, internal and external force vectors, contact force vector, displacements, velocities, and accelerations.

(15) Regenerate the information of boundary conditions for the new mesh, including supports, prescribed displacements, and the contact surfaces.

(16) Recalculate the size of matrices and reallocate memory for the stiffness, damping and mass matrices.

(17) Go to Step (23).

(18) Retrieve the information of the material points on the boundaries.

(19) Relocate the nodes along all boundaries,

(20) Perform an elastic analysis using boundary displacements obtained in Step (19) as prescribed nodal displacements, and calculate the new locations of all nodal points.

(21) Transfer all state variables from the old mesh to the new mesh as explained in Section 6.2.2.

(22) Go to Step (25)

(23) Transfer all state variables from the old mesh to the new mesh as explained in Section 4.4.

(24) If required, free the memory allocated for old mesh.

(25) Retrieve the equilibrium and the satisfy the principle of plasticity consistency at all integration points by conducting further iterations as explained in Section 5.3.4.

(26) If this is the last increment, exit with the solution. Otherwise, go to Step (2), increasing the increment number.

CHAPTER 7

APPLICATIONS

7.1. INTRODUCTION

The *h*-adaptive and the *rh*-adaptive finite element methods presented in the previous chapters have been implemented into SNAC, the in-house finite element code developed by the Geotechnical Group at the University of Newcastle, Australia. SNAC has been used to analyse the numerical examples in this section. Although the methods described in this Thesis can be used to analyse general large deformation problems in continuum mechanics, applications are limited to geotechnical problems here.

7.2. NUMERICAL EXAMPLES

This chapter includes 8 numerical examples. The first three examples present the application of the *h*-adaptive finite element method in tackling large deformation problems of geomechanics, and they address the cylindrical cavity expansion problem, the biaxial test, and the large deformation analysis of a strip footing. The error estimator used in the first three examples is based only on the energy norm. The forth and the fifth examples present a comparative study of three error estimation techniques introduced in Chapter 4 of this Thesis. These error estimation techniques include the energy norm, the Green-Lagrange strain, and the rate of plastic dissipation. The efficiency and applicability of these techniques are studied by analysing the soil behaviour under a rigid footing undergoing static as well as dynamic loads, and the penetration of a cone into a soil layer at slow and fast rates. The last three numerical examples address the efficiency and robustness of the *rh*-adaptive technique, developed in Chapter 6 of this Thesis, compared to the *h*-adaptive

finite element method. This is conducted by analysing a vertical cut, the indentation of a cylindrical object into a soil layer, and the bearing capacity of a two-layered soil under a rigid footing.

All examples have been analysed using 6-node triangular elements, with six integration points. Since the performance of such elements for the problems solved is quite satisfactory, other types of elements, such as quadrilateral rectangles, have not been used here. On a smooth boundary the displacements are restrained in the normal direction only while the displacements of a coarse (or rigid) boundary are restrained in the normal as well as the tangential directions. For some examples, a very fine mesh has been employed without refinement to produce benchmark results. These benchmarks are then used to check the results of a coarse mesh without refinement and the effect of the *h*-adaptive procedures.

It should be noted that the *h*-adaptive finite element method is able to analyse the problem in hand based on a desired degree of accuracy. The minimum element area in each example is approximately the largest value of area which can provide results within a prescribed precision.

7.2.1. Elastoplastic cylindrical cavity expansion

The cavity expansion problem is one of the few cases that can be solved analytically using finite-strain plasticity, and is thus very useful for validating the finite element analyses. The internal radius of a cylindrical cavity is denoted as r_0 while the outer radius is set to $60r_0$.

To simulate the effects of an infinite medium, a correcting elastic layer is added to the soil layer (Burd, 1986). Figure 7.1 represents the boundary conditions and material properties of the cavity used in this analysis. The soil is modelled by a Tresca material. In Figure 7.1, G, s_u, and ν, respectively, represent the shear modulus, the undrained shear strength, and Poisson's ratio of the soil. A total prescribed radial displacement of magnitude $6r_0$ is

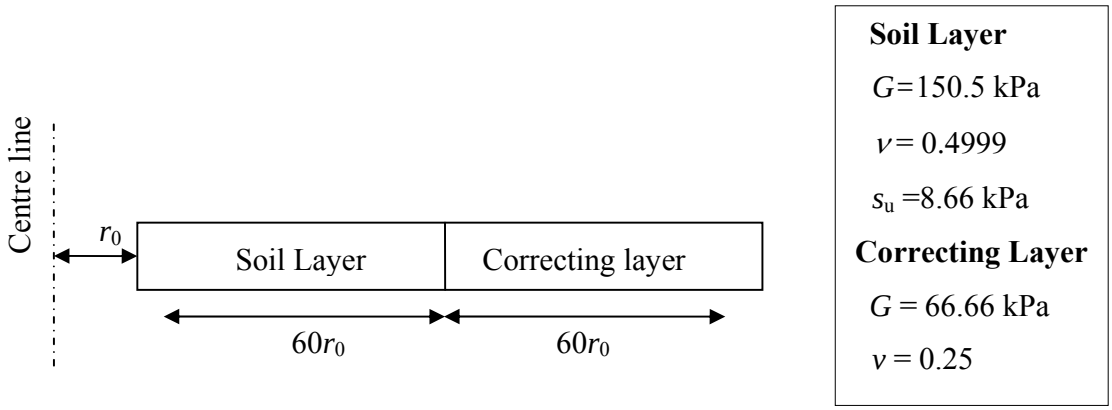

Figure 7.1. The cavity expansion problem (geometry not to scale)

applied over 200 equal time increments.

The analytical solution according to Yu (2000) is:

$$\frac{\Psi}{s_u} = 1 + \ln\left[\frac{G}{s_u}\left(1 - \frac{r_0^2}{r^2}\right) + \frac{r_0^2}{r^2}\right] \tag{7.1}$$

where Ψ represents the internal pressure of the cavity and r is the current internal radius of the cavity. The numerical solution for the normalised internal pressure of the cavity

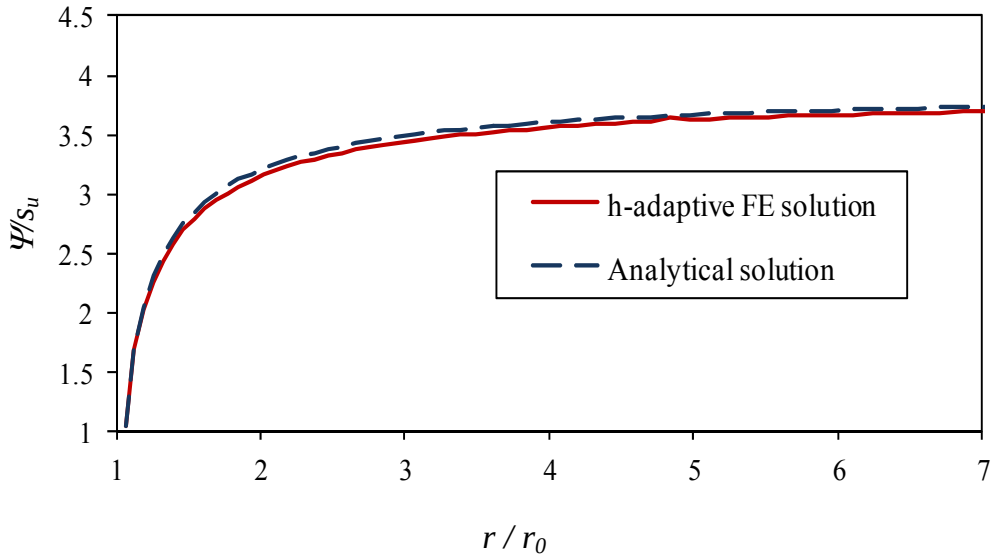

Figure 7.2. Normalised internal pressure of cavity versus normalised radial displacement

versus the normalised radial displacement is compared with the analytical solution in Figure 7.2. Good agreement between the analytical and the numerical solutions is observed.

7.2.2. Biaxial test

In this example, a biaxial test is simulated using the Mohr-Coulomb model with a non-associated flow rule. The problem is analysed for two different scenarios. In the first case, the soil specimen is assumed to have uniform properties over the entire domain. In the second case, a small area in the soil specimen is assumed to have a different set of material parameters than the rest of the specimen, to initiate localised failure.

The geometry of the problem, material properties and boundary conditions are shown in Figure 7.3. The soil is modelled using a rounded Mohr-Coulomb model proposed by Sheng et al. (2000):

$$q = \frac{6\sin\phi'}{3-\sin\phi'}\left(\frac{2\alpha^4}{1+\alpha^4-(1-\alpha^4)\sin 3\theta}\right)^{1/4}\left(p'+\frac{c'}{\tan\phi}\right), \qquad \alpha = \frac{3-\sin\phi'}{3+\sin\phi'} \tag{7.2}$$

where q is the deviator stress, p is the effective mean stress, and θ is the Lode angle. In Figure 7.3, E', c', ϕ' and ψ' represent the drained Young's modulus, the drained cohesion, the drained friction angle of the soil and the dilation angle, respectively.

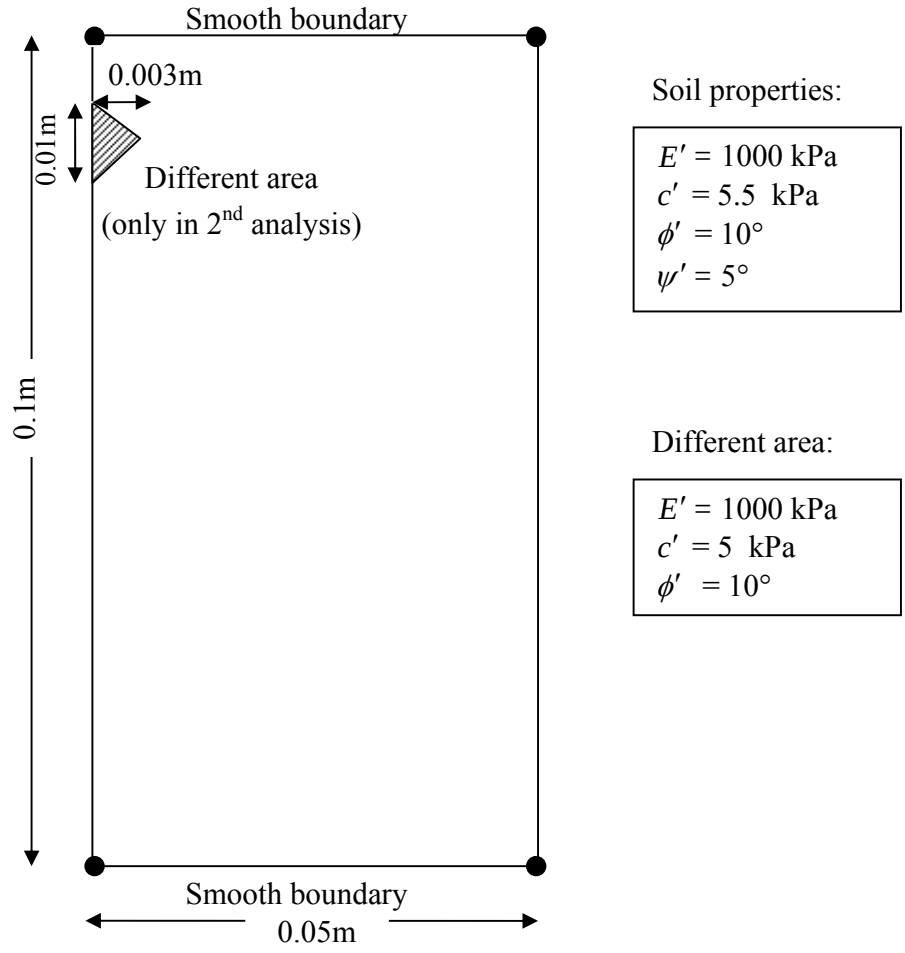

Figure 7.3. Biaxial test

A total prescribed displacement of 0.35 cm is applied vertically at the top and the bottom of the specimen, in 100 equal increments. Figure 7.4 shows the initial meshes, the meshes at the 10^{th} and 20^{th} increments for the uniform soil specimen and at the 20^{th} and 40^{th} increments for the non-uniform soil specimen with a minimum element area of 0.004 m^2. Benchmark analyses using 7763 elements and 15768 nodes were carried out for both the uniform specimen and non-uniform specimen. The applied pressure normalized by c' is plotted versus the axial strain in Figure 7.5 for both the adaptive mesh and the fixed fine mesh in each analysis. Obviously, the analysis using a fixed fine mesh does not lead to the localised failure (shear band). However as shown in Figure 7.6, the *h*-adaptive method can predict the location and formation of the shear band in this problem. To prove the effect of chosen minimum area on the accuracy of the solution in both problems are also analysed with a larger minimum area of 0.08 m^2 and also a much finer minimum area of 0.008 m^2. As shown in Figure 7.5 as the minimum element area gets smaller the accuracy of solution will increase. Although with the area defined less than 0.004 m^2 the result remains unchanged. Therefore, no refinement seems necessary where the minimum area reaches 0.004 m^2. Also, by increasing the number of elements in the very fine fixed mesh, the result of the solution remained unchanged. Therefore, it seems that load deflection curves are converged as the number of degrees of freedom goes to infinity. It is interesting to note that the *h*-adaptive method leads to localised failure even for the soil specimen with uniform properties. One possible reason is that the initial mesh is not symmetric (uniform). It is also interesting to note that the constitutive model used here does not have a length scale and as such the mesh will continuously be refined, which leads to an unrealistically thinner

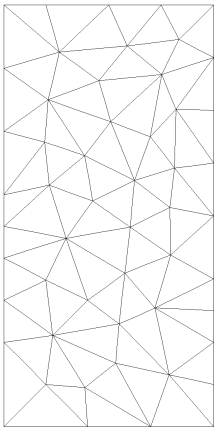

1. Coarse mesh
(80 elements)

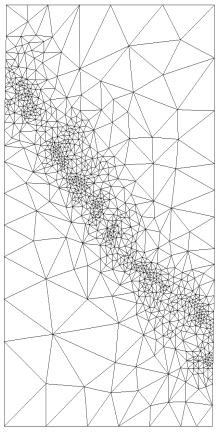

2. After 10 remeshing
(731 elements)

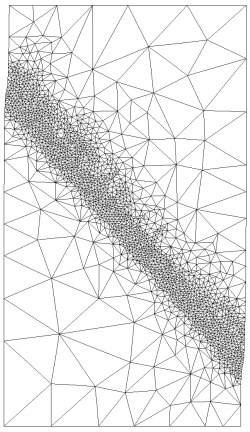

3. After 20 remeshing
(1658 elements)

a. Uniform soil properties

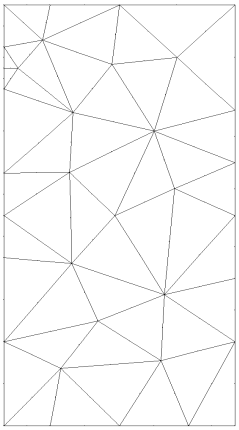

1. Coarse mesh
(47 elements)

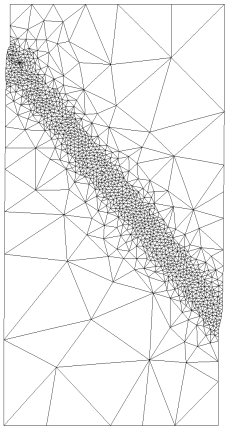

2. After 20 remeshing
(2337 elements)

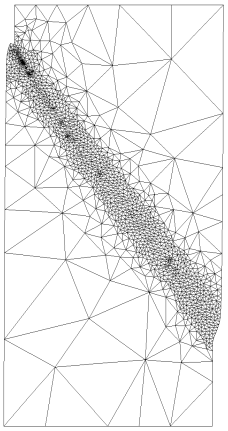

3. After 40 remeshing
(2792 elements)

b. Non-uniform soil properties

Figure 7.4. Mesh results of the biaxial tests

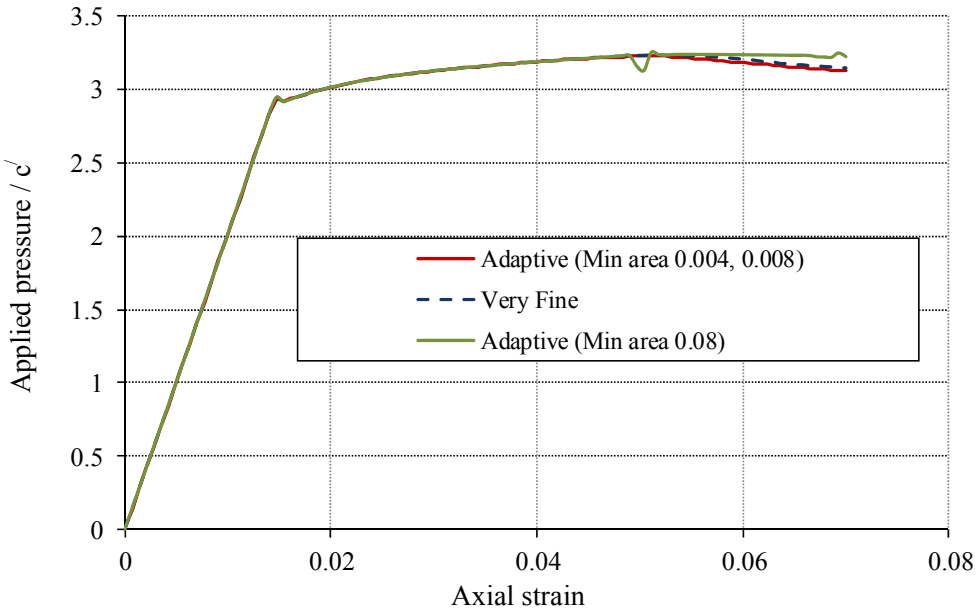

a. Uniform soil properties

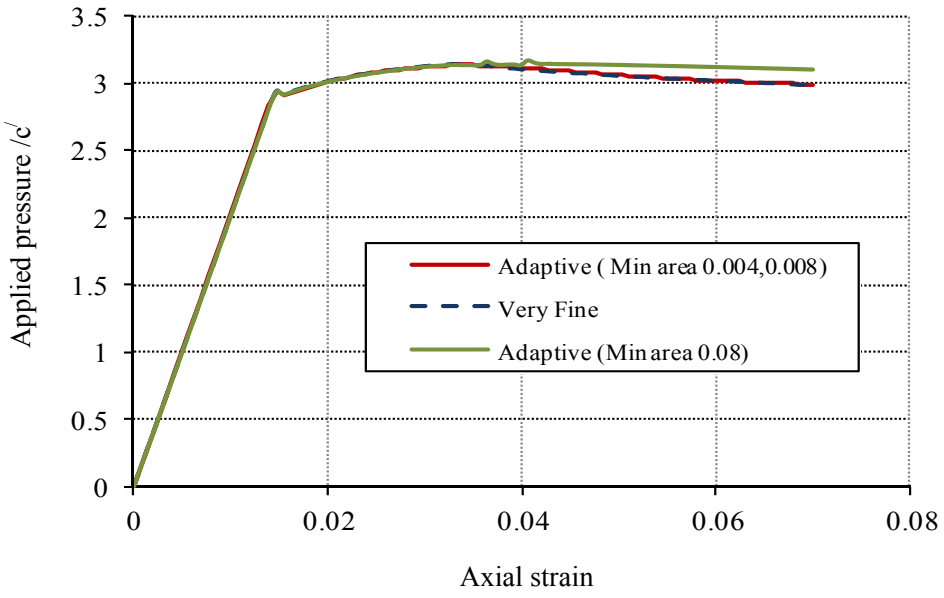

b. Non-uniform soil properties

Figure 7.5. Load-displacement response of the biaxial test

And thinner shear band. However, the predicted load-displacement curves shown in Figure 7.5 seem to converge to a unique solution, suggesting that the length scale does not affect the numerical results here. Runesson et al. (1991) also showed that introducing some softening to the associated model or using a non-associated model would permit bifurcation. In general, a more robust method to tackle this localisation problem is perhaps

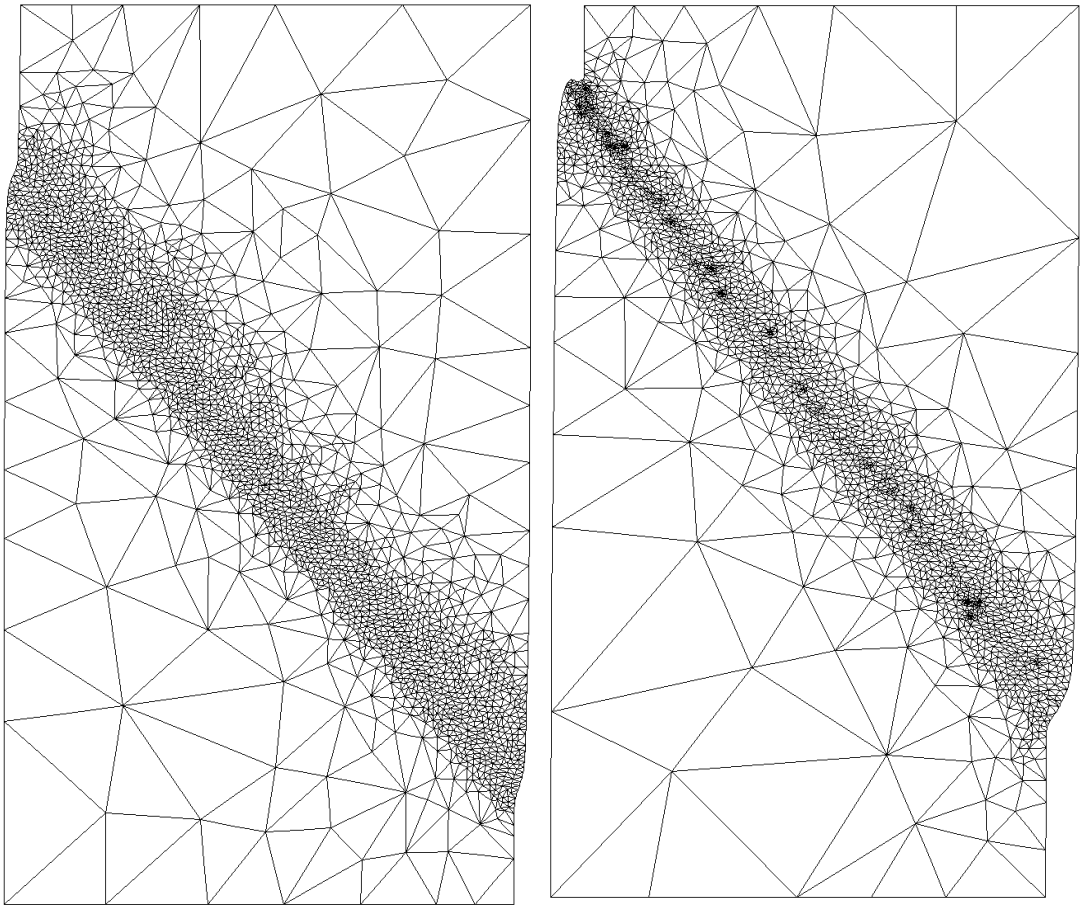

a. Uniform soil properties (2964 elements and 6001

b. Non-uniform soil properties (3363 elements and 6802 nodes)

Figure 7.6. Final deformed *h*-adaptive meshes for biaxial test

to combine the adaptive finite element method with appropriate constitutive models for the localising material (Mühlhaus and Vardoulakis, 1987; Tejchman and Bauer, 1996), so that the remeshing process will stop once the mesh size is approaching the length scale in the constitutive model.

7.2.3. Bearing capacity of soil under a strip footing

In the third example, a strip footing on an undrained soil layer of Tresca material is considered. Only half of the footing is analysed due to symmetry, and the domain, its boundary conditions and material properties are shown in Figure 7.7. The footing is assumed to be either flexible or rigid.

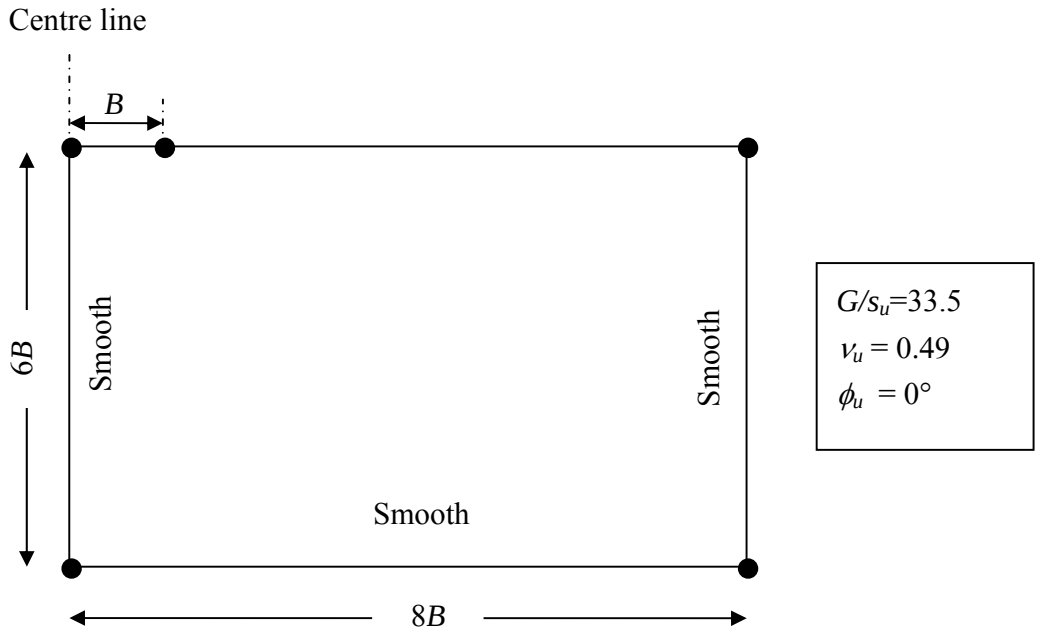

Figure 7.7. Footing problem

To model a flexible footing, a vertical pressure $6.5s_u$ is applied on the footing in 200 equal time steps. The domain is analysed by two different finite element meshes: a very fine mesh and a relatively coarse mesh. The coarse mesh has only 299 elements and a maximum element area of $0.25B^2$, while the fine mesh has 3713 elements and a maximum element area of $0.02B^2$. Table 7.1 provides the minimum element area, number of nodes, number of elements and the consumed CPU time in each analysis. The topology of the domain is kept constant in the fine mesh, while the coarse mesh is refined continuously using the *h*-adaptive technique. The numbers of nodes and the elements in the *h*-adaptive analysis provided in Table 7.1 correspond to those at the start and end of analysis. The *h*-adaptive solution was found using a total of 32 mesh refinements. The evolution of the adaptive mesh shown in Figure 7.8 indicates the finite element meshes at the beginning of the analysis and after 10, 25 and 30 mesh refinements, respectively, respectively. This figure clearly shows that the *h*-adaptive method is able to predict the occurrence and location of the shear band under the footing successfully. Figure 7.9 plots the applied pressure on the

Analysis	Minimum element area (B^2)		Number of Nodes	Number of Elements	CPU Time (sec)
Very Fine	0.02		7604	3713	8013
h-adaptive	Initial	0.25	648	299	589
	Final	0.002	2132	1025	

Table 7.1. Results for analysis of flexible strip footing

footing, normalised with respect to s_u, versus the vertical displacement normalised with respect to the half width of the footing. The results presented in Figure 7.9 are based upon the large deformation formulation where the limit pressure does not necessarily converge to Prandtl's plasticity solution, $(2+\pi)s_u$. The two load-displacement plots perfectly coincide with each other, while the *h*-adaptive analysis is approximately 14 times faster than the analysis using the fixed fine mesh (Table 7.1).

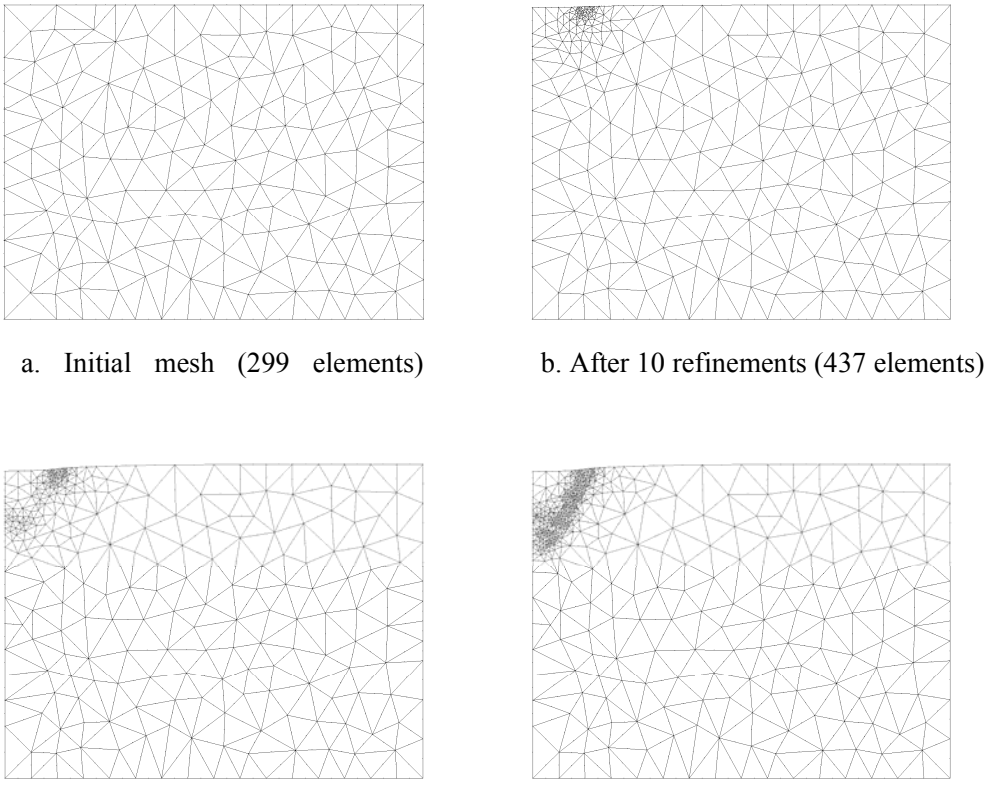

a. Initial mesh (299 elements) b. After 10 refinements (437 elements)

c. After 25 refinements (539 elements) d. After 30 refinements (888 elements)

Figure 7.8. Finite element mesh during analysis of flexible strip footing

In another attempt to solve this example the minimum element area of $0.01B^2$ was selected and no mesh refinement was permitted. As a result, a new fine mesh with 15168 nodes and 7467 elements leads to almost an identical load-displacement curve as shown in Figure 7.9.

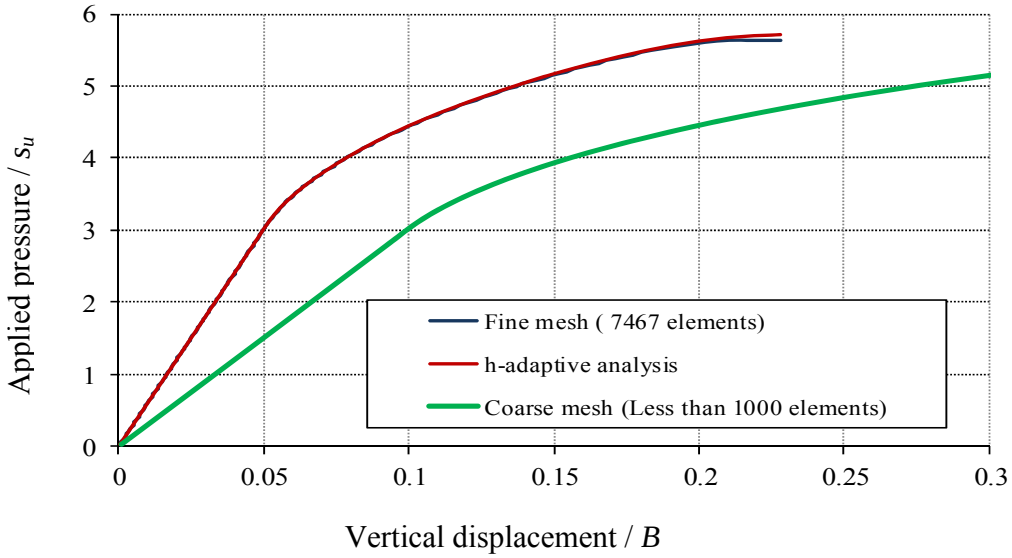

Figure 7.9. Load-displacement response of flexible strip footing

On the other hand, a fixed mesh with less than 1000 elements would lead to significantly different load-displacement response. Figure 7.10 shows the final deformed meshes at the end of *h*-adaptive analysis and the UL analysis. Again, the localised failure mechanism is well captured.

For the case of a rigid footing, a vertical displacement of $0.5B$ is applied on the footing in 100 equal steps. The problem is analysed as a large deformation formulation. Some of the

intermediate meshes are shown in Figure 7.11.

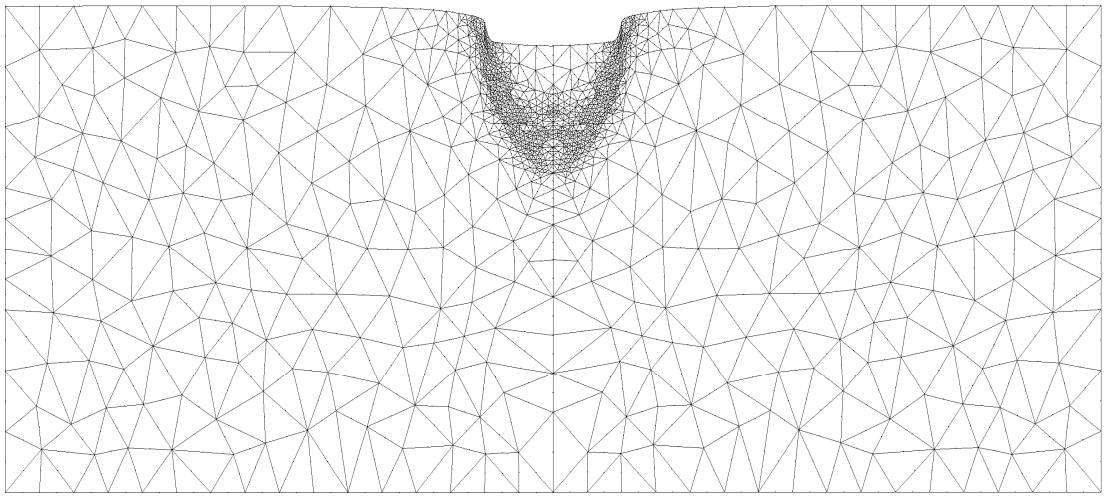

a. *h*-adaptive analysis

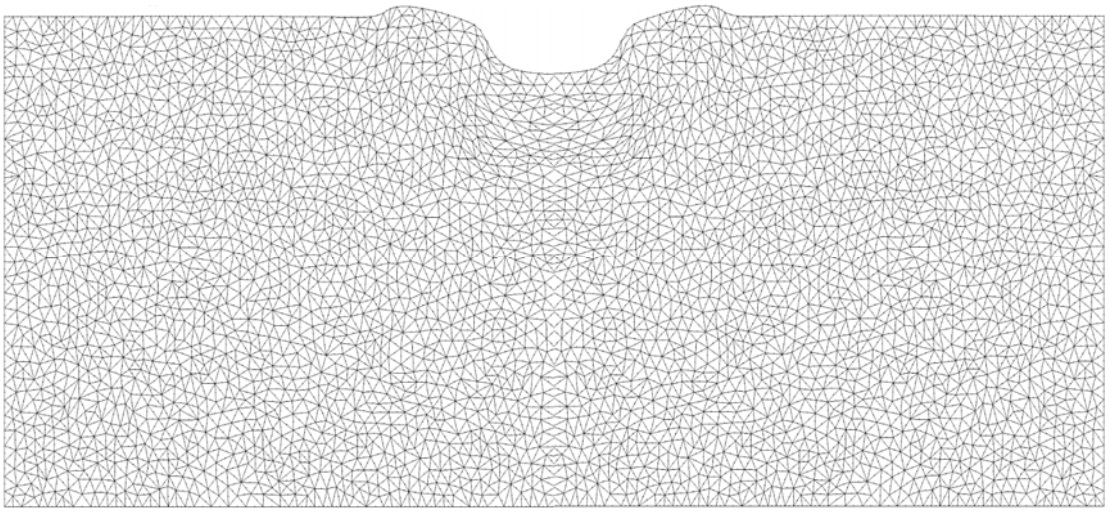

b. UL analysis

Figure 7.10. Final deformed meshes for flexible strip footing

The final result is achieved after 32 refinement steps. For comparison, the problem is also analysed by a small deformation assumption where the configuration remains unchanged during the analysis. Figure 7.12 plots the applied pressure on the footing, normalised with respect to s_u, versus the vertical displacement, normalised with respect to the half width of the footing. The small deformation analysis results in a final applied pressure of $5.18s_u$, which is only 0.8% above the Prandtl plasticity solution, $(2+\pi)\, s_u$. The final deformed mesh at the end of *h*-adaptive large deformation analysis is shown in Figure 7.13.

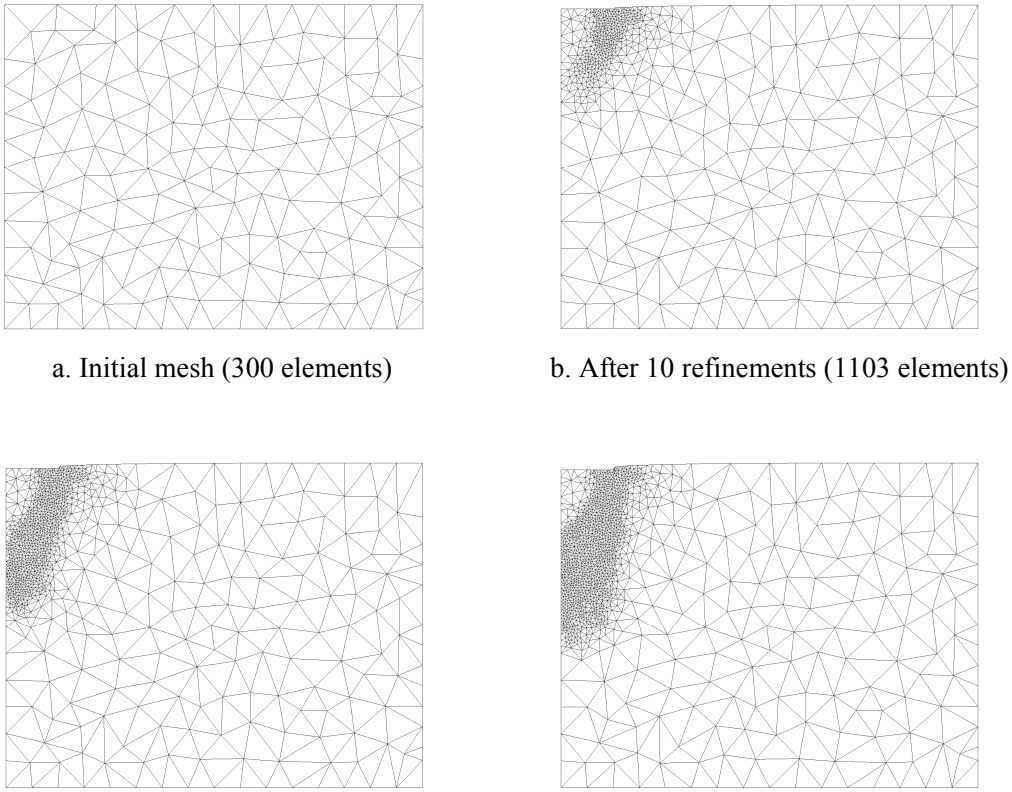

a. Initial mesh (300 elements)

b. After 10 refinements (1103 elements)

c. After 15 refinements (1730 elements)

d. After 20 refinements (2143 elements)

Figure 7.11. Finite element meshes during analysis of rigid strip footing

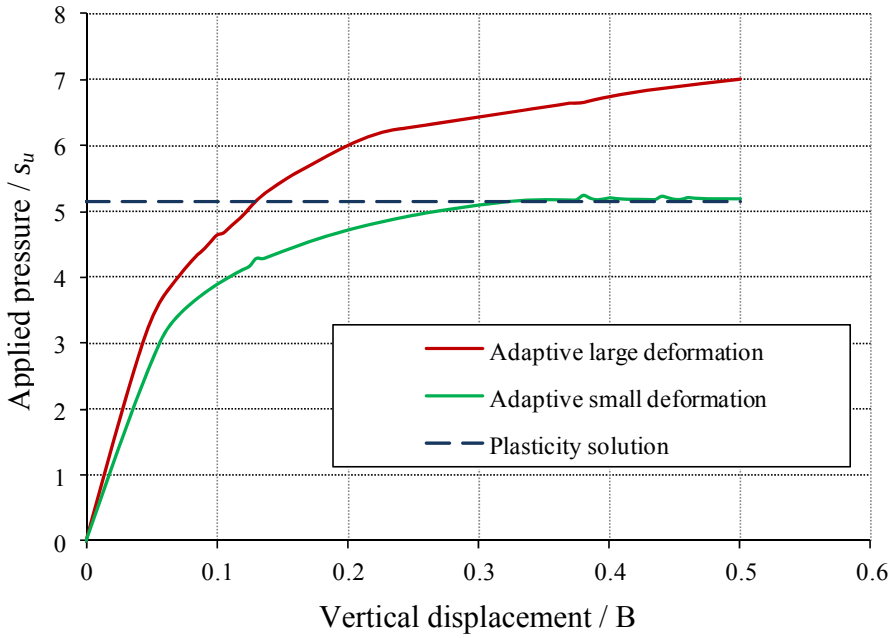

Figure 7.12. Load-displacement response of rigid strip footing

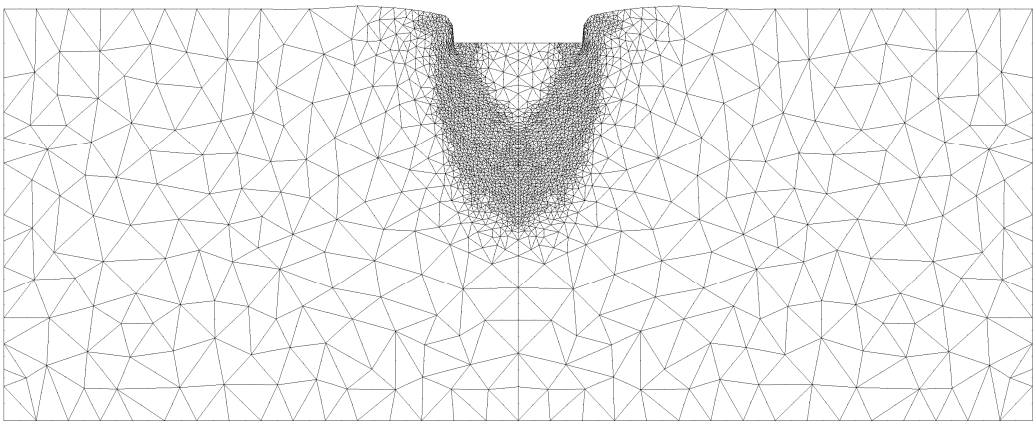

Figure 7.13. Final deformed mesh for rigid strip footing

7.2.4. Undrained behaviour of a soil layer under a rigid footing

To compare the performance of the three error estimation techniques and the accuracy of the *h*-adaptive method presented here an undrained layer of soil under a rough rigid footing is considered. The footing, the soil layer, and the boundary conditions are shown in Figure 7.14. The soil was modelled as a Tresca material, and any increase in shear strength due to strain rate effects was neglected to avoid further complexity. The material properties describing the soil behaviour include the shear modulus, G, undrained shear strength, s_u, and the density, γ. The undrained friction angle of the soil and its material damping are assumed to be zero. To approximate elastic incompressibility of the soil, a Poisson's ratio of 0.49 was adopted in all analyses.

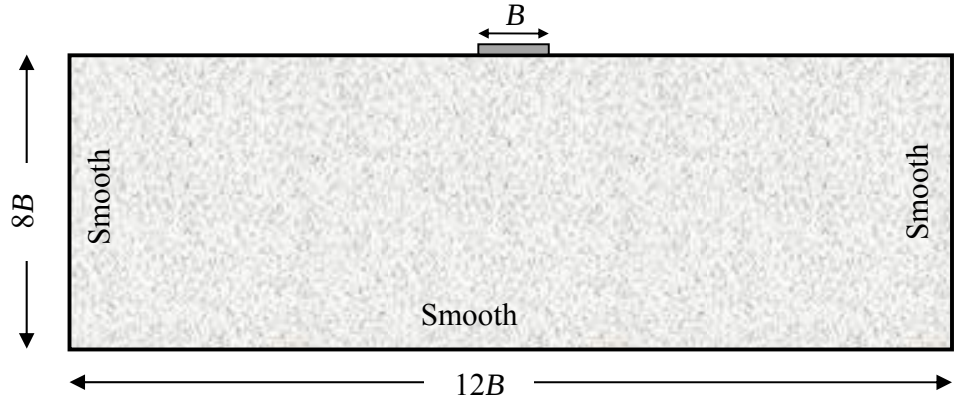

Figure 7.14. An undrained layer of soil under a rigid footing

a) Small deformation bearing capacity

Firstly, the static bearing capacity of the soil assuming small deformations is investigated using the three error assessment methods. According to Prandtl's plasticity solution the

static undrained bearing capacity of the soil under a rigid strip footing is given by $(2+\pi)s_u$. To estimate the capacity numerically, a prescribed vertical displacement of 0.04B was applied to the footing, and due to symmetry only one half of the problem domain was analysed. In all analyses the initial topology, number of time steps, and the error tolerance were identical. Table 7.2 shows the bearing capacity predicted by each method, the total number of the elements and the nodes at the end of each analysis, and the CPU time normalised by the CPU time of the fastest analysis.

Error assessment method	Predicted bearing capacity	Total number of elements	Total number of nodes	Normalised CPU time
Energy norm	$5.16s_u$	3962	8059	20.0
Green-Lagrange strain	$4.99s_u$	2521	5146	15.7
Plastic dissipation	$5.10s_u$	1122	2331	1.0

Table 7.2. Performance of the error assessment methods, static bearing capacity of the soil under a rigid footing assuming small deformations

Table 7.2 shows that the error assessment based on plastic dissipation requires the minimum number of elements and nodes as well as the minimum CPU time to estimate the undrained bearing capacity of the soil, assuming small deformations only. The values of bearing capacity predicted by the energy norm, the Green-Lagrange strain, and the plastic dissipation error assessment methods are, respectively, 0.39%, 2.9% and 0.78% different from Prandtl's exact plasticity solution. Compared to the Green-Lagrange strain error estimator, the plastic dissipation is about 16 times faster and requires a significantly smaller number of nodes and elements, but yet provides a more accurate result. The error assessor

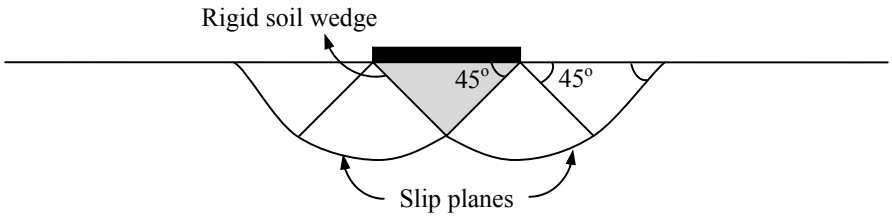

a. Failure mechanics, static undrained bearing capacity.

b. Error assessment based on the energy norm

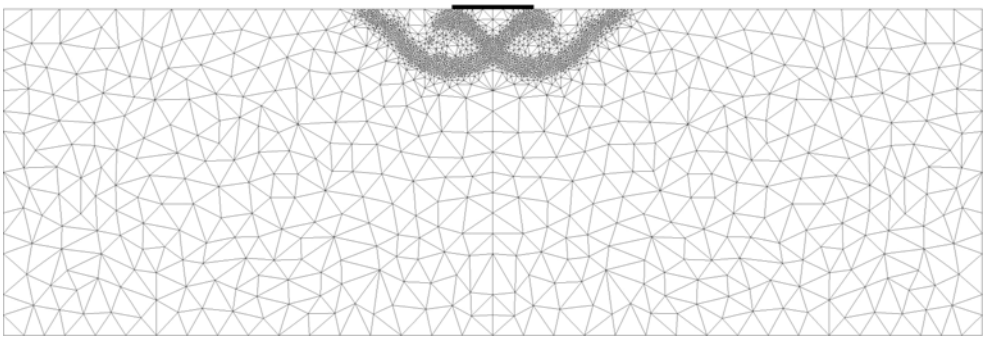

c. Error assessment based on the Green-Lagrange strain

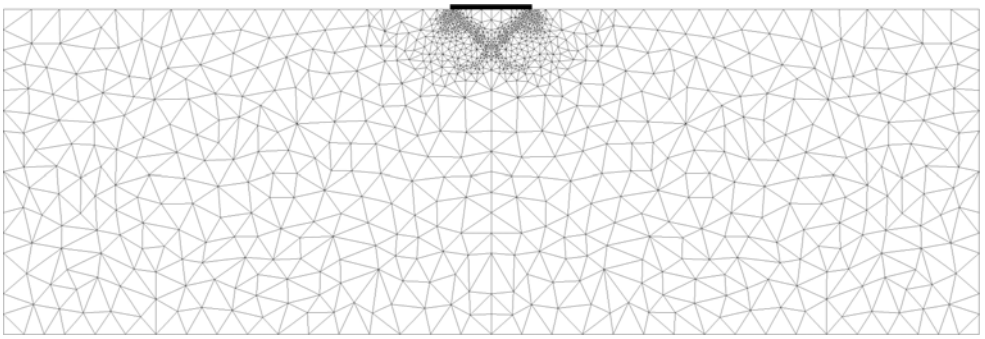

d. Error assessment based on plastic dissipation

Figure 7.15. Small deformation bearing capacity, final meshes at the end of each analysis

based on the energy norm predicted the bearing capacity of the soil most accurately but was computationally the slowest method. Figure 7.15 depicts the failure mechanism of the soil under a rigid strip as well as the finite element meshes at the end of each analysis. Although only half of the geometry was considered in all analyses the entire problem domains are shown in Figure 7.15, presenting a more meaningful visualisation. According to Figures 7.15(b-d), the *h*-adaptive method can successfully predict the location and the orientation of the slip surfaces generated due to the shear failure of the soil.

b) Dynamic small deformation analysis

Next we investigate the behaviour of the same soil and footing under a dynamic pressure loading of total magnitude $10s_u$, applied at a uniform rate over a period of 1 second. Small deformation conditions were also assumed in this example. The magnitude of the pressure loading, being applied rapidly, can exceed the static bearing capacity of the soil since it contributes to the development of inertia forces in the elastoplastic continuum.

Error assessment method	Final settlement/*B*	Total number of elements	Total number of nodes	Normalised CPU time
Energy norm	0.665	9005	18196	3.6
Green-Lagrange strain	0.652	5154	10467	1.0
Plastic dissipation	0.648	7390	14941	2.8

Table 7.3. Performance of the error assessment methods for an undrained layer of soil under a dynamically applied pressure assuming small deformation

In all analyses, it was assumed that $G/s_u = 33$ and the soil has mass density of 1 t/m^3 (Nazem et al., 2009). In order to avoid reflection of the outgoing stress waves, viscous energy absorbing boundaries were used in all dynamic analyses. Predictions of the applied pressure normalised by the static shear strength of the soil are plotted versus the vertical displacement of the footing normalised by the footing width in Figure 7.16a. Almost identical predictions were obtained in all analyses performed using the three error assessment methods. However, the final vertical settlements of the footing predicted by the three methods are slightly different, as shown in Table 7.3. This table also presents the performance of each error assessment technique by comparing the final densities of the various finite element meshes and the normalised CPU times. According to Table 7.3 the error assessor based on the Green-Lagrange strain tensor represents the best performance. Alternatively, the performance of the *h*-adaptive strategies considered in this study can be compared by plotting the growth of the total number of degrees of freedom versus the analysis time, as in Figure 7.16b. According to Figure 7.16b, the error estimator based on the Green-Lagrange strain requires the minimum number of the elements and nodal points to finalise the dynamic analysis, suggesting that for dynamic analysis of the footings this method is probably the most efficient strategy among those methods studied here. The final element meshes obtained at the end of each analysis are shown in Figure 7.17, which represent consistent plastic zones predicted by each method. However, for the rate of loading considered in this problem no clear shear failure mechanism can be observed.

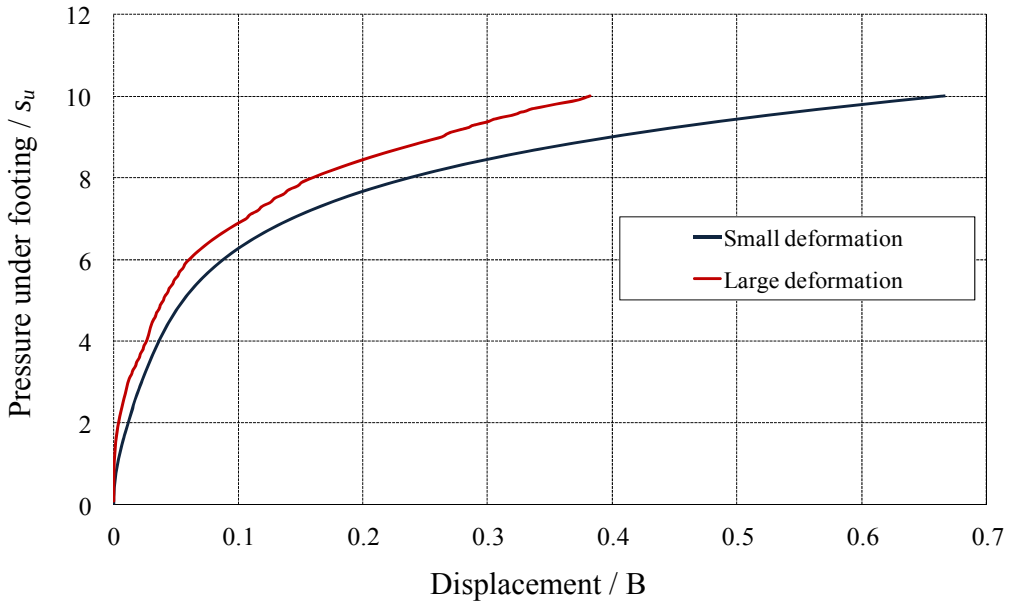

a. Settlement of the footing versus the normalised dynamic pressure

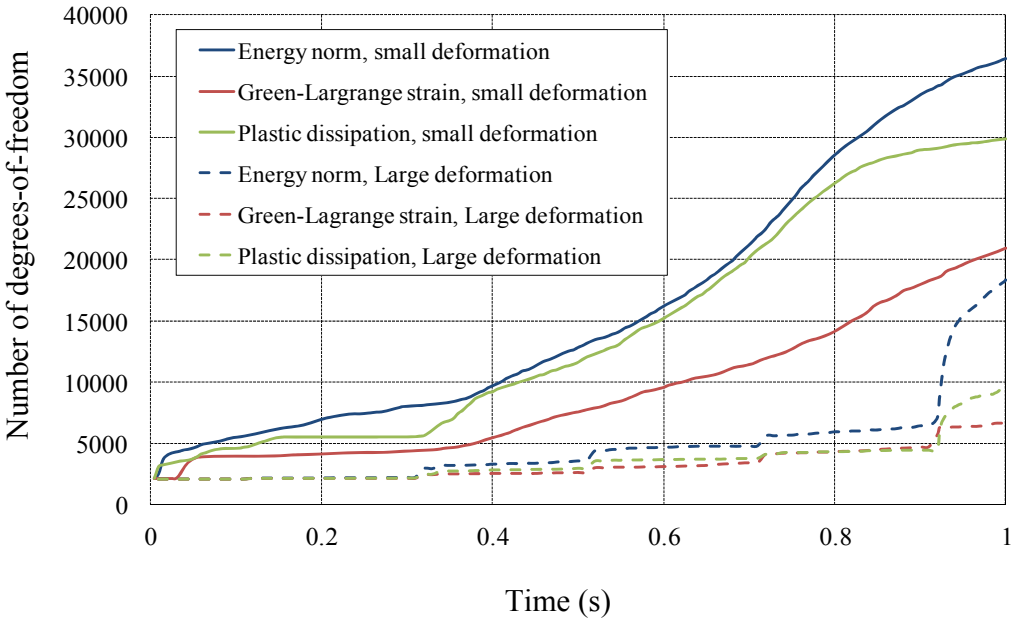

b. Growth in degrees of freedom versus time

Figure 7.16. Dynamic analysis of soil under a footing

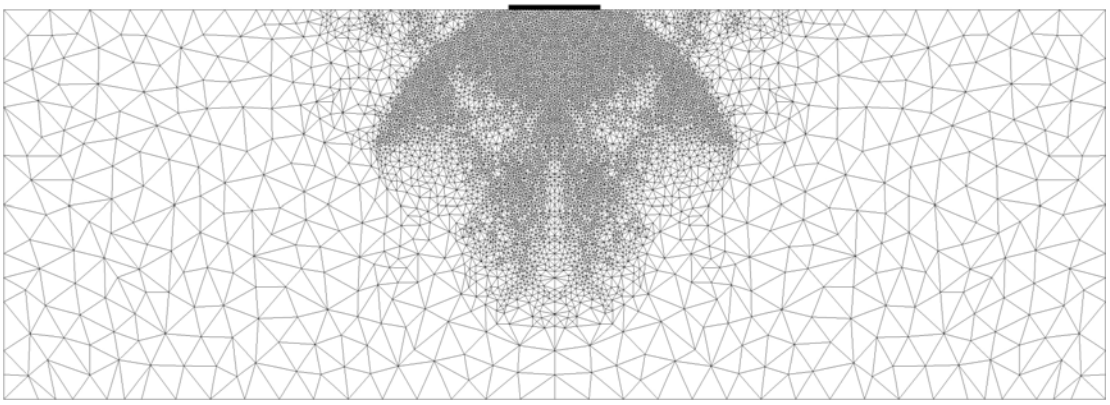

a. Error assessment based on energy norm

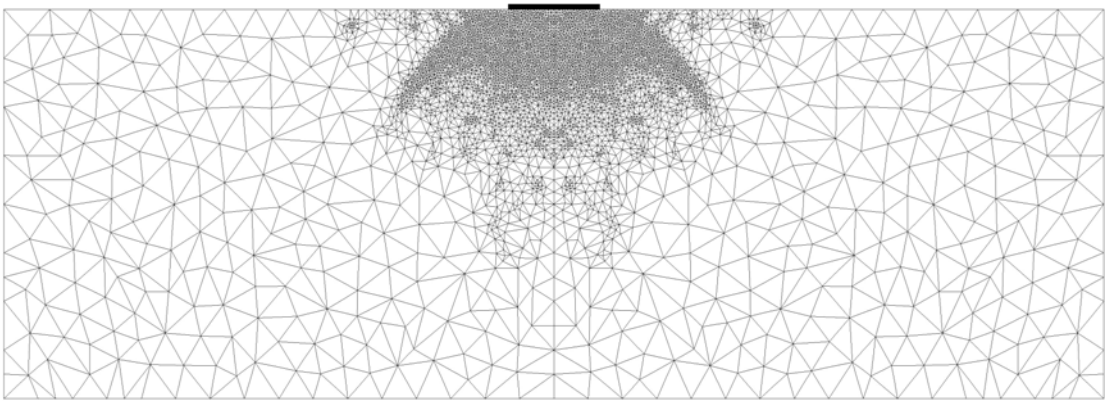

b. Error assessment based on Green-Lagrange strain

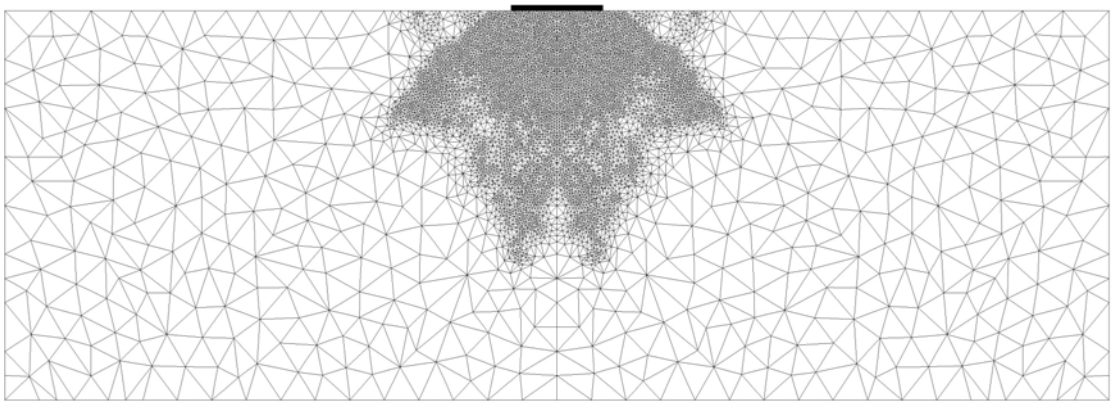

c. Error assessment based on plastic dissipation

Figure 7.17. Dynamic small deformation analysis, final meshes at the end of each analysis

c) Dynamic large deformation analysis

Finally, the footing problem solved in Section 7.2.4.b was reanalysed by considering identical conditions but assuming large deformations**.** Nazem et al. (2009) studied the behaviour of this soil layer for pressure loading applied at rates of $2s_u$ and $20s_u$ per second, using the Arbitrary Lagrangian-Eulerian (ALE) method. In this work the behaviour of the same ideal soil and footing for a loading rate of $10s_u$/s is studied, i.e., a total pressure $10s_u$ applied at a uniform rate over 1 s. The problem was analysed using the three different error assessment techniques described in chapter 4 of this Thesis. By using a very fine mesh and employing the ALE method, Nazem et al. (2011) found that the final settlement of the footing under the applied dynamic pressure load was $0.322B$. This value was also approximated by the three *h*-adaptive methods, as presented in Table 7.4. In addition, Table 7.4 provides the normalised CPU times as well as the topology information at the end of each analysis. These data show that in terms of efficiency, the Green-Lagrange strain error estimator outperforms the other two methods.

Error assessment method	Final settlement/B	Total number of elements	Total number of nodes	Normalised CPU time
Energy norm	0.318	4509	9178	5.2
Green-Lagrange strain	0.332	1600	3303	1.0
Plastic dissipation	0.312	2289	4700	1.6

Table 7.4. Performance of the error assessment methods for an undrained layer of soil under a dynamically applied pressure assuming large deformation

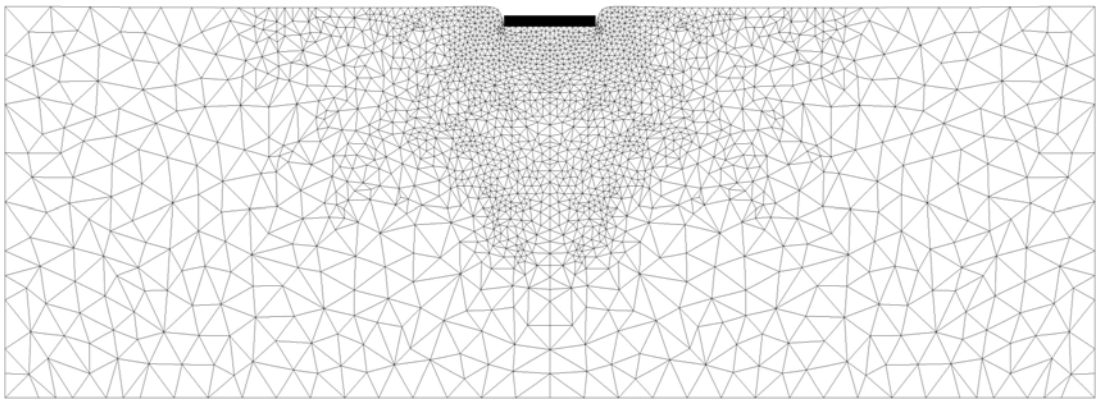

a. Error assessment based on energy norm

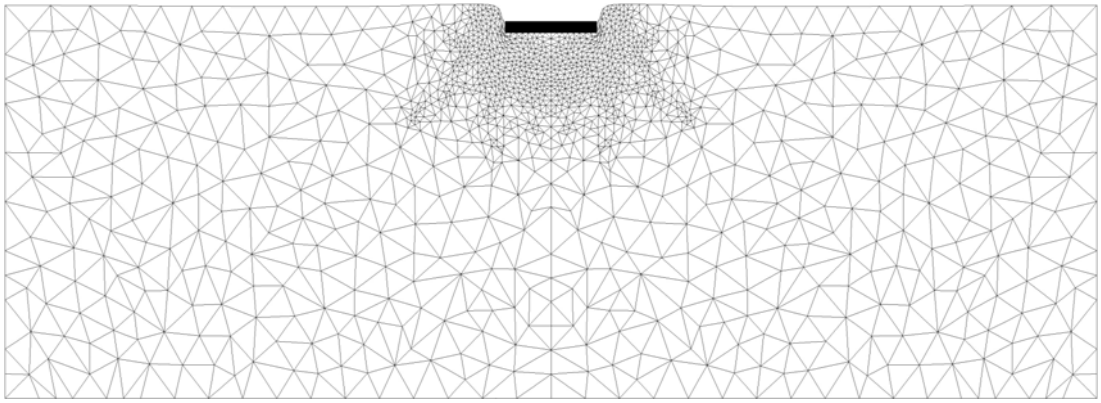

b. Error assessment based on Green-Lagrange strain

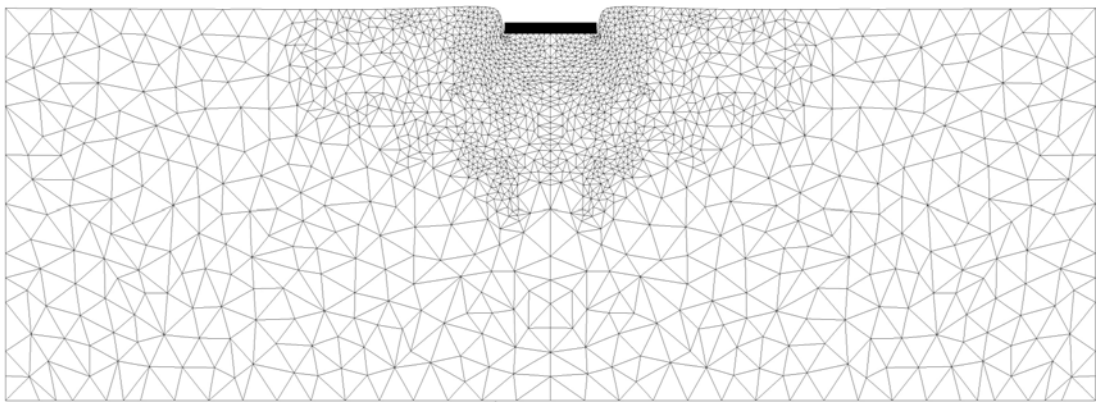

c. Error assessment based on plastic dissipation

Figure 7.18. Dynamic large deformation analysis, deformed meshes at the end of each analysis

A typical plot of the applied pressure normalised by the shear strength of the soil versus the settlement of the footing normalised by its width is shown in Figure 7.16a. According to Figure 7.16a, the predicted resistance of the soil at any given displacement in a large deformation analysis is higher than the resistance predicted assuming small deformations. For all analyses, the growth of the total number of degrees of freedom versus the analysis time is plotted in Figure 7.16b, which shows that the Green-Lagrange error estimator generates the minimum number of nodes as the analysis proceeds, and thus is the most efficient method of those considered. The deformed meshes at the end of each analysis are shown in Figure 7.18.

7.2.5. Cone penetration into a drained soil layer

In the fifth example, the performance of the error assessment methods is studied by analysing a relatively complicated problem in geomechanics, the penetration of an object into a soil layer, which requires contact mechanics to deal with the interface between the object and the soil. Figure 7.19 represents a rigid cone penetrating into a layer of sand. The soil is modelled by a Mohr-Coulomb material with a non-associated flow rule. The Young's modulus, Poisson ratio, unit weight, cohesion, friction angle and dilation angle of the soil are assumed to be 500 kPa, 0.3, 19.6 kN/m^3, 2.0 kPa, 30^o and 20^o, respectively. The diameter of the penetrometer, d, is 0.05 m and its length is assumed to be 10d. For simplicity, the friction forces between the cone and the soil are considered negligible. Due to symmetry, only half of the problem domain is modelled in the axi-symmetric analysis.

As the purpose of these analyses was to compare the efficiency and effectiveness of the methods of error estimation, for simplicity the initial stress state throughout the sand was assumed to be zero, i.e., the effect of self weight on the initial stress state were ignored.

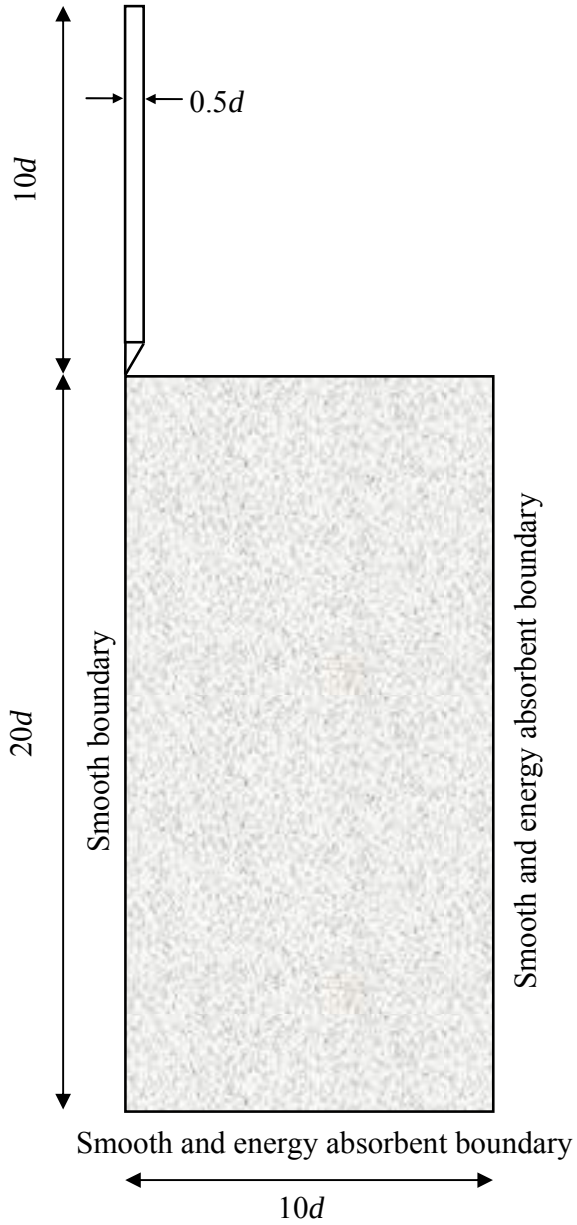

Figure 7.19. Penetration of an object into a soil layer

However, the finite mass density of the sand was used in the dynamic analysis. This may mean that the magnitude of the predicted cone penetration resistance may be somewhat unrealistic, although it is noted that maximum penetration is only 0.5 m, so that the magnitude of the initial stress field, prior to penetration, is expected to be relatively small.

a) Static analysis

In field tests the penetrometer is usually pushed into the ground at a relatively slow velocity of 0.02 m/s in which case it is reasonable to ignore inertia effects. To simulate static penetration numerically, a total prescribed vertical displacement of $10d$ was applied to the penetrometer. The three error estimation techniques were used separately to analyse the problem and to predict the soil resistance. In each analysis the maximum value of an element area in the initial mesh was $1.2d^2$, representing a relatively coarse mesh. During the adaptive analysis the minimum area of new elements was limited to $0.02d^2$.

The soil resistance normalised by its cohesion versus the vertical displacement of the penetrometer normalised by its diameter is plotted in Figure 7.20a. The three error assessment methods predict similar curves, but the *h*-adaptive method based on the energy norm failed to complete the analysis due to mesh distortion occurring at a penetration of $8.97d$. Figure 7.20b displays the growth in the number of degrees of freedom versus the analysis time obtained by each method. As shown in Figure 7.20b, the adaptive method based on the Green-Lagrange strain, compared to the other two error estimation techniques, required significantly fewer nodal points to estimate the soil resistance. This is also evident in the finite element meshes at the termination of each analysis, as represented in Figure

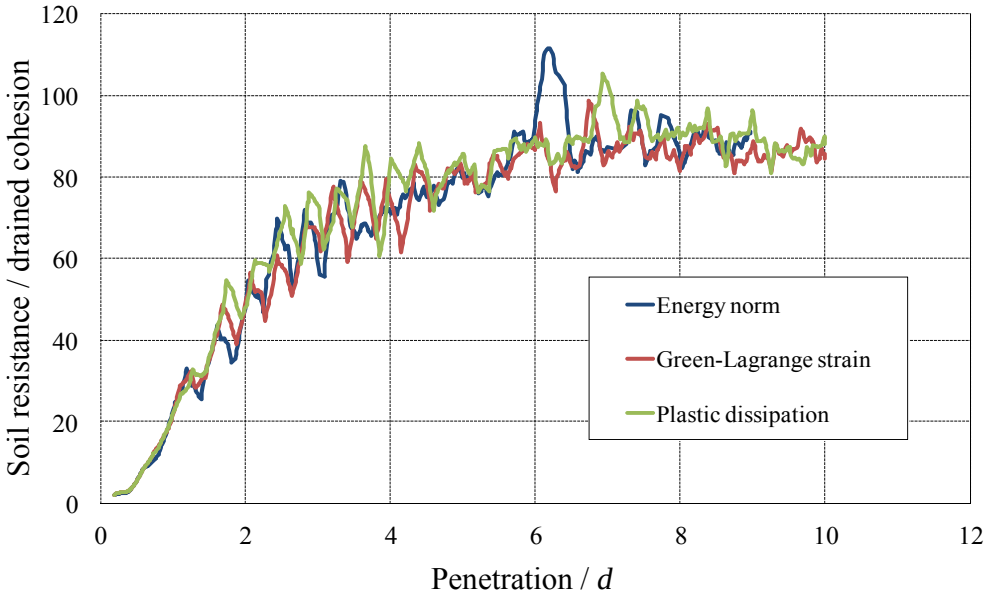

a. Normalised penetration versus normalised soil resistance

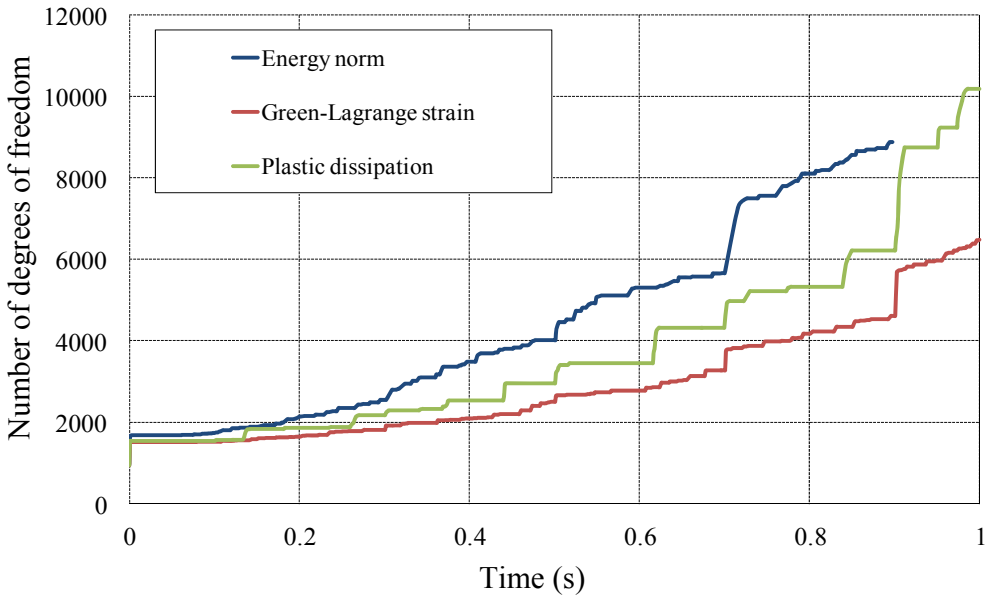

b. Growth of degrees of freedom versus time

Figure 7.20. Static penetration of an object into a drained layer of soil

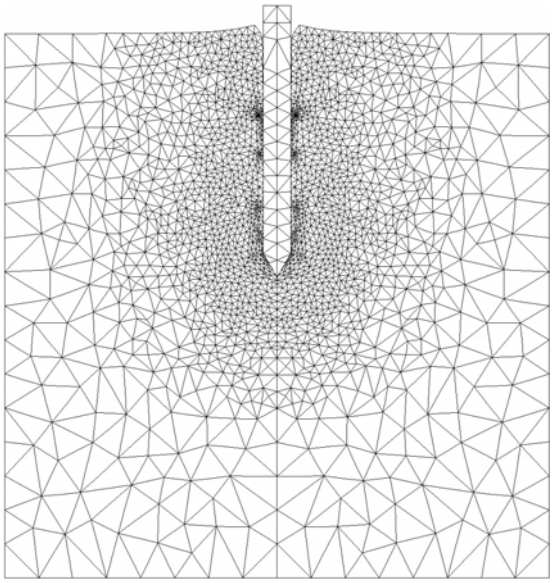

a. Error assessment based on energy norm, analysis terminated due to mesh distortion at 8.97*d* penetration

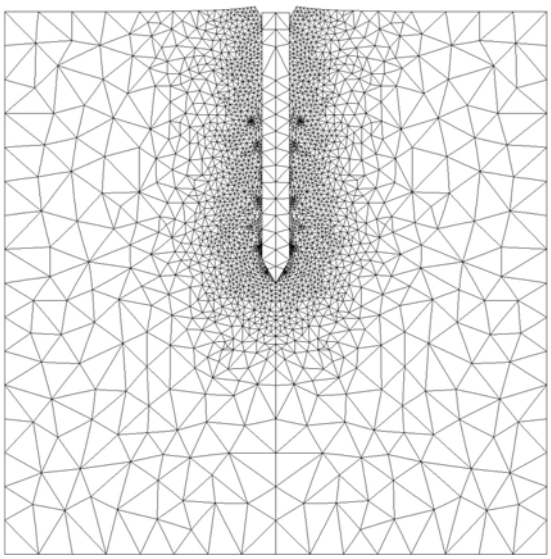

c. Error assessment based on plastic dissipation, mesh at the end of analysis

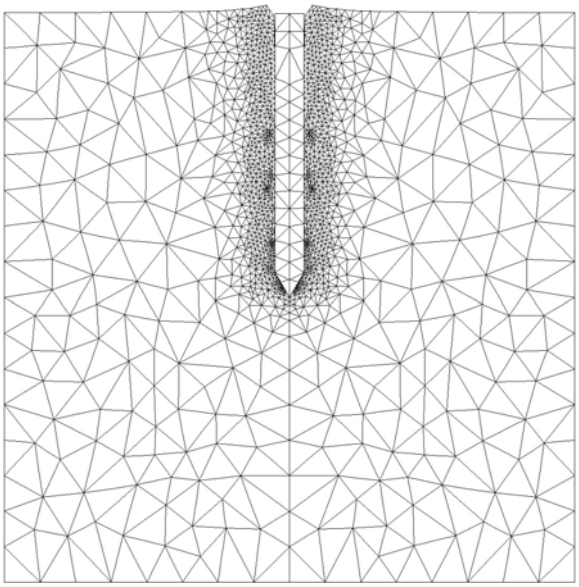

b. Error assessment based on Green-Lagrange strain, mesh at the end of analysis

Figure 7.21. Static cone penetration

7.21. For the static cone penetration analysis presented here, it was observed that the Green-Lagrange strain error assessor is approximately five times faster than the plastic dissipation error estimator.

b) Dynamic analysis

To compare the performance of the three *h*-adaptive methods for a dynamic contact problem**,** a prescribed vertical displacement of 10*d* was applied to the same penetrometer over a period of 1 s, and inertia forces were considered in the analysis. The mass density of the soil was assumed to be 2 t/m^3. For this case in which $d = 0.05$m, the cone penetrates into the soil layer at a velocity of 0.5 m/s, which is 25 times faster than the standard penetration rate of a static test, 0.02 m/s. As depicted in Figure 7.19, energy absorbent boundaries were used in all dynamic analyses and the material damping was assumed to be zero. Similar to the static analyses presented in the previous section, the initial mesh is relatively coarse, including 285 elements and 468 nodal points. This configuration was obtained by initially limiting the maximum value of an element area to 1.2 d^2, while the elements were permitted to attain a minimum area of 0.02 d^2 during the adaptive analysis.

The predicted load-displacement curves for the dynamic analyses are shown in Figure 7.22a. Only the analysis in which the error estimator was based on the Green-Lagrange strain was able to complete the analysis, i.e., to an overall penetration of 10*d*. The analyses assuming the energy norm and the plastic dissipation error estimators failed to provide a complete solution for the problem due to mesh distortion occurring at penetrations of 4.64*d* and 1.49*d*, respectively. The increase in degrees of freedom versus the analysis time is

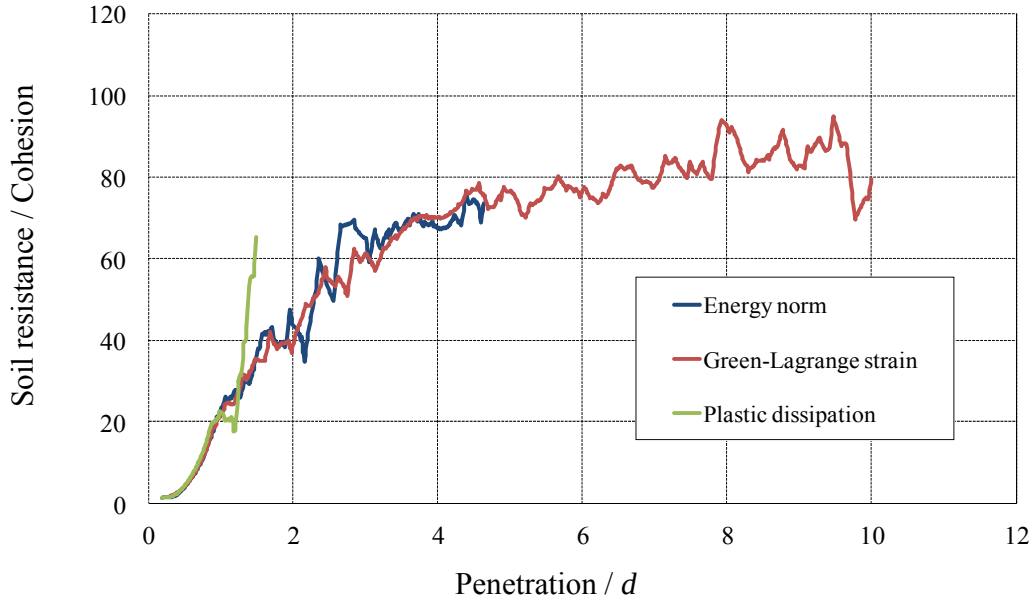

a. Normalised penetration versus normalised soil resistance.

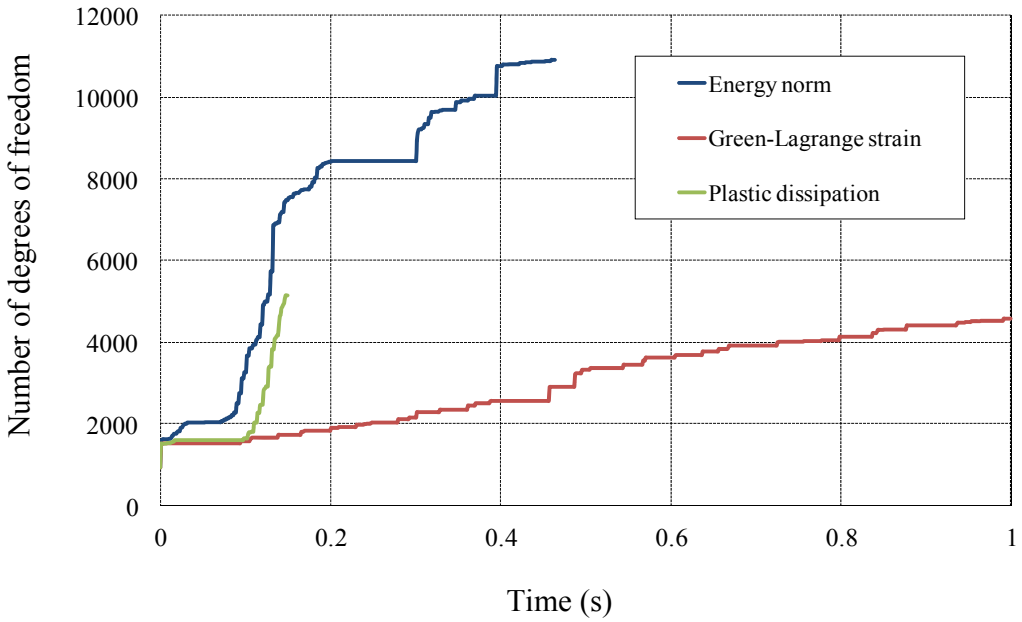

b. Increase in degrees of freedom versus time

Figure 7.22. Dynamic penetration of an object into a drained layer of soil

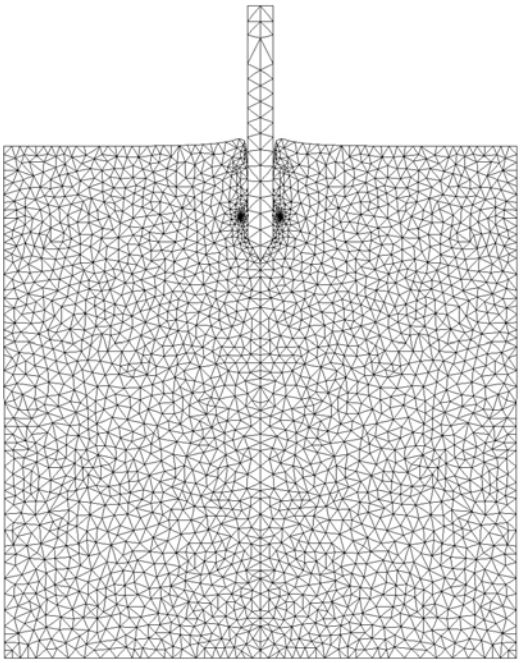

a. Error assessment based on energy norm, analysis terminated due to mesh distortion at 4.64*d* penetration

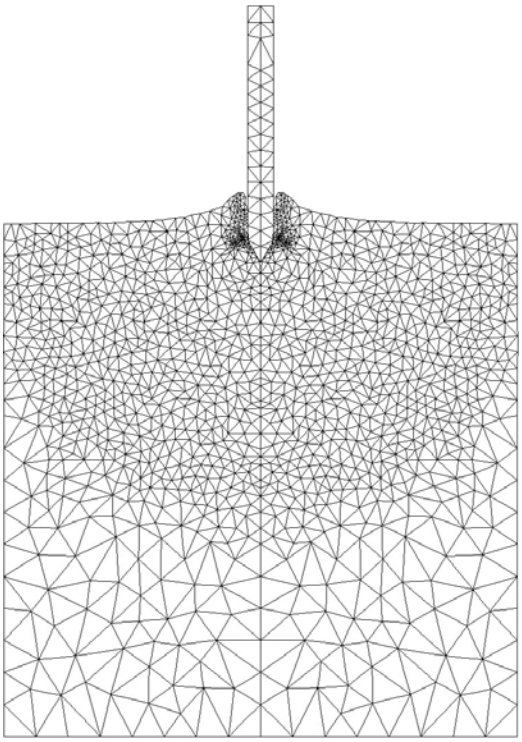

b. Error assessment based on plastic dissipation, mesh distortion occurred at 1.52*d* penetration

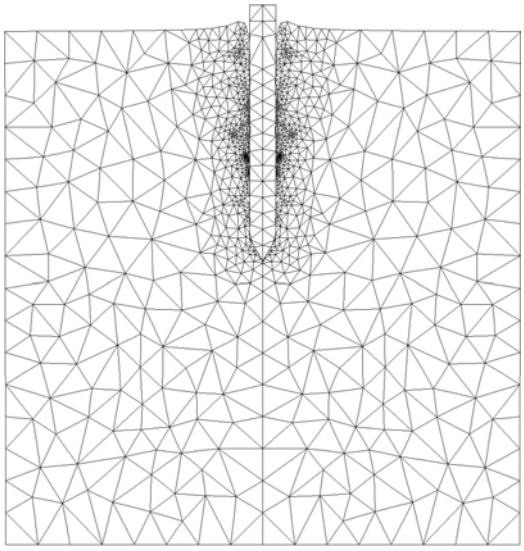

c. Error assessment based on Green-Lagrange strain, mesh at the end of analysis

Figure 7.23. Dynamic cone penetration analysis

plotted in Figure 7.22b. In each analysis, when a penetration of 1.49d (t = 0.149 s) was attained, i.e., the point at which the plastic dissipation error assessor failed to proceed, the total number of degrees of freedom in the adaptive finite element meshes predicted by the energy norm, Green-Lagrange strain, and plastic dissipation error assessments were 7474, 1732, and 5152, respectively. The rapid increase in degrees of freedom predicted by the energy norm and the plastic dissipation error assessment methods was unexpected, and shows that these two techniques are neither applicable nor efficient for this dynamic contact problem. This is also shown graphically by plotting the finite element meshes at the end of each analysis in Figure 7.23. Use of the energy norm and plastic dissipation error estimators resulted in an increase in the density of the mesh in regions distant from the penetrometer. This phenomenon could be due to the propagation of stress waves in the continuum resulting from the initial impact of the penetrometer with the soil, but it does not necessarily improve the predicted results, and as observed, eventually it causes unacceptable mesh distortion.

7.2.6. Vertical cut

In this example, the combined *rh*-adaptive method explained in Chapter 6 is used to analyse the vertical slope problem. Figure 7.24 shows the hypothetical problem of a vertical slope including its dimensions, boundary conditions and material properties. The bottom and right boundaries are restrained from vertical and horizontal displacement, respectively, while the left boundary is free to move in all directions. Except for the portion with prescribed vertical displacement, the top boundary is also free to move in all directions.

Note that this example does not address the stability analysis of a slope under its self-weight, but it aims to investigate the pure resistance of a weightless soil in a vertical slope when a rigid area adjacent to the slope is loaded in the vertical direction. The width of this area is B and vertical pressure is mobilised by specifying a prescribed downward displacement of $0.25B$ uniformly across the width B. Plane strain conditions are assumed and the soil is modeled as an elastoplastic Tresca material.

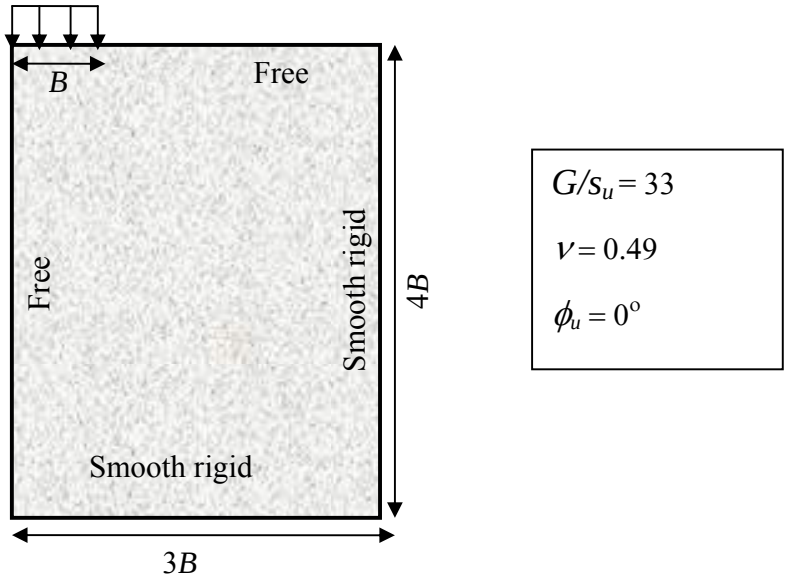

Figure 7.24. A vertical slope under vertical prescribed displacement

The problem was solved using three different approaches, including the UL method, the *h*-adaptive method, and the *rh*-adaptive method. The UL mesh consists of 7909 elements and 15692 nodal points, while the initial mesh at the beginning of the adaptive analyses includes 72 elements and 167 nodes. The error estimation method in the adaptive analyses

was based on plastic dissipation. According to the plasticity solution of this problem, the average value of the ultimate vertical pressure by the soil should be $2s_u$.

Predictions of the applied pressure normalised by the shear strength of the soil versus the vertical displacement normalised by the width of the loaded area are plotted in Figure 7.25.

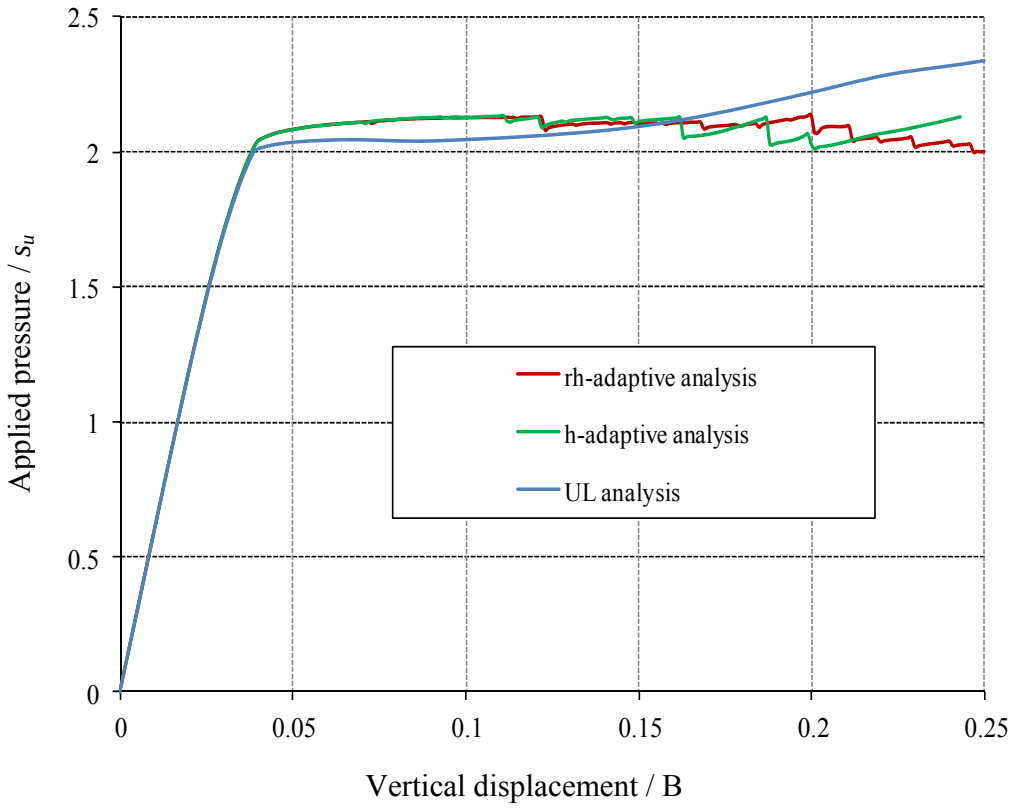

Figure 7.25. Load-displacement response of a vertical cut

Note that the *h*-adaptive method fails to complete the analysis due to excessive mesh distortion occurring in a few small elements, while the combined *rh*-adaptive method is able to finish the analysis. The UL method overpredicts the soil resistance since the

process of continuously updating the nodal coordinates tends to decrease the quality of the mesh and to distort the shape of triangular elements. This poor performance of the UL method in analysing problems involved with relatively large deformations has been previously reported (see Nazem et al., 2006).

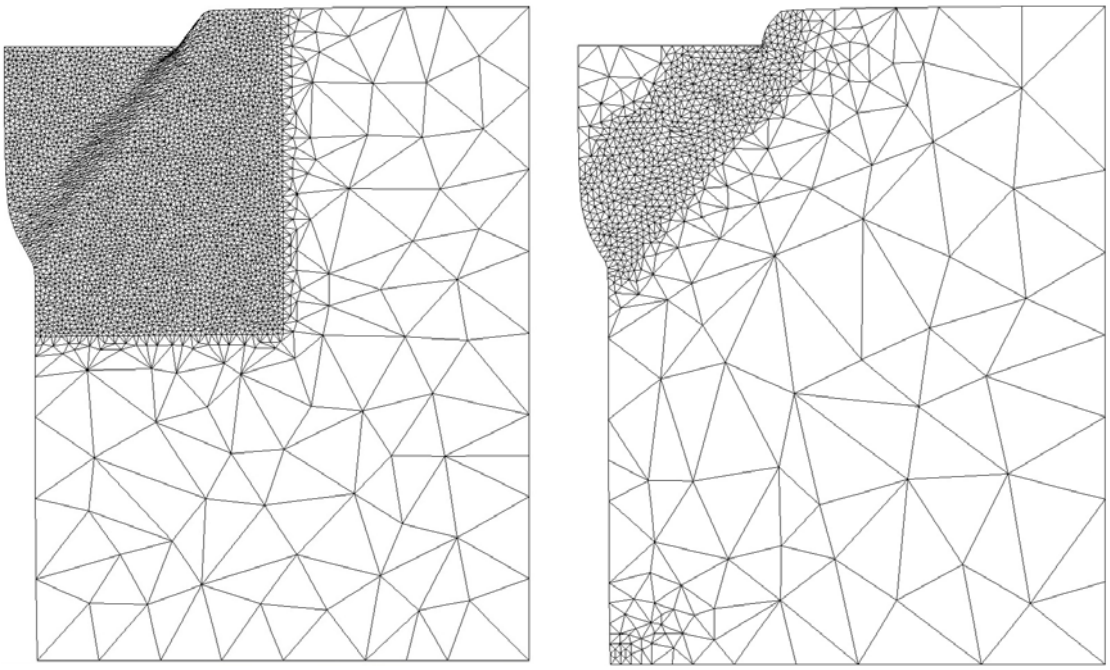

a. The deformed mesh at the end of the UL analysis

b. The final mesh at the end of rh-adaptive analysis, 2418 elements and 4969 nodes

Figure 7.26. Finite element meshes at the end of analyses

The finite element meshes at the end of the UL and the *rh*-adaptive analyses are depicted in Figure 7.26. The finite element mesh at the end of the *rh*-adaptive analysis includes 2418 elements and 4969 nodes. By comparing the CPU time of the analyses, it was observed that the *rh*-adaptive method is almost 12 times faster than the UL method.

7.2.7. Indentation of a cylinder into a soil layer

In this example, the indentation of a long rigid cylinder with diameter D into an undrained layer of soil is analysed. The soil is modelled using an associated Tresca material. Only half of the problem is considered due to symmetry. Figure 7.27 shows the topology of the problem and as well as the material properties.

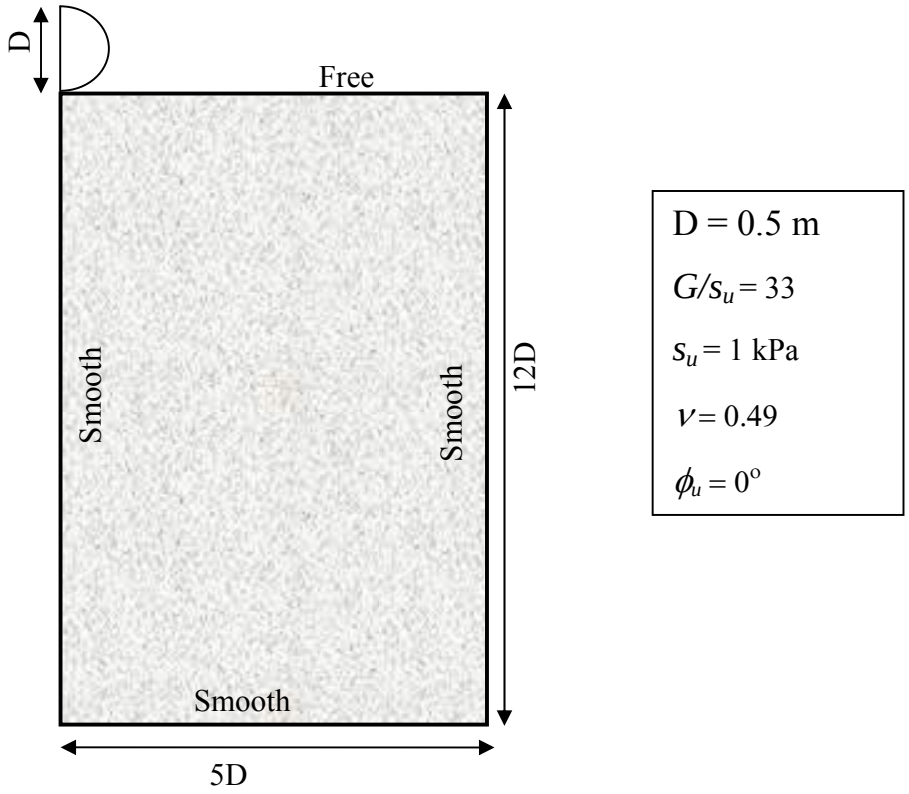

Figure 7.27. Rigid cylinder on cohesive soil

To study the soil behaviour under the indentation of the cylinder a vertical prescribed displacement of 0.8D is applied on the cylinder, and a static analysis is performed ignoring the friction between the cylinder and the soil to avoid further complexity. This example

involves both large deformation and changing boundary conditions. The *h*-adaptive method failed to finish the analysis due to severe mesh distortion occurring at ~0.1D of indentation. As the mesh is continuously refined in the *h*-adaptive procedure, some finest elements may become vulnerable of losing positive Jacobian within one single time step and hence lead to numerical breakdown. By contrast, the combined *rh*-adaptive method developed in Chapter 6 of this Thesis was able to successfully finish the analysis for the prescribed indentation. Figure 7.28 plots the indentation, normalised by the diameter of the cylinder, versus the vertical force under the cylinder, normalised by D×s_u obtained by the *rh*-adaptive method under static loading. Figure 7.29 shows the final mesh at the end of *rh*-adaptive analysis with 620 elements and 1312 nodes.

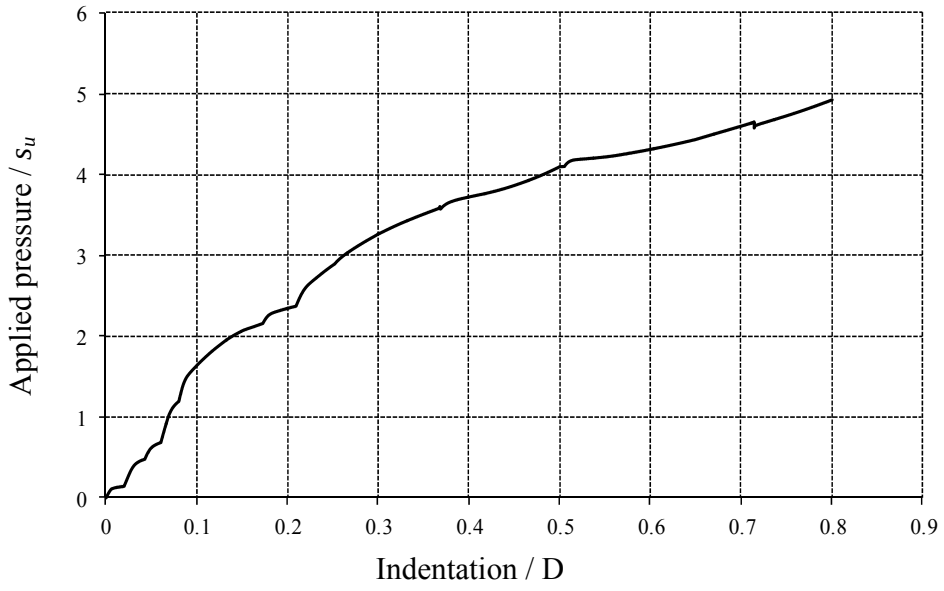

Figure 7.28. Load-displacement response of indentation of a cylinder into a soil layer

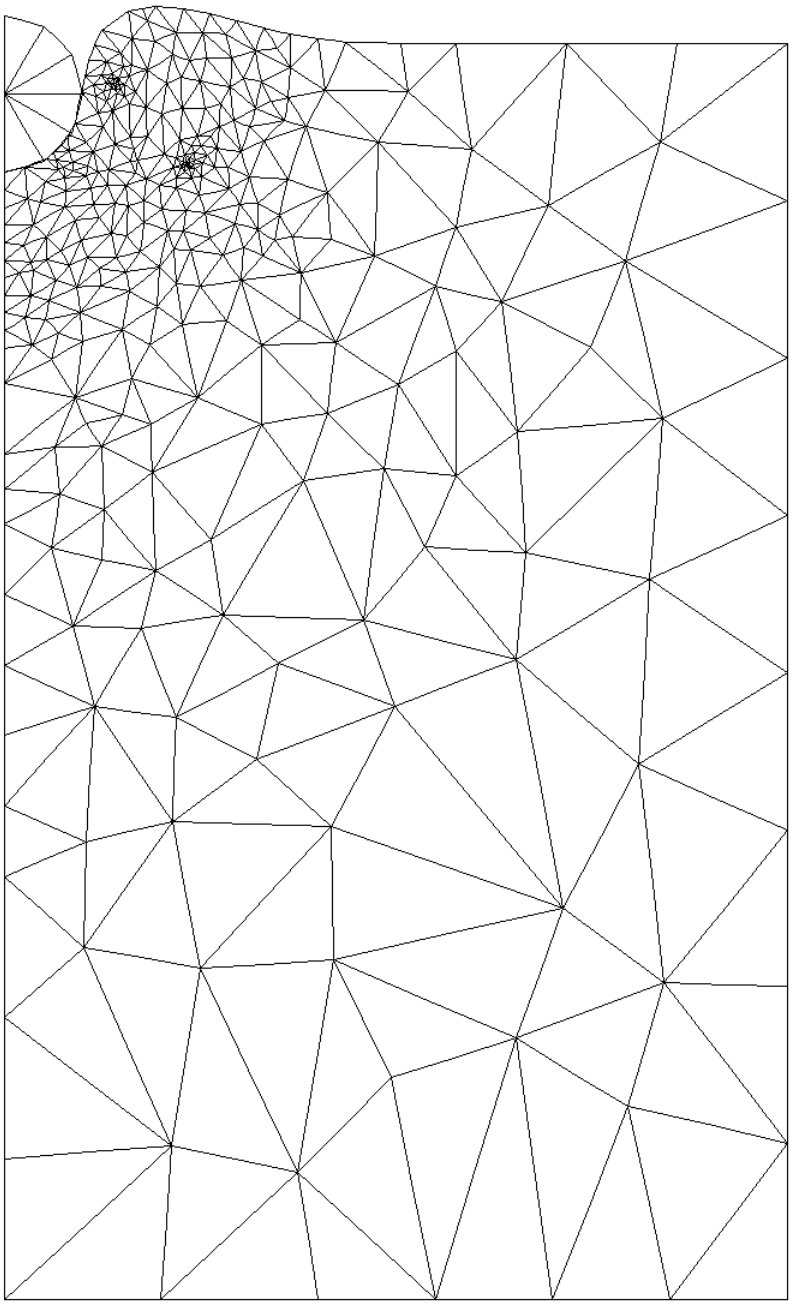

Figure 7.29. Finite element mesh at the end of analysis

7.2.8. Large deformation analysis of a footing on a two-layered undrained soil

In this example, the behaviour of a two-layered weightless soil under a strip rigid footing is studied, considering large deformations only. Figure 7.30 depicts the right half of the problem, its geometry, its boundary conditions and the material properties of the soil layers.

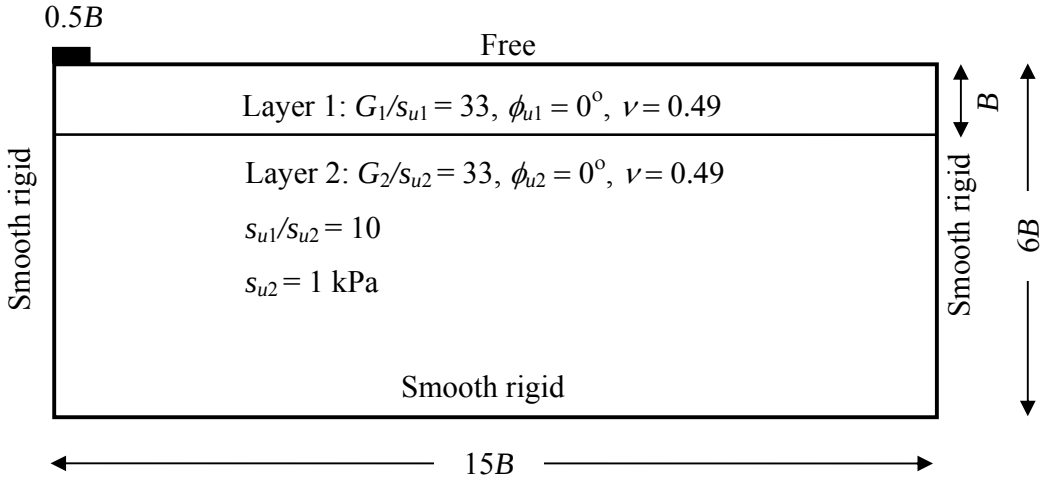

Figure 7.30. A rigid strip footing resting on a two-layered soil

The width of the footing as well as the thickness of the top layer is assumed to be *B*. The rigidity indexes (G1/su) of the two layers are identical, but the top layer is 10 times stronger than the bottom layer. Both layers are modelled as a Tresca material. Previously, Wang and Carter (2002) comprehensively studied the behaviour of layered clays supporting the strip and the circular footings and undergoing large deformations. To address the advantages of the *rh*-adaptive technique developed here, this numerical example only considers a special case of a two layered soil where the upper layer is relatively stronger

than the lower layer. To compare the performance of the *rh*-adaptive method with the *h*-adaptive method a vertical prescribed displacement of B is applied on the footing in 1000 equal time steps. The problem is analysed by the *rh*- and *h*-adaptive methods based on the Green-Lagrange strain as well as the plastic dissipation error estimators. The initial finite element mesh in all adaptive analyses includes 184 nodal points and 79 6-node triangular elements, and the minimum element area is $0.01B^2$. The *h*-adaptive analyses using the Green-Lagrange strain and the plastic dissipation error estimators fail to finish the analysis at $0.75B$ and $0.47B$, respectively, due to excessive mesh distortion causing a negative Jacobian of a few elements. This mesh distortion usually occurs in elements with a very small size during integration constitutive equations and results in spontaneous termination of the analysis. The combined *rh*-adaptive methods, on the other hand, are able to finish the

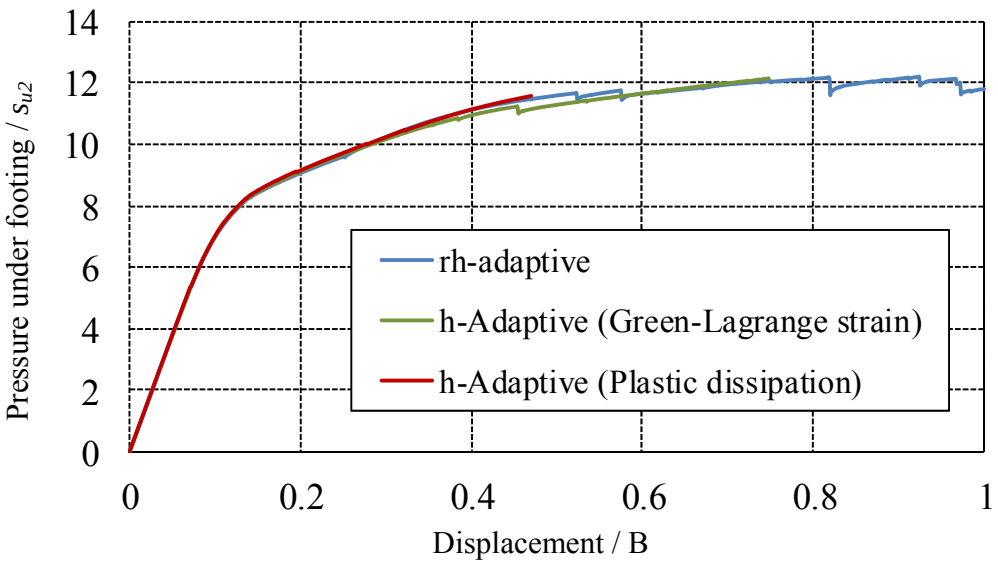

Figure 7.31. Footing on a two-layered undrained soil

analysis. The vertical displacement of the footing, normalised by B, versus the pressure under the footing, normalised by s_{u2}, predicted by the *rh*-adaptive methods is plotted in Figure 7.31. Although this example presents the advantage and the robustness of the *rh*-adaptive finite element strategy developed here, the performance of the two *rh*-adaptive finite element techniques based on the Green-Lagrange strain and the plastic dissipation error estimators is also studied by plotting the growth of the total number of degrees of freedom versus the analysis progress as in Figure 7.32. In terms of CPU time, the *rh*-adaptive analysis based on plastic dissipation is ~25% faster than the other method considered in this study. The final deformed finite element meshes at the end of the *rh*-adaptive analyses are depicted in Figure 7.33. Note that the entire problem domains are

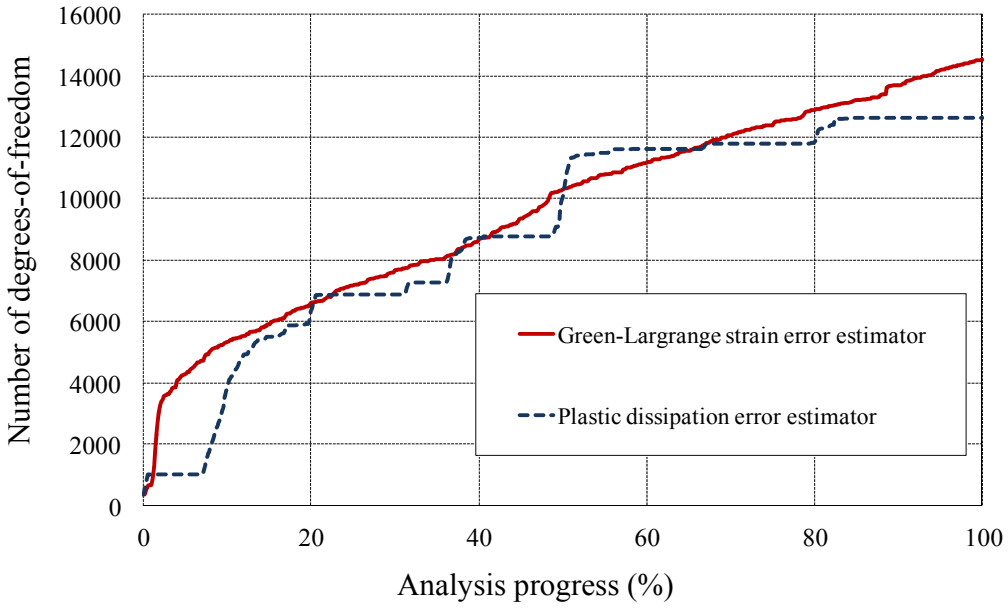

Figure 7.32. Two-layered soil under a strip footing

shown in Figure 7.33 to present a more meaningful visualisation. The total number of elements and nodal points at the end of analysis based on Green-Lagrange strain error

a. Error assessment based on Green-Lagrange strain

b. Error assessment based on plastic dissipation

Figure 7.33. Rigid strip footing on a two-layered soil, finite element meshes at the end of analysis.

estimator are 7260 and 3555, respectively, whereas the *rh*-adaptive analysis based on the plastic dissipation generated 6317 nodes and 3104 elements at the end.

CHAPTER 8

CONCLUSION AND

FUTURE WORK

8.1. SUMMERY

In this Thesis, adaptive techniques for solving large deformation problems of geomechanics have been studied and improved. The main areas covered in this study are summarised in the following.

- Alternative adaptive techniques have been investigated by considering their advantages and disadvantages and focusing mainly on large deformation problems of geomechanics.
- The main components of an adaptive finite element method including error estimation, mesh generation and remapping have been studied and their application in geotechnical problems have been addressed in this Thesis.
- A new *h*-adaptive technique has been presented with the ability to estimate the error in the analysis using one of three error estimators based on the energy norm, the Green-Lagrange strain or the plastic dissipation, to refine the mesh where a finer mesh is required and to transfer all the state variables from previous mesh to the new mesh.
- The efficiency and the accuracy of the *h*-adaptive method presented in this study have been tested by analysing some well known static geomechanics problems with either small or large deformation.
- The *h*-adaptive method in this study has been generalised for geotechnical problems involving dynamic analysis and contact mechanics.

- The efficiency and applicability of three main error assessor techniques including the energy norm, the Green-Lagrange strain, and the plastic dissipation in solving geotechnical problems involved with dynamic forces and changing boundary conditions have been address in this Thesis.
- A new combined *rh*-adaptive finite element strategy to solve geotechnical problems involved with material nonlinearity, large deformations, changing boundary conditions, and dynamic forces has been developed in this Thesis. This new method combines the *h*-adaptive method introduced in this study with an *r*-adaptive technique (ALE) to benefit from both methods simultaneously, and overcome the drawbacks of each individual adaptive technique. Then, the efficiency of this combined *rh*-adaptive method has shown by analysing some large deformation problems of geomechanics.

8.2. EFFICIENCY OF *h*-ADAPTIVE METHOD

The *h*-adaptive finite element method presented here is able to solve a wide range of nonlinear geotechnical problems efficiently and accurately. It is particularly effective in capturing localised failure and shear bands, which are difficult to predict using fixed grids. This *h*-adaptive technique also seems to be quite efficient in dealing with problems involving large deformation, where mesh distortion can affect the accuracy of the solution. In terms of efficiency, the *h*-adaptive technique is able to produce accurate results with considerably less numbers of elements and nodes and significantly less computational time.

8.3. ALTERNATIVE ERROR ESTIMATORS

The performance of three alternative error assessment techniques was investigated within the framework of an *h*-adaptive finite element method. This was achieved by studying the static and dynamic behaviour of soil under a strip footing as well as the response of soil to a penetrating object in the examples 7.2.4 and 7.2.5. For the static problems studied here it was observed that, in terms of accuracy, the three error assessment techniques provide similar results. For the footing problem, the plastic dissipation error estimator outperformed the other two techniques. However, for the case of static cone penetration involving an analysis of contact behaviour, it was demonstrated that the error assessor based on the Green-Lagrange was the most efficient technique.

For the dynamic problems considered in this study it was found that the Green-Lagrange strain error estimator can provide a solution with a minimum number of required degrees of freedom. In the case of dynamic penetration, the Green-Lagrange strain error estimator is the only one which was able to complete the analysis without any difficulty, while the other two techniques failed to provide a complete solution due to excessive mesh distortion caused by relatively large deformations occurring at the interface between the soil and the penetrometer. In addition, the plastic dissipation and energy norm error estimators tended to increase the density of the mesh unnecessarily, which increased the computational time significantly.

Numerical results indicate that the choice of a suitable error estimator depends on the problem and its complexity. In general, for the geomechanics problems presented here, the energy norm error estimator demonstrated the lowest performance while the Green-Lagrange strain error assessor was found to be most optimal. The results show that no unique error estimator may be generally prescribed for geotechnical problems. However, for dynamic contact problems, the choice of an error estimator based on the Green-Lagrange strain tensor is recommended.

8.4. COMBINED RH-ADAPTIVE METHOD

A combined *rh*-adaptive finite element method for analysing large deformation problems of geomechanics was presented in this study. The proposed method takes advantage of the *h*-adaptive finite element technique as well as the Arbitrary Lagrangian-Eulerian method, and eliminates the individual drawbacks of each method. For the numerical examples considered in this Thesis, it was shown that the proposed *rh*-adaptive method outperforms the *h*-adaptive finite element technique as well as the Updated-Lagrangian method.

8.5. FUTURE WORK

Based on the conclusions obtained in this Thesis, the following research topics are recommended by the author for future research works.

- The *h*- and *rh*-adaptive finite element techniques developed in this study can be generalised to solve geotechnical problems in which the pore water pressure is coupled with displacements under static or dynamic loads.

- The performance and applicability of alternative error estimator techniques in solving coupled problems of geomechanics is not addressed in the literature, and is yet to be understood.
- For all adaptive methods considered in this study, a robust strategy for transferring the state variables between the old mesh and the new mesh, which guarantees satisfaction of the equilibrium as well as the plasticity consistency, is still in demand.

REFERENCES

ABAQUS, Dassault Systemes, *Version 6.8EF Documentation*, 2008

Ainsworth M, Oden JT, "A unified approach to a-posteriori error estimation using element residual methods", *Numerical Mathematics*, 23-50, 1993

Allix O, Kerfriden P, Gosselet P, "On the control of the load increments for a proper description of multiple delamination in a domain decomposition framework", *International Journal for Numerical Methods in Engineering*, 83, 1518-1540, 2010

Ammons BA, Vable M, "An *hr*-method of mesh refinement for boundary element method", *International Journal for Numerical Methods in Engineering*, 43, 979-996, 1998

Argyris JH, Kelsey S, "Energy Theorems and Structural Analysis", *Aircraft Engineering*, 26 and 27, Part I is by JH Argyris and Part II is by JH Argyris and S Kelsey, 1954, 1955

Armero F, Petocz E, "Formulation and analysis of conserving algorithms for frictionless dynamic contact/impact problems", *Computer Methods in Applied Mechanics and Engineering*, 158, 269-300, 1998

Arney DC, Flaherty JE, "An adaptive local mesh refinement method for time-dependent partial differential equations", *Applied Numerical Mathematics*, 5, 257-274, 1989

Askes H, Rodriguez-Ferran A, "A combined *rh*-adaptive scheme based on domain subdivision. Formulation and linear examples", *International Journal for Numerical Methods in Engineering*, 51, 253-273, 2001

Babuska I, Chandra J, Flaherty JE, editors, "Adaptive Computational Methods for Partial Differential Equations", Philadelphia, SIAM, 1983

Babuska I, Flaherty JE, Hanshaw WD, Hopcroft JE, Oliger JE, Tezduyay T, editors, "Modelling, Mesh Generation, Adaptive Numerical Methods for Partial Differential Equations", *the IMA Volumes in Mathematics and its Applications*, 75, New York Springer- Verlag, 1995

Babuska I, Strouboulis T, Upadhyay CS, Gangaraj S.K, "A model study of the quality of a posteriori estimators for linear elliptic problems error estimation in the interior of patchwise uniform grids of triangles", *Computer Methods in Applied Mechanics and Engineering*, 114, 307-378, 1994a

Babuska I, Strouboulis T, Upadhyay CS, Gangaraj SK, Copps K, "Validation of posteriori error estimators by numerical approach", *International Journal for Numerical Methods in Engineering*, 37, 1073-1123, 1994b

Babuska I, Rheinboldt WC, "A posteriori error estimates for the finite element method", *International Journal for Numerical Methods in Engineering*, 12, 1597-1615, 1978

Babuska I, Zienkiewicz OC, Cago J, Olivira ER de A, editors, "Accuracy Estimates and Adaptive Refinements in Finite Element Computations", *John Wiley and Sons*, Chichester, 1986

Bank RE, Weiser A, "Some a posteriori error estimators for elliptic partial differential Equations", *Mathematics of Computation*, 44, 283-301, 1985

Becker R, Rannacher R, "A feed-back approach to error control in finite element methods: Basic analysis and examples", EAST-WEST, *Journal of Numerical Mathematics*, 4, 237-264, 1996

Belytschko T, "Adaptive refinement for explicit nonlinear finite element analysis", Technical Report DNA-TR-95-92, Defence Nuclear Agency Alexandria, VA 22310-3398, 1996

Belytschko, T and Kennedy, JM, "Computer models for subassembly simulation", *Nuclear Engineering and Design*, 49, 17-38, 1978

Belytschko T, Liu WK, Moran B, "Nonlinear Finite Elements for Continua and Structures", *John Wiley*, Chichester, New York, 2000

Belytschko T, Tabbara M, "*h*-adaptive finite element methods for dynamic problems, with emphasis on localization", *Journal for Numerical Methods in Engineering*, 36, 4245-4265, 1993

Benson DJ, "An efficient, accurate and simple ALE method for nonlinear finite element programs", *Computer Methods in Applied Mechanics and Engineering*, 72, 305-350, 1989

Bern MW, Flaherty JE, Luskin M, editors, "Grid Generation and Adaptive Algorithms", t*he IMA Volumes in Mathematics and its Applications*, 113, New York Springer, 1999

Bernardi C, Patera A, "A domain decomposition by the mortar element method. Asymptotic and numerical methods for partial differential equations with critical parameters", *Kluwer Academic Publisher,* Netherlands, 269- 286, 1993

Bessette GC, Becker EB, Taylor LM, Littlefield DL, "Modelling of impact problems using an *h*-adaptive, explicit Lagrangian finite element method in three dimensions", *Computer Methods in Applied Mechanics and Engineering*, 192, 1649-1679, 2003

Blacker TD, Belytschko T, "Superconvergent patch recovery with equilibrium and conjoint interpolant enhancements", *International Journal for Numerical Methods in Engineering*, 37, 517-536, 1994

Blum H, Jansen T, Rademacher A, Weinert K, "Finite element in space and time for dynamic contact problems", *International Journal for Numerical Methods in Engineering*, 76, 1632-1644, 2008

Boroomand B, Zienkiewicz OC, "Recovery by equilibrium in patches (REP)", *International Journal for Numerical Methods in Engineering*, 40, 137-154, 1997

Boroomand B, Zienkiewicz OC, "Recovery procedures in error estimation and adaptivity, Part II: adaptivity in nonlinear problems of elasto-plasticity behavior", *Computer Methods in Applied Mechanics and Engineering*, 176, 27-146, 1999

Brebbia CA, Aliabadi MH (Eds.), "Adaptive finite and boundary element methods", *Computational Mechanics Publications*, Southampton, Elsevier Applied Science, London, 1993

Buell WR, Bush BA, "Mesh generation- a survey", *Journal of Engineering for Industry Transactions of the ASME*, ser. B, 332-338, 1973

Burd HJ, "A large displacement finite element analysis of a reinforced unpaved road", *PhD Thesis*, Oxford University, England, 1986

Buscaglia1 GC, Duran R, Fancello EA, Feijoo RA, Padra1 C, "An adaptive finite element approach for frictionless contact problems", *International Journal for Numerical Methods in Engineering*, 50, 395-418, 2001

Cao T, “Adaptive H- and H-R methods for Symm's integral equation”, *Computer Methods in Applied Mechanics and Engineering*, 162, 1-17, 1998

Cescotto S, Wu ZD, “A variable-density mesh generation for planar domains”, *Communications in Applied Numerical Methods*, 5, 473-481, 1989

Chew LP, “Constrained Delaunay triangulations”, *Algorithmica*, 4, 97-108, 1989

Chung J, Hulbert GM, “A time integration algorithm for structural dynamics with improved numerical dissipation: the generalized-a method”, *Journal of Applied Mechanics*, 60, 371–375, 1993

Clark K, Flaherty JE, Shephard MS, editors, “Applied Numerical Mathematics”, *Special Issue on Applied Methods for Partial Differential Equations*, 14, 1994

Clough RW, “The Finite Element Method in Plane Stress Analysis,” Proceedings, *Second ASCE Conference on Electronic Computation*, Pittsburgh, PA, 345-378, 1960

Crane HL, Gibbs N, Poole W, Stockmeyer P, “Algorithm 508: Matrix bandwidth and profile reduction”, *ACM Transaction on Mathematical Software*, 2, 375-377, 1976

Cuthill E, McKee J, “Reducing the bandwidth of spare symmetric matrices”, *Proceeding of ACM National Conference*, New York, 151-172, 1969

Deb A, Prevost JH, Loret B, “Adaptive meshing for dynamic strain localization”, *Computer Methods in Applied Mechanics and Engineering*, 137, 285-306, 1996

Di Y, Sato T, “An operator-split ALE model for large deformation analysis of geomaterials”, *International Journal for Numerical and Analytical Methods in Geomechanics*, 31, 1375-1399, 2007

Diez P, Huerta A, "A unified approach to remeshing strategies for finite element *h*-adaptivity", *Computer Methods in Applied Mechanics and Engineering*, 176, 215-229, 1999

Duncan DB, editor, "Applied Numerical Mathematics", *Special Issue on Grid Adaptation in Computational PDEs: Theory and Applications*, 26, 1998

El-Hamalawi A, "Adaptive refinement of finite element methods for geotechnical analysis", *PhD Thesis*, Cambridge University, Cambridge, UK, 1997

El-Hamalawi A, "A 2D combined advancing front-Delaunay mesh generation scheme", *Finite Element in Analysis and Design*, 40, 967-989, 2004

Fischer KA, Wriggers P, "Frictionless 2D contact formulations for finite deformations based on the mortar method", *Computational Mechanics*, 36, 226-244, 2005

Fischer KA, Wriggers P, "Mortar based frictional contact formulation for higher order interpolation using the moving friction cone", *Computer Methods in Applied Mechanics and Engineering*, 195, 5020- 5036, 2006

Flaherty JE, Paslow PJ, Shephard MS, Vasilakis JD, editors, "Adaptive Methods for Partial Differential Equations", Philadelphia, SIAM, 1989

Fortune SJ, "A sweep line algorithm for Voronoi diagrams", *Algorithmica*, 2, 153-174, 1987

Franke D, Düster A, Nübel V, Rank E, "A comparison of the *h*-, *p*-, *hp*-, and *rp*- version of the FEM for the solution of the 2D Hertzian contact problem", *Computational Mechanics*, 45, 513-522, 2010

Frey PJ, George PL, "Mesh generation-Application to finite elements", *Hermes Science Europe Ltd.*, Oxford, UK, 2000

Gallimard L, Ladevèze P, Pelle JP, "Error estimation and adaptivity in elastoplasticity", *International Journal for Numerical Methods in Engineering*, 39, 189–217, 1996

George JA, "Computer implementation of the finite element method", *PhD Thesis*, Stanford University, California, USA, 1971

George PL, "Automatic Mesh Generation: Application to Finite Element Methods", *John Wiley & Sons*, 1991

Green PJ, Sibson R, "Computing Dirichlet tessellation in the plane", *The Computer Journal*, 21-2, 168-173, 1978

Habashi W, Dompierre J, Bourgault Y, Ait-Ali-Yahia D, Fortin M, Vallet M, "Anisotropic mesh adaption: Towards user-independent, mesh-independent and solver-independent CFD. Part I: General principles", *International Journal for Numerical Methods,* Fluids, 32, 725–744, 2000

Hlavacek I, Haslinger J, Necas J, Lovisek J, Solution of variational inequalities in mechanics, Springer-Verlag, Berlin, New York, 1988

Ho-Le K, "Finite element mesh generation methods: a review and classification", *Computer Aided Design*, 10, 27-38, 1988

Hu G, Wriggers P, "On the adaptive finite element method of steady-state rolling contact for hyperelasticity in finite deformation", *Computer Methods in Applied Mechanics and Engineering*, 191, 1333-1348, 2002

Hu Y, Randolph MF, "*h*-adaptive FE analysis of elasto-plastic non-homogeneous soil with

large deformation", *Computers and Geotechnics*, 23, 61-83, 1998

Hu Y, Randolph MF, "Plate-penetrometer penetration into NC soil using *h*-adaptive FE method", NUMOG VII International Symposium on Numerical Models in Geomechanics, Netherlands, A.A.Balkema, 501-506, 1999

Huerta A, Diez P, "Error estimation including pollution assessment for nonlinear finite element analysis", *Computational Methods for Applied Mechanics and Engineering*, 181, 21-41, 2000

Huerta A, Rodriguez-Ferran A, Diez P, Sarrate J, "Adaptive finite element strategies based on error assessment", *International Journal for Numerical Methods in* Engineering, 46, 1803-1818, 1999

Jin H, Wiberg NE, "Two dimensional mesh generation, adaptive remeshing and refinement", *International Journal for Numerical Methods in Engineering*, 29, 1501-1526, 1990

Johnson C, Hansbo P, "Adaptive finite element methods in computational mechanics", *Computer Methods in Applied Mechanics and Engineering*, 101, 143-181, 1992

Kellezi, L, "Dynamic soil-structure interaction. Transmitting boundary for transient analysis", *PhD Thesis*, Series R No. 50, Department of Structural Engineering & Materials, DTU, Denmark, 1998

Kelly DW, Gago J, Zienkiewicz OC, "'A posteriori error analysis and adaptive processes in the finite element method, Part I", *International Journal for Numerical Methods in Engineering*, 19, 1593-1619, 1983

Khoei AR, Lewis RW, "*h*-adaptive finite element analysis for localization phenomena with reference to metal powder forming", *Finite Elements in Analysis and Design*, 38, 503-519, 2002

Khoei AR, Tabarraie AR, Gharehbaghi SA, "*h*-Adaptive mesh refinement for shear band localization in elasto-plasticity Cosserat continuum", *Communications in Nonlinear Science and Numerical Simulation*, 10, 253-286, 2005

Khoei AR, Gharehbaghi SA, Tabarraie AR, Riahi A, "Error estimation, adaptivity and data transfer in enriched plasticity continua to analysis of shear band localization", *Applied Mathematical Modelling*, 31, 983-1000, 2007

Khoei AR, Biabanaki M, Anahid M, "Extended finite element method for three dimensional large plasticity deformation on arbitrary interfaces", *Computer Methods in Applied Mechanics and Engineering*, 197, 1100-1114, 2008

Kikuchi N, Oden JT, "Contact problems in elasticity: A study of variational inequalities and finite element methods", Vol 8 of SIAM studies in applied mathematics, Society for Industrial and Applied Mathematics, Philadelphia, 1988

Kita E, Higuchi K, Kamiya N, "*r*- and *hr*-adaptive boundary element method for two-dimensional potential problem", *Computers and Structures*, 74, 11-19, 2000

Kontoe S, "Development of time integration schemes and advanced boundary conditions for dynamic geotechnical analysis", *PhD Thesis*, Imperial College, London, 2006

Kontoe, S, Zdravkovic, L, Potts, D.M. , "An assessment of time integration schemes for dynamic geotechnical problems", *Computers and Geotechnics*, 35, 253-264, 2008a

Kontoe S, Zdravkovic L, Potts D, "The generalised-alpha algorithm for dynamic coupled consolidation problems in geotechnical engineering", 12th International Conference of International Association for Computer Methods and Advances in Geomechanics (IACMAG), 1449-1558, 2008b

Ladevèze P, Moës N, "Adaptive control for time-dependent nonlinear finite element analysis", *Advances in Finite Element Technology*, Civil-Comp Press, 79-92, 1996

Ladevèze P, Oden JT, "Advances in adaptive computational methods in Mechanics", Elsevier, Amsterdam, 1998

Lang J, Cao W, Huang W, Russell RD, "A two-dimensional moving finite element method with local refinement based on a posteriori error estimates", *Applied Numerical Mathematics*, 46, 75-94, 2003

Lau TS, Lo SH, "Finite element mesh generation over analytical curved surfaces", *Computer and Structures*, 59, 301-309, 1996

Lawson CL , "Software for C1 surface interpolation", in Rice, J.R., Editor, *Mathematical Software III*, 161-194, Academic Press, New York, USA, 1977

Lee DT, Schachter BJ, "Two algorithms for constructing a Delaunay triangulation", *International journal of computer and information sciences*, 9, 219-242, 1980

Lee NS, Bathe KJ, "Error indicators and adaptive remeshing in large deformation finite element analysis", *Finite Element in Analysis and Design*, 16, 99-139, 1994

Lee T, Park HC, Lee SW, "A superconvergent stress recovery technique with equilibrium constraint", *International Journal for Numerical Methods in Engineering*, 40, 1139-1160, 1997

Li LY, Bettess P, "Notes on mesh optimal criteria in adaptive finite element Computations", *Communications in Numerical Methods in Engineering*, 11, 911-915, 1995

Li LY, Bettess P, "Adaptive finite element methods: a review", *Applied Mechanics Review*, 50, 581-591, 1997

Lo SH, "A new mesh generation scheme for arbitrary planar domains", *International Journal for Numerical Methods in Engineering*, 21, 1403-1426, 1985

Lo SH, Lee CK, "Generation of gradation meshes by the background technique", *Computer and Structures*, 50, 21-32, 1994

Lopez, R.J., *Advanced Engineering Mathematics*, Addison Wesley, New York, 2001

Loze MK, Saunders R, "Two simple algorithms for constructing a two-dimensional constrained Delaunay triangulation", *Applied Numerical Mathematics*, 11, 403-418, 1993

Lysmer JR, Kuhlemeyer L, ''Finite dynamic model for infinite media", *Journal of the Engineering Mechanics Division, ASCE*, 95(EM4), 859-77, 1969

McFee S, "H-p adaptive numerical integration techniques for finite element analysis in magnetic", *Journal of IEEE Transactions on Magnetics*, 33, No. 5, 1997

Mahomed N, Kekana M, "An error estimator for adaptive mesh refinement analysis based on strain energy equalisation", *Computational mechanics*, 22, 355-366, 1998

Mühlhaus HB, Vardoulakis I, "The thickness of shear bands in granular materials", *Geotechnique*, 37, 271-283, 1987

Nazem M, "Numerical Algorithms for Large Deformation Problems in Geomechanics", *PhD Thesis*, the University of Newcastle, Australia, 2006

Nazem M, Sheng D, Carter JP, "Stress integration and mesh refinement for large deformation in geomechanics", *International Journal for Numerical Methods in Engineering*, 65, 1002-1027, 2006

Nazem, M, Sheng D, Carter JP, Sloan SW, "Arbitrary Lagrangian-Eulerian method for large-strain consolidation problems", *International Journal for Numerical and Analytical Methods in Geomechanics*, Vol. 32, 1023-1050, 2008

Nazem M, Carter JP, Sheng D, Sloan SW, "Alternative stress-integration schemes for large-deformation problems of solid mechanics", *Finite Elements in Analysis and Design*, 45-12, 934-943, 2009

Nazem M, Kardani M, Carter JP, Sheng D, "Application of *h*-adaptive FE method for dynamic analysis of geotechnical problems", Proceedings of the 2nd International Symposium on Computational Geomechanics (COMGEO II), Cavtat-Dubrovnik, Croatia, 490-495, 2011

Newmark NM, "A method of computation for structural dynamics", *Journal of Engineering Mechanics Division*, 85, 67-94, 1959

Noh WF, "A time-dependent two-space-dimensional coupled Eulerian-Lagrangian code", in: Alder, B, Fernbach, S and Rotenberg, M, *Methods in Computational Physics*, 3, Academic Press, New York, 1964

O'Rourke J, "Computational geometry in C", *Cambridge University Press*, 1993

Oden JT, Brauchli HJ, "On the calculation of consistent stress distributions in finite element approximation", *International Journal for Numerical Methods in Engineering*, 3, 317-325, 1971

Oden JT, Demkowicz L, Rachowicz W, Westermann TA, "Toward a universal *h-p* adaptive finite element strategy-Part 2: A posteriori error estimation", *Computer Methods in Applied Mechanics and Engineering*, 77, 113-180, 1989

Oden JT, Prudhomme S, "Goal-oriented error estimation and adaptivity for the finite element method", *Computers and Mathematics with Applications*, 41, 735-756, 2001

Onate E, Bugeda G, "A study of mesh optimality criteria in adaptive finite element analysis", *Engineering Computations*, 10, 307-321, 1993

Ortiz M, Quigley JJ, "Adaptive mesh refinement in strain localization problems", *Computer Methods in Applied Mechanics and Engineering*, 90, 781-804, 1991

Owen SJ, "A survey of unstructured mesh generation technology", Proceedings, *Seventh International Meshing Roundtable*, Sandia National Laboratories, Albuquerque, NM, 239–267, 1998

Partheymuller P, Bialecki RA, Kuhn G, "Self-adapting algorithm for evaluation of weakly singular integrals arising in the boundary element method", *Journal of Engineering Analysis with Boundary Elements*, 14, 285-292, 1995

Paulino GH, Shi F, Mukhrejee S, Ramesh P, "Nodal sensitivities as error estimates in computational mechanics", *Acta Mechanica*, 121, 191-213, 1997

Peano AG, Pasini R, Sardella, "Adaptive approximation in finite element structural analysis", *Computer and Structures*, 10, 332-342, 1979

Peraire J, Morgan K, "Unstructured mesh generation including directional refinement for aerodynamic flow simulation", *Finite Elements in Analysis and Design*, 25, 343-355, 1997

Peraire J, Vahdati M, Morgan K, Zienkiewicz OC, "Adaptive remeshing for compressible flow computations", *Journal of Computational Physics*, 72, 449-466, 1987

Peric D, Hochard Ch, Dutko M, Owen DRJ, "Transfer operators for evolving meshes in small strain elasto-plasticity", *Computer Methods in Applied Mechanics and Engineering*, 137, 331-344, 1996

Peric D, Vaz Jr. M and Owen DRJ, "On adaptive strategies for large deformations of elasto-plastic solids at finite strains: computational issues and industrial applications", *Computer Methods in Applied Mechanics and Engineering*, 176, 279-312, 1999

Peric D, Yu J, Owen RJ, "On error estimates and adaptivity in elastoplastic solids: Applications to the numerical simulation of strain localization in classical and Cosserat continua", *International Journal for Numerical Methods in Engineering*, 37, 1351-1379, 1994

Potts DM, Zdravkovic L, "Finitet element analysis in geotechnical engineering: Application", London, Thomas Telford, 2001, ISBN: 9780727727831

Puso MA, Laursen TA, "Mesh tying on curved interfaces in 3D", *Engineering Computations*, 20(3), 305-319, 2003

Qian YY, Dhatt G, "A Simple adaptable 2D mesh generation package", *Computer and Structures*, 53, 801-810, 1994

Ramm E, Rank E, Rannacher R, Schweizerhof K, Wendland W, Wittum G, Wriggers, Wunderlich W, “Error-controlled adaptive finite elements in solid mechanics”, *Wiley*, Chichester, 2003

Rank E, Zienkiewicz OC, “A simple error estimator in finite element method”, *Computer Methods in Applied Mechanics and Engineering*, 3, 243-250, 1987

Rannacher R, Suttmeier FT, “A posteriori error control in finite element method via duality technique: Application to perfect plasticity”, *Computational Mechanics*, 21, 123-133, 1998

Rannacher R, Suttmeier FT, “A posteriori error estimation and mesh adaption for finite element models in elsto-plasticity”, *Computer Methods in Applied Mechanics and Engineering*, 176, 333-361, 1999

Rebay S, “Efficient unstructured mesh generation by means of Delaunay triangulation and Bowyer-Watson algorithm”, *Journal of Computational Physics*, 106, 125-138, 1993

Rieger A, Wriggers P, "Comparison of different error estimators for contact problems", *Engineering Computations*, 17, 255 – 273, 2000

Rieger A, Wriggers P, "Adaptive methods for frictionless contact problems", *Computers and Structures*, 79, 2197-2208, 2001

Runesson K, Ottosen NS, Peric D, “Discontinuous bifurcations of elastic-plastic solutions at plane stress and plane strain", *International journal of plasticity*, 7, 99-121, 1991

Schwab C, “P- And Hp- Finite Element Methods: Theory and Applications in Solid and Fluid Mechanics”, *Numerical Mathematics and Scientific Computation*, Clarendon, London, 1999

Shamos MI, Hoey D, "Closest-point problems", in proceeding of the 16th *annual symposium on the foundations of computer science*, 151-162, 1975

Sheng D, Eigenbrod P, Wriggers P, "Finite element analysis of pile installation using large slip frictional contact", *Computer and Geotechnics*, 32, 17-26, 2005

Sheng D, Nazem M, Carter JP, "Some computational aspects for solving deep penetration problems in geomechanics", *Computational Mechanics*, 44, 549-561, 2009

Sheng D, Sloan SW, "Load stepping schemes for critical state models", *International Journal for Numerical Methods in Engineering* , 50(1), 67-93, 2001

Sheng D, Sloan SW, "Time stepping schemes for coupled displacement and pore pressure analysis", *Computational Mechanics*, 31, 122-134, 2003

Sheng D, Sloan SW and Yu HS, "Aspects of finite element implementation of critical state models", *Computational Mechanics*, 26, 185-196, 2000

Sheng D, Wriggers P, Sloan SW, 'Improved numerical algorithms for frictional contact in pile penetration analysis', *Computers and Geotechnics*, 33, 341-354, 2006

Shephard MS, "Adaptive finite element analysis and CAD; In: Babuska *et al.* (Eds.), Accuracy Estimates and Adaptive Refinement in Finite Element Computations", *John Wiley & Sons*, 205-225, 1986

Shephard MS, "Approaches to the automatic generation and control of finite element meshes", *Applied Mechanics Review ASME*, 41, 169-185, 1988

Shewchuk JR, "Delaunay refinement mesh generation", *PhD thesis*, Carnegie Mellon University, Pittsburgh, PA, USA, 1997

Shewchuk JR, "Triangle: Engineering a 2D quality mesh generator and Delaunay Triangulator", Applied Computational Geometry: Toward Geometric Engineering", 1148, Lecture Notes in Computer Science, Springer-Verlag, Berlin, 203-222, 1996

Sibson R, "Locally equiangular triangulations", *The Computer Journal*, 2, 243-245, 1973

Silva RCC, Landau L, Ribeiro FLB, "Visco-Plastic *h*-adaptive analysis", *Computers and Structures* , 78, 123-131, 2000

Sloan SW, "Substepping schemes for the numerical integration of elastoplastic stress-strain relations", *International Journal for Numerical Methods in Engineering*, 24(5), 893-911, 1987

Sloan SW, "A fast algorithm for generating constrained Delaunay triangulations", *Computer and Structures*, 47, 441-450, 1993

Sloan SW, Abbo AJ, "Biot consolidation analysis with automatic time stepping and error control Part 1: Theory and implementation", *International Journal for Numerical and Analytical Methods in Geomechanics*, 23, 467-492, 1999

Sloan SW, Abbo AJ, "Biot consolidation analysis with automatic time stepping and error control Part 2: Applications", *International Journal for Numerical and Analytical Methods in Geomechanics*, 23, 493-529, 1999

Sloan SW, Abbo AJ, Sheng D, "Refined explicit integration of elastoplastic models with automatic error control", *Engineering Computations*, 18, 121-154, 2001

Szabo BA, "Some recent development in finite element analysis", *Computers and Mathematics with Applications*, 5, 99-115, 1979

Szabo BA, "Mesh design for the p-version of the finite element method", *Computer Methods in Applied Mechanics and Engineering*, 55, 181-197, 1986

Szabo BA, Babuska I, "Finite Element Analysis", *John Wiley & Sons*, New York, 1991

Tabbara M, Blacker TP, Belytschko T, "Finite element derivative recovery by moving least square interpolants", *Computational Methods in Applied Mechanics and Engineering,* 117, 211-223, 1994

Tejchman J and Bauer E, "Numerical simulation of shear band formation with a polar hypoplastic constitutive model", *Computer and Geotechnics,* 19-3, 221-244, 1996

Thacker WC, "A brief review of techniques for generating irregular computational grids", *International Journal for Numerical Methods in Engineering,* 15, 1335-1342, 1980

Turner MJ, Clough RW, Martin HC, Topp LJ, "Stiffness and Deflection Analysis of Complex Structures", *Journal of the Aeronautical Sciences*, 23(1956), 805-823, 1956

Verfurth R, "A Review of Posteriori Error Estimation and Adaptive Mesh Refinement Techniques", *Teubner-Wiley*, Stuttgart, 1996

Wang CX, Carter JP, "Deep penetration of strip and circular footings into layered clays", *The International Journal of Geomechanics*, 2, 2, 205-232, 2002

Watson DF, "Computing the n-dimensional Delaunay tessellation with application to Voronoi polytopes", *the Computer Journal*, 24, 167-172, 1981

Wiberg NE, Abdulwahab F, "Patch recovery based on superconvergent derivatives and equilibrium", *International Journal for Numerical Methods in Engineering*, 36, 2703-2724, 1993

Wiberg NE, Abdulwahab F, Ziukaz S, "Enhances superconvergent patch incorporating equilibrium and boundary condition", *International Journal for Numerical Methods in Engineering*, 37, 3417-3440, 1994

Wiberg NE, Li XD, "A postprocessed error estimate and an adaptive procedure for the semidiscrete finite element method in dynamic analysis", *International Journal for Numerical Methods in Engineering*, 37, 3585-3603, 1994

Wriggers P, "Computational Contact Mechanics", Chichester: John Wiley & Sons, 2002

Wriggers P, "Nonlinear Finite Element Methods", Springer-Verlag, Austria, 2010

Wriggers P, Scherf O, Carstensen C, "Adaptive techniques for the contact of elastic bodies", In Recent Developments in Finite Element Analysis, (Edited by JR Hughes, E Onate and OC Zienkiewicz), CIMNE, Barcelona, 1994

Wriggers P, Scherf O, "Different a posteriori error estimators and indicators for contact problems", *Mathematical and Computer Modelling*, 28, 437-447, 1998

Wriggers P, Simo JC, "A note on tangent stiffness for fully nonlinear contact problems", *Communications in Applied Numerical Methods*, 203, 1- 199, 1985

Wriggers P, Rieger A, Scherf O, "Comparison of different error measures for adaptive finite element technique applied to contact problems involving large elastic strain", *Computer Methods in Applied Mechanics and Engineering*, 2000

Yu HS, "Cavity expansion methods in geomechanics", Kluwer Academic Publishers, Netherlands, 2000

Zienkiewicz OC, Irons BM, Scott FE, Campbell, "High speed computing of elastic structures", *International Union of Theoretical and Applied Mechanics*, Liege, 1970

Zienkiewicz OC, Irons BM, Scott FE, Campbell, "High speed computing of elastic structures", *International Union of Theoretical and Applied Mechanics*, Liege, 1970

Zienkiewicz OC, Philips DV, "An automatic mesh generation scheme for plane and curved surfaces by isoparametric coordinates", *International Journal for Numerical Methods in Engineering*, 3, 519-528, 1971

Zienkiewicz OC, Taylor RL, "The Finite Element Method, Vol. 1: Basic Formulation and linear problems", *McGraw-Hill*, London, 1989

Zienkiewicz OC, Zhu JZ, Wu J, "Superconvergent recovery techniques, some further tests", *Comm. Appl. Sci. Eng.* **9** (1993), pp. 251–258Zienkiewicz OC, Wu J, "Automatic directional refinement in adaptive analysis of compressible flows", *International Journal for Numerical Methods in Engineering*, 37, 2189-2210, 1994

Zienkiewicz OC, Zhu JZ, "A simple error estimator and adaptive procedure for practical engineering analysis", *International Journal for Numerical Methods in Engineering*, 24, 337-357, 1987

Zienkiewicz OC, Zhu JZ, "Adaptivity and mesh generation", *International Journal for Numerical Methods in Engineering*, 32, 783-810, 1991

Zienkiewicz OC, Zhu JZ, "The superconvergent patch recovery and a posteriori error estimate. Part I: The recovery technique", *International Journal for Numerical Methods in Engineering*, 33, 1331-1364, 1992a

Zienkiewicz OC, Zhu JZ, "The superconvergent patch recovery and a posteriori error estimate. Part II: Error estimates and adaptivity", *International Journal for Numerical Methods in Engineering*, 33, 1365-1382, 1992b

Zienkiewicz OC, Zhu JZ, Wu J, "Superconvergent patch recovery techniques-some further tests", *Communications in numerical methods in engineering*, 9, 251-258, 1993

Zienkiewicz OC, Zhu JZ, "The SPR recovery and boundaries", *International Journal for Numerical Methods in Engineering*, 37, 3195-3196, 1994